DFO TANKER SAFETY 2016 PROJECT REPORT

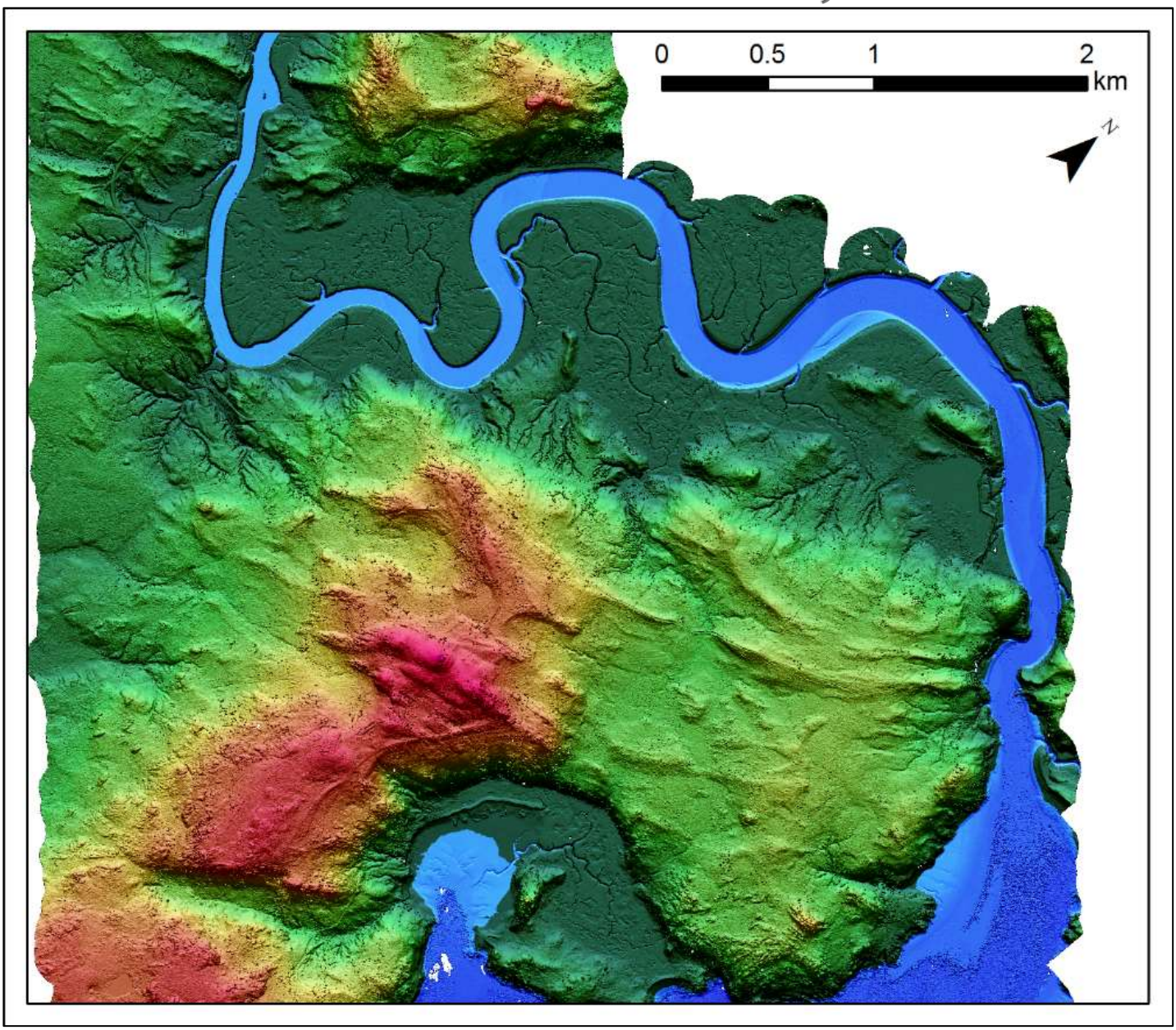

Prepared by

Applied Geomatics Research Group
NSCC, Middleton
Tel. 902 825 5475
email: tim.webster@nscc.ca

Submitted to

Fisheries and Oceans Canada
Pêches et Océans Canada

Scott Coffen-Smout
Oceans and Coastal Management Division
Ecosystem Management Branch

June 22, 2016

How to cite this work and report:

Webster, T., Crowell, N., Collins, K., McGuigan, K., MacDonald, C., 2016. DFO Tanker Safety 2016 Project Report. Technical report, Applied Geomatics Research Group, NSCC Middleton, NS.

Executive Summary

Topographic-bathymetric lidar surveys were flown at six study areas in Nova Scotia and New Brunswick as part of the Government of Canada's World-Class Tanker Safety Program, in collaboration with Fisheries and Oceans Canada in the fall of 2015. Digital elevation models, colour shaded relief models, and aerial photograph mosaics were generated for each study area.

Oil tankers approaching the Port Hawkesbury, Nova Scotia terminal sail through the Strait of Canso past the complex bathymetry and morphology of Isle Madame. A portion of that area was surveyed using lidar in 2014, and two additional surveys were completed there on Oct. 28 and Nov. 11, 2015, with a maximum depth penetration of 12 m. Validation of the topographic lidar was achieved using differential GPS data obtained for hard, flat surfaces; mean difference in elevation between the GPS data and lidar data was -0.04 m. Bathymetric lidar was validated at the Isle Madame study area using direct seabed elevation measurements obtained using differential GPS; the mean difference in elevation between the GPS data and the lidar data was -0.19 m.

A hydrodynamic model was developed for the Isle Madame study area using the lidar bathymetry data from 2014 combined with the 2015 data and traditional echo sounding depths. The model was validated using a pressure sensor deployed in Isle Madame for 48 days in 2015. The modelled and observed depths comparison was represented by a linear relationship with a Pearson's Coefficient of 0.975, with p value < 0.01 and random residual distribution. The model was used to simulate flow through the complex morphology and bathymetry of the Isle Madame coastline, and to simulate the timing and dispersion of a simulated oil spill.

Four lidar surveys were completed near the port of Saint John, New Brunswick, in the Bay of Fundy. The Saint John approach study area was surveyed on Nov. 7, 2015, and had maximum depth penetration of 4.5 m. Topographic validation was completed with mean elevation difference between the GPS data and lidar data of -0.09 m. Musquash was surveyed on Nov. 9 and had maximum depth penetration of ~3 m; topographic validation had mean difference of -0.05 m. Campobello Island and Grand Manan were surveyed on Oct. 27 and had maximum depth penetration of 8.4 m. No topographic validation was completed at Campobello or Grand Manan, and no bathymetric validation has yet been completed at any of the Bay of Fundy sites.

A narrow area along the Nova Scotia shoreline of the Bay of Fundy was surveyed on Oct. 27 to assess the penetration of the lidar in the varying water clarity conditions of that coast. Near Brier Island depth penetration reached 10 m, and penetration decreased towards the upper Bay of Fundy, achieving a maximum depth penetration in the Northeastern strip of 3 m.

Table of Contents

Table of Figures

List of Tables

1 Introduction

The Government of Canada established the World-Class Tanker Safety program to strengthen Canada's current tanker safety program by preventing oil spills and improving response and cleanup (Government of Canada, 2016). Spill-response planning partnerships were developed as part of the program for several high-traffic ports, including Saint John, New Brunswick (NB) and Port Hawkesbury, Nova Scotia (NS). The Area Response Planning Project is a regional, risk-based planning approach that reflects local environmental sensitivities and marine activity; the project aims to establish a new level of oil spill preparedness and response capacity to match the level of regional risk (Government of Canada, 2012).

Nova Scotia Community College's Applied Geomatics Research Group (NSCC-AGRG) is participating in the Atlantic component of the project by surveying several areas in the Atlantic Ocean and Bay of Fundy using an airborne topographic-bathymetry (topo-bathy) lidar sensor and high resolution digital camera. Six areas were surveyed in 2015 using topo-bathy lidar: four in the Bay of Fundy near the Port of Saint John and two in the Strait of Canso near the Port Hawkesbury terminal (Figure 1.1). Addionally, a narrow strip of NS Bay of Fundy coastline was surveyed as a test area to assess the water quality and success of the lidar in this region (Figure 1.1). Over the two-year project, AGRG will use these data to generate high resolution near-shore bathymetry maps, derive substrate and vegetation habitat types, and develop coastal hydrodynamic models. The results of the project will be used as part of the World-Class Tanker Safety program to ensure safe navigation of tankers into the port, and to better manage response time and logistics.

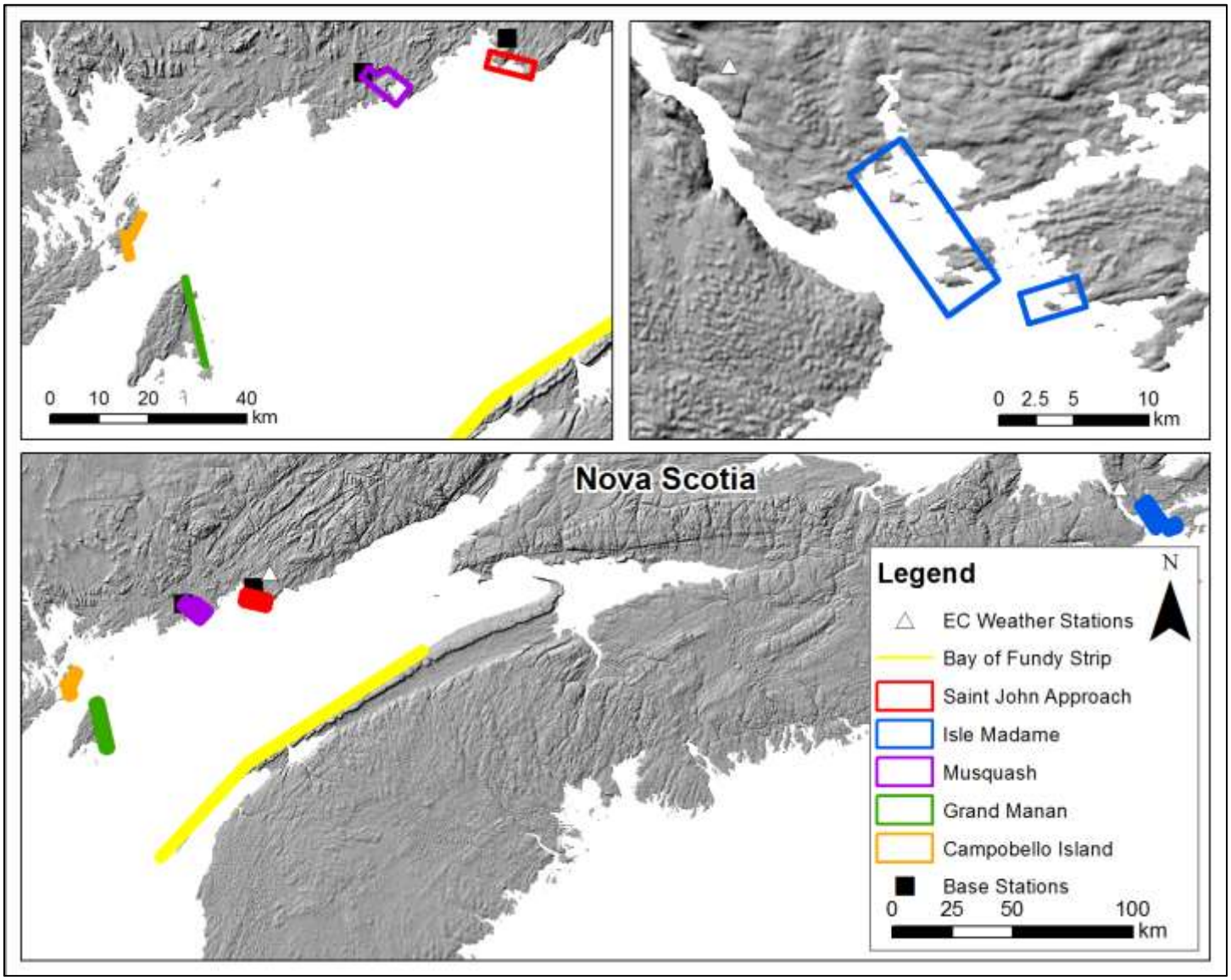

Figure 1.1: The bathymetric lidar study areas.

This report describes the methods for data collection and processing in Section 2. Results are presented in Section 3.

2 Methods

2.1 Sensor Specifications and Installation

The lidar sensor used in this study is a Chiroptera II integrated topographic-bathymetric lidar sensor equipped with a 60-megapixel multispectral camera. The system incorporates a 1064 nm near-infrared laser for ground returns and sea surface and a green 515 nm laser for bathymetric returns (Figure 2.1). The lasers scan in an elliptical pattern, which enables coverage from many different angles, on vertical faces, causes less shadow effects in the data, and is less sensitive to wave interaction. The bathymetric laser is limited by depth and clarity, and has a depth penetration rating of 1.5 x the Secchi depth (a measure of turbidity or water clarity using a black and white disk). The Leica RCD30 camera

collects co-aligned RGB+NIR motion compensated photographs which can be mosaicked into a single image in post-processing, or analyzed frame by frame for maximum information extraction.

The calibration of the sensor has been documented in a separate report included as part of the Deliverables for this project.

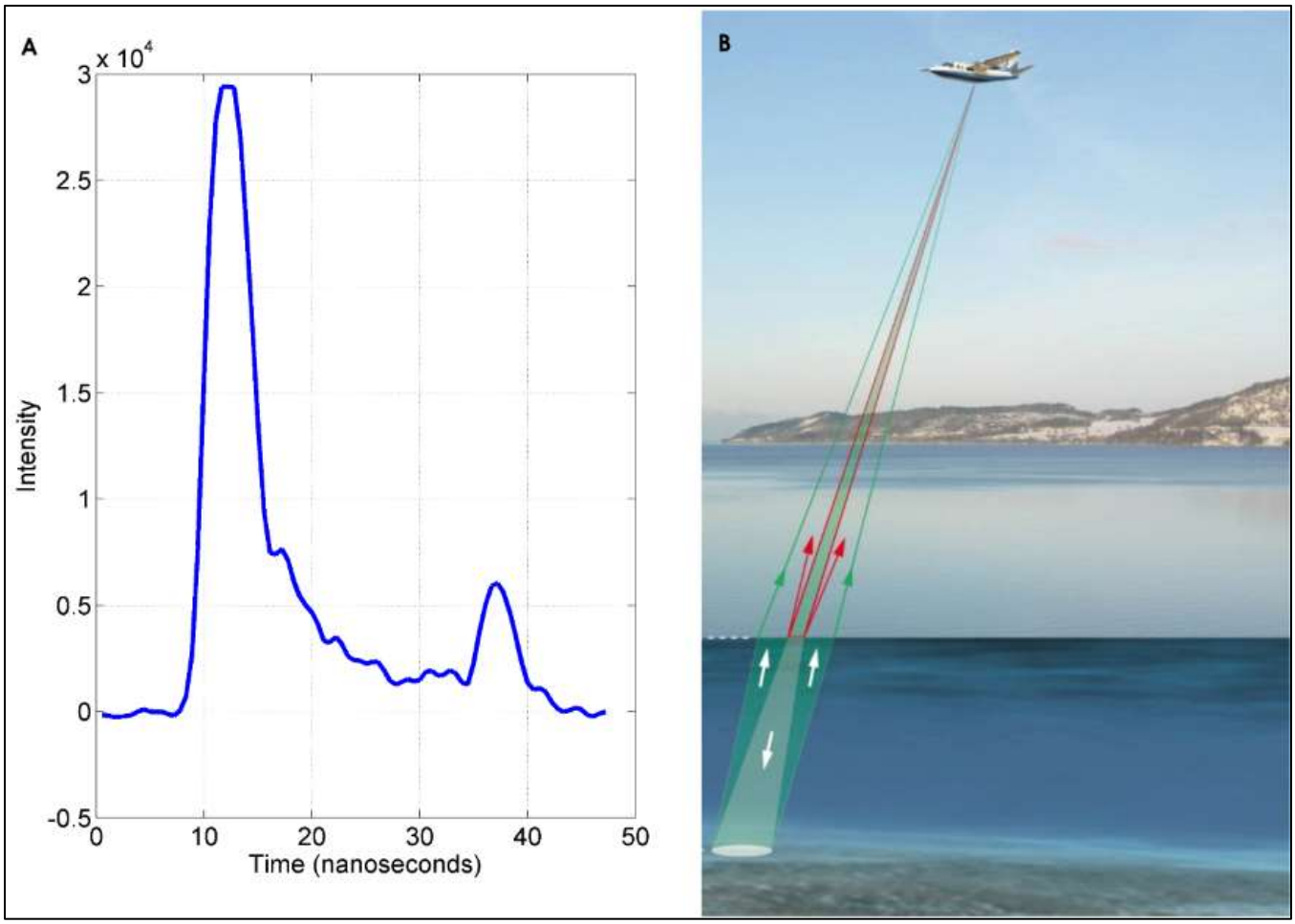

Figure 2.1: (A) Example of the Chiroptera II green laser waveform showing the large return from the sea surface and smaller return from the seabed. (B) Schematic of the Chiroptera II green and NIR lasers interaction with the sea surface and seabed (adapted from Leica AHAB).

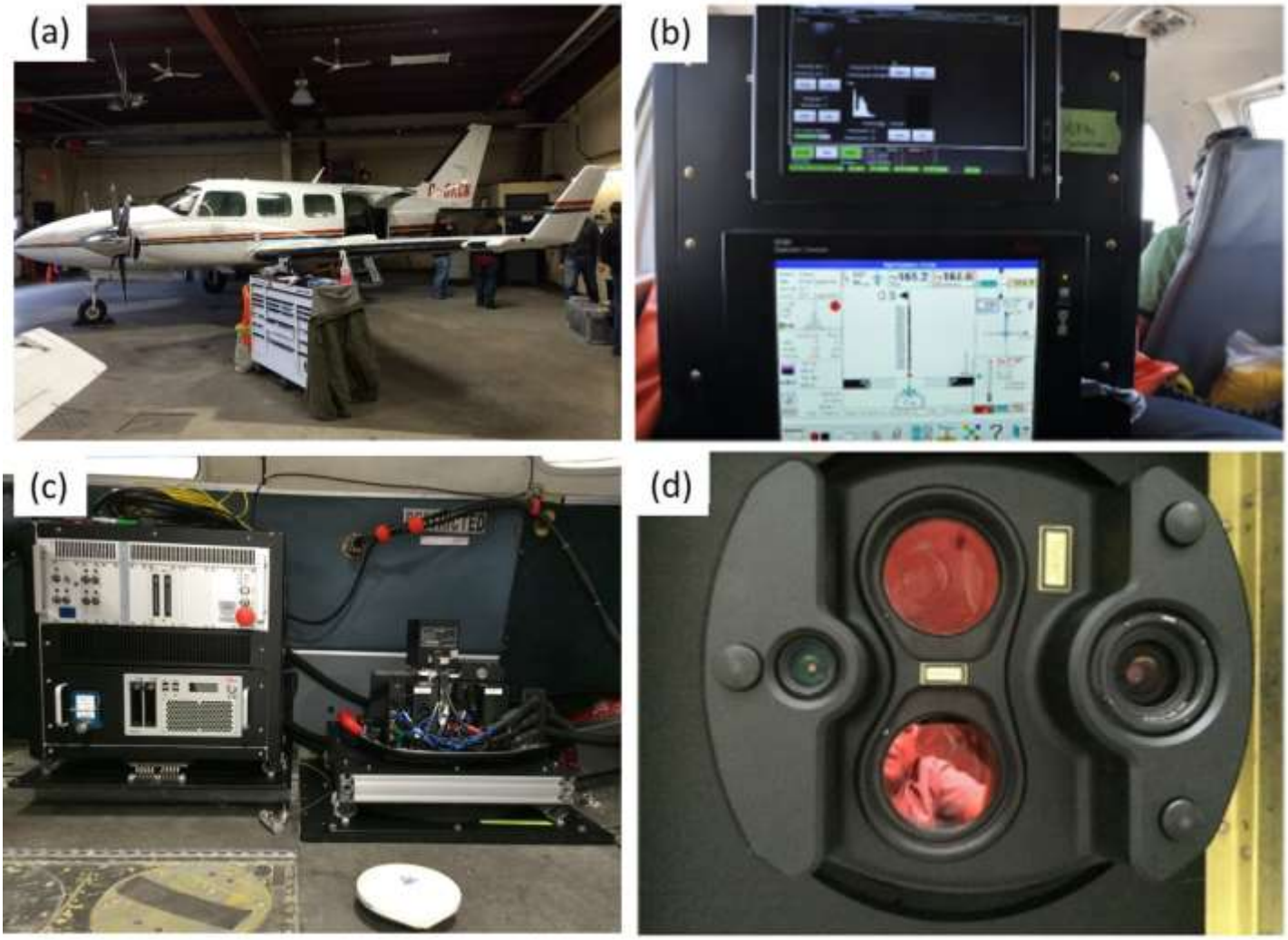

Figure 2.2: (a) Aircraft used for 2015 lidar survey; (b) display seen by lidar operator in-flight; (c) main body of sensor (left) and laser heads pointing through a hole cut in the bottom of the plane (right); (d) large red circles are the lasers; the RCD30 lens (right) and low resolution camera (left).

2.2 Lidar Survey Details

The lidar surveys were conducted in October and November, 2015 (Table 2.1). The surveys were planned using Leica Mission Pro software and flown at an altitude of 400 m above ground at a flying speed of 62.0 m/s. The planned flight lines for each study area are shown in Figure 2.3 -Figure 2.6. Average tidal state and meteorological conditions are summarized in Table 2.1 and are presented in greater detail in Section 2.4.

The Musquash survey was attempted on November 8 under scattered cloud conditions which cause different light conditions between flight lines and make it difficult to generate a consistent and seamless mosaicked orthophoto. The priority for Musquash was good quality photographs, so the survey was aborted. The survey was completed successfully on the following day when cloud conditions had improved.

The aircraft required ground-based high precision GPS data to be collected during the lidar survey in order to provide accurate positional data for the aircraft trajectory. For Isle Madame South ground crews established a benchmark to gather observations to use as control for the aircraft during the survey, while for the other stations observations were obtained from a virtual network. The control used for each survey are noted in Table 2.1 and the control stations are shown in in Figure 2.3 - Figure 2.6. The Leica GS14 GPS base station at Isle Madame was set to log observations at 1 second intervals and the RTK rover was used to collect lidar validation points on hard flat surfaces.

Study Area	AOI Code	Survey Date (mm/dd/yy)	Survey Time (UTC)	Tide	Wind Spd (km/hr)	Wind Dir	Sun Angle (°)	Cloud State	Control
Isle Madame West, NS	IMW	11/19/15	13:43 – 16:40	MTR	9	SE	22	Overcast	ACHT
Isle Madame South, NS	IMS	10/28/15	17: 48 – 18:52	LT	11	NW	21	Open	IMBENCH
Saint John Approach, NB	SJA	11/07/15	16:37 – 19:12	MTF	27	NW	22	Overcast	STJN
Musquash, NB, Survey 1	MQ	11/08/15	17:10 – 17:40	MTF	28	NW	24	Scattered	STJN
Musquash, NB, Survey 2	MQ	11/09/15	16:42 – 19:33	MTF	17	W	20	Open	STJN
Campobello Island - Grand Manan, NB	CAMP, GM	10/27/15	12: 39 – 13:49	HT	11	W	20	Open	PENF
Bay of Fundy Strip	BOFS	10/27/15	15:36-16:55	MTF	15	NW	32	Open	MTGN,DIGBY, AGRG_Roof

Table 2.1: Lidar survey details summary. Tide, wind speed and direction, sun angle and cloud state are all average values for the duration of the survey. Tidal states: MTR= Mid-Tide Rising, MTF=Mid-Tide Falling, HT=High Tide, LT= Low Tide; weather information is from nearest airport (shown on flight line figures?). Note that Musquash Survey 1 was aborted due to poor meteorological conditions.

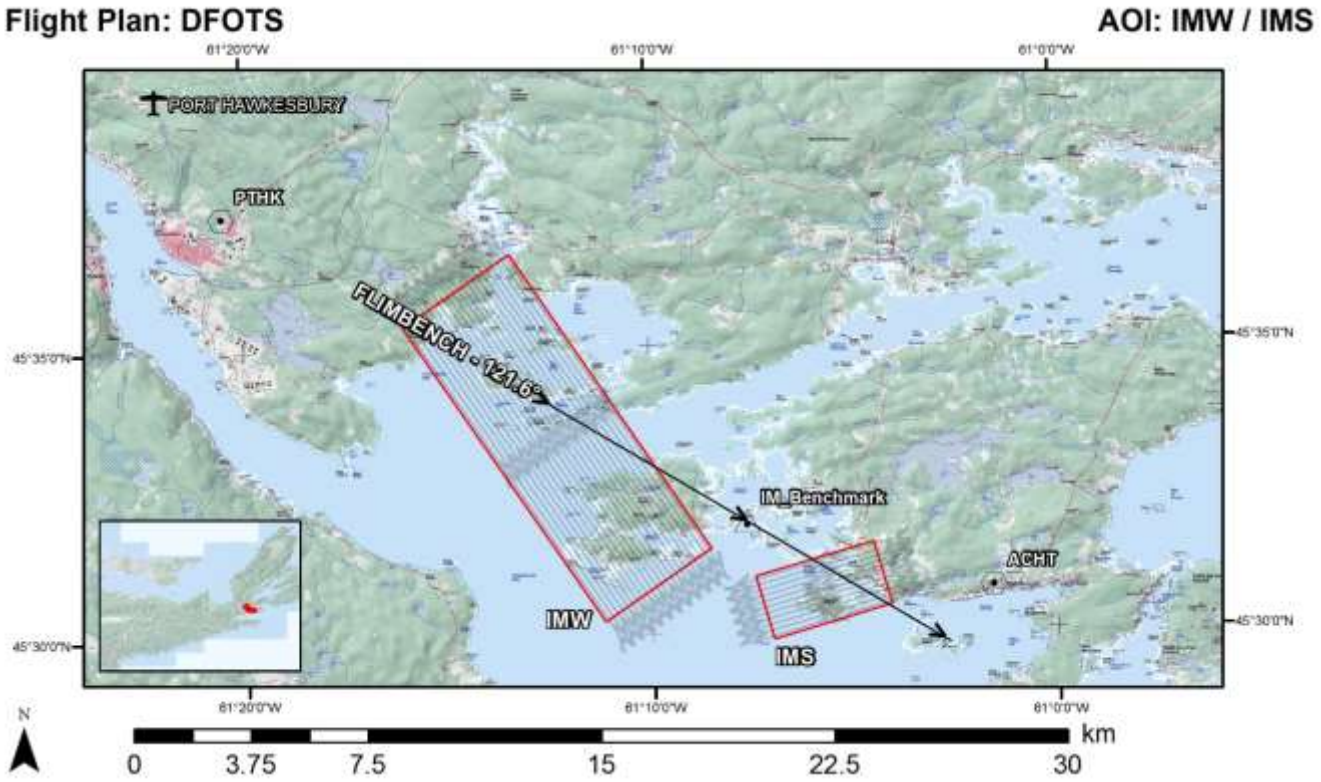

Figure 2.3: Flight lines planned for the Isle Madame West and South study areas showing the flat and level flight line over the base station (IMBENCH), and showing the virtual control station used for the IMS survey (ACHT).

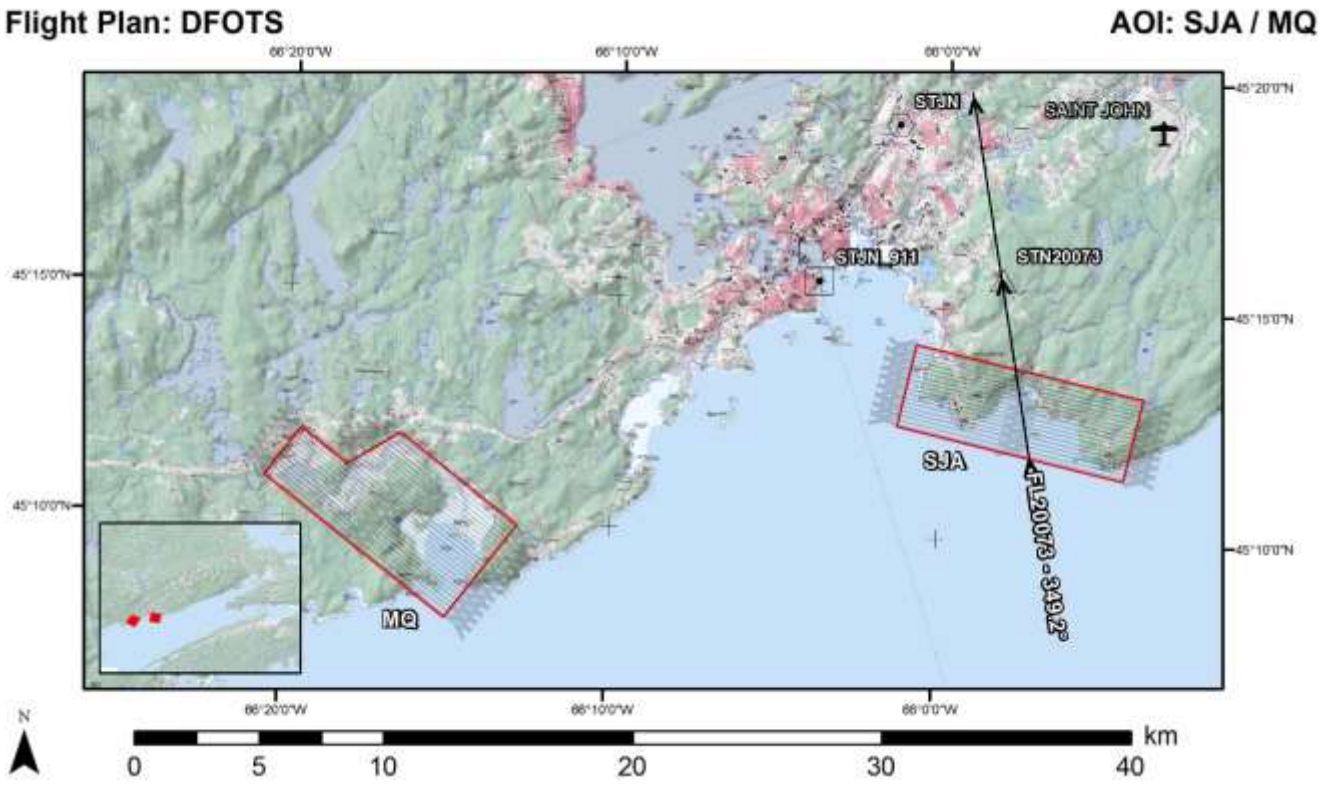

Figure 2.4: Flight lines planned for the Musquash and Saint John Approach study areas showing the flat and level flight line over the base station (STJN).

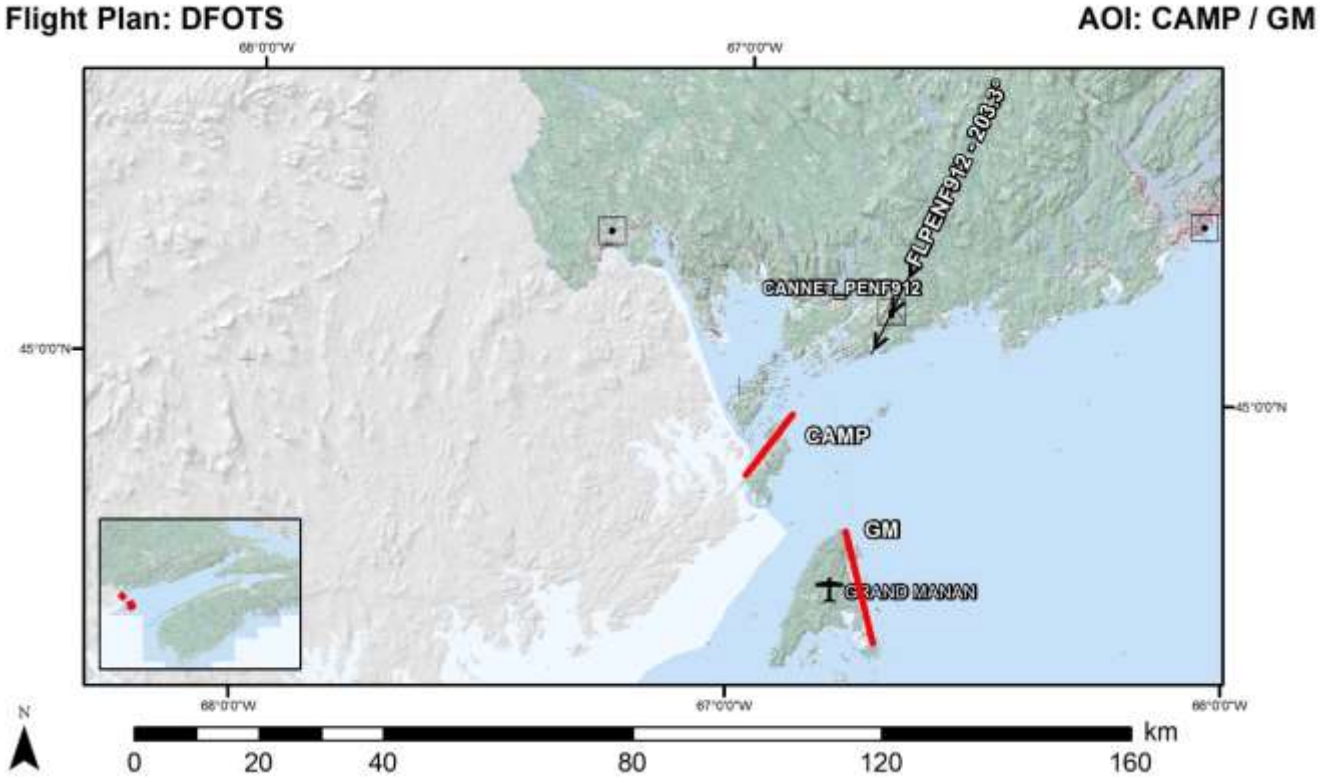

Figure 2.5: Flight lines planned for the Grand Manan and Campobello Island study areas.

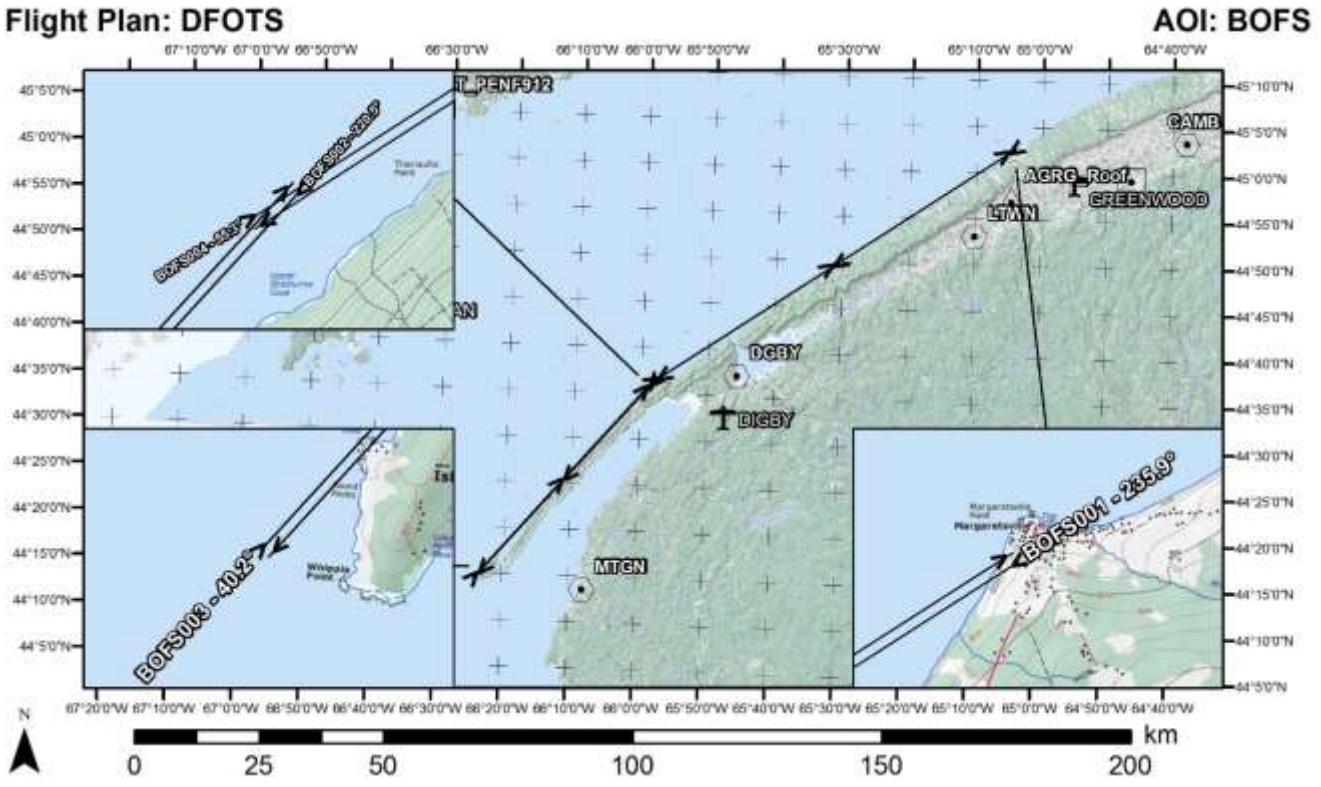

Figure 2.6: Flight lines planned for the Bay of Fundy strip study area and the base station used.

2.3 Ground Truth Data Collection

Ground truth data collection is an important aspect of topo-bathymetric lidar data collection. In 2015 land-based hard surface ground truth data were collected at all study sites except Grand Manan and Campobello Islands, and boat-based ground truth data were collected at Isle Madame (Table 2.2). The boat-based observations included depth measurements to validate the lidar, Secchi depth measurements for information on water clarity, and underwater photographs to obtain information on bottom type and vegetation (Figure 2.6). For the 2015 field season, a new system was employed to measure the seabed elevation directly using a large pole onto which the RTK GPS antenna was threaded. This system helped to overcome the challenges of validating 1 m resolution lidar bathymetry using 3-5 m resolution code-based GPS top obtain the boat-based bathymetry spatial information. By threading the RTK GPS antenna on the pole and measuring the elevation of the seabed directly we not only benefitted from the higher resolution spatial data of the RTK GPS (<5 cms of cm accuracy), we also eliminated errors introduced into depth measurements obtained from a boat such as water tidal variation, angle of rope for lead ball measurements, etc. (Figure 2.6b).

Location	Date	Base station	GPS System	Secchi	Depth	Light and Pressure Sensors	Underwater Photos	Hard Surface GPS
Isle Madame	09/23/15	imbenchmark	GS14, 530	-	CTD	Deployed	Q_1	Y
	10/28/15*	imbenchmark	GS14	-	-	-	-	Y
	11/19/15*	Imbenchmark	GS14, 530	Y	P,M,ES	Retrieved	P,Q_{50}	-
Saint John Approach	10/09/15	HPN 20073	530	-	-	-	-	Y
Musquash	10/09/15	HPN 28125	530	-	-	-	-	Y

Table 2.2: Ground truth data summary. * Indicates that the ground truth survey was occurring simultaneously with the lidar survey. GPS Column: Two Leica GPS systems were used the GS14 and the 530. Depth Column: CTD=Conductivity Temperature Depth profiler; P=GPS antenna threaded onto the large pole for direct bottom elevation measurement; M=manual depth measurement using lead ball or weighted Secchi disk; ES=Single beam commercial grade Humminbird Echo Sounder. Underwater Photos: P=GoPro camera secured to pole for underwater still photos; Q_1=1 m^2 quadrat with downward-facing and side-facing GoPro cameras; Q_{50}=50 cm^2 quadrat with downward-facing GoPro camera.

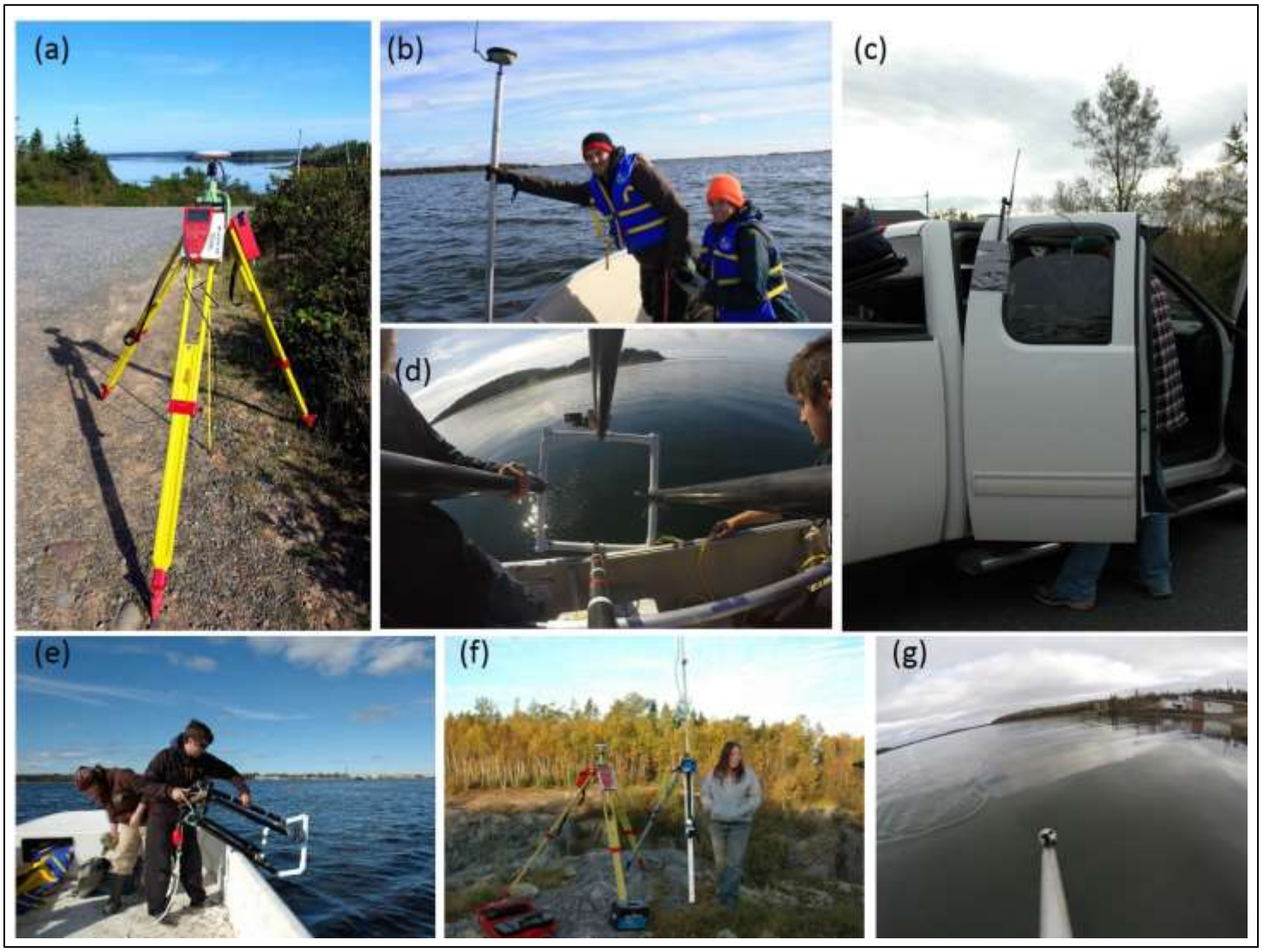

Figure 2.7: Ground truth images (a) GPS base station set up over benchmark at IM; (b) RTK GPS depth measurement using pole; (c) radio antenna mounted to truck for hard surface validation at MQ and SJA; (d,e) 0.5 m^2 quadrat being deployed;(f) base station set up at MQ; (g) GoPro camera mounted to pole being deployed for depth measurements and underwater photographs at IM.

2.3.1 Light and Pressure Sensors

The 2015 ground truth campaign also included the deployment of two sets of underwater light sensors and one pressure sensor. The light sensors were Onset HOBO Light and Temperature Pendant Sensors, which are wireless monitoring devices that can be deployed remotely for months at a time and will log data at user selected intervals. For this study two of the Hobo sensors were secured to a cinder block (Figure 2.7) and deployed at IMW and IMS (Figure 2.8), approximately two months prior to the lidar surveys (Table 2.2). The RTK pole was used to store the location of the sensor deployment, and a rope was attached to a second block which was deployed nearby, so that the equipment could be retrieved by dragging the anchor between the two GPS points. At IMW the elevation of the light sensors was -1.98 m CGVD28, while the IMS sensors were deeper at -3.53 m CGVD28 (elevations obtained from the lidar Digital Elevation Model, DEM). The light sensors were retrieved following the lidar surveys.

The Hobo light sensors measure ambient light rather than the narrower bandwidth of light that is available for biology, but they are inexpensive and provide data for research on how a water clarity in each study area responded to physical forcing such as wind speed and direction. The light sensor data are presented in Section 2.4.3.

A Hobo Onset Pressure sensor was deployed attached to the light sensor cinder block at IMS (Figure 2.7c). The pressure sensor recorded data from Sept. 23 until the battery failed on Nov. 10. The data were recorded to use in validating the Isle Madame hydrodynamic model and are presented in Section 2.4.2.

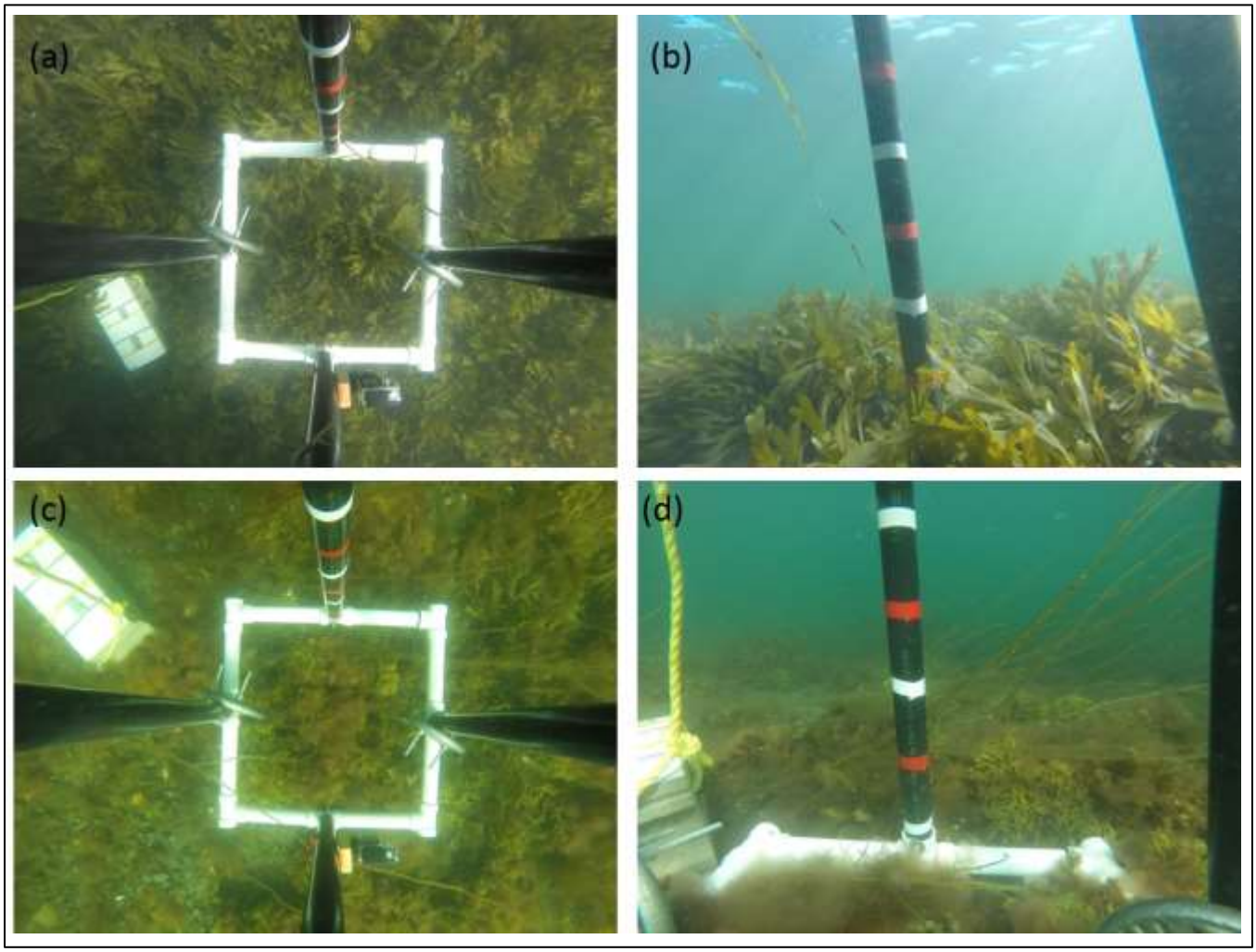

Figure 2.8: (a) Light sensors deployed at IMW; (b) location of light sensors deployed at IMW; (c,d) light sensors and pressure sensor deployed at IMS on Sept. 23, 2015, as photographed with the downward-facing (a,c) and side-facing (b,d) GoPro cameras on the 1 m^2 quadrat.

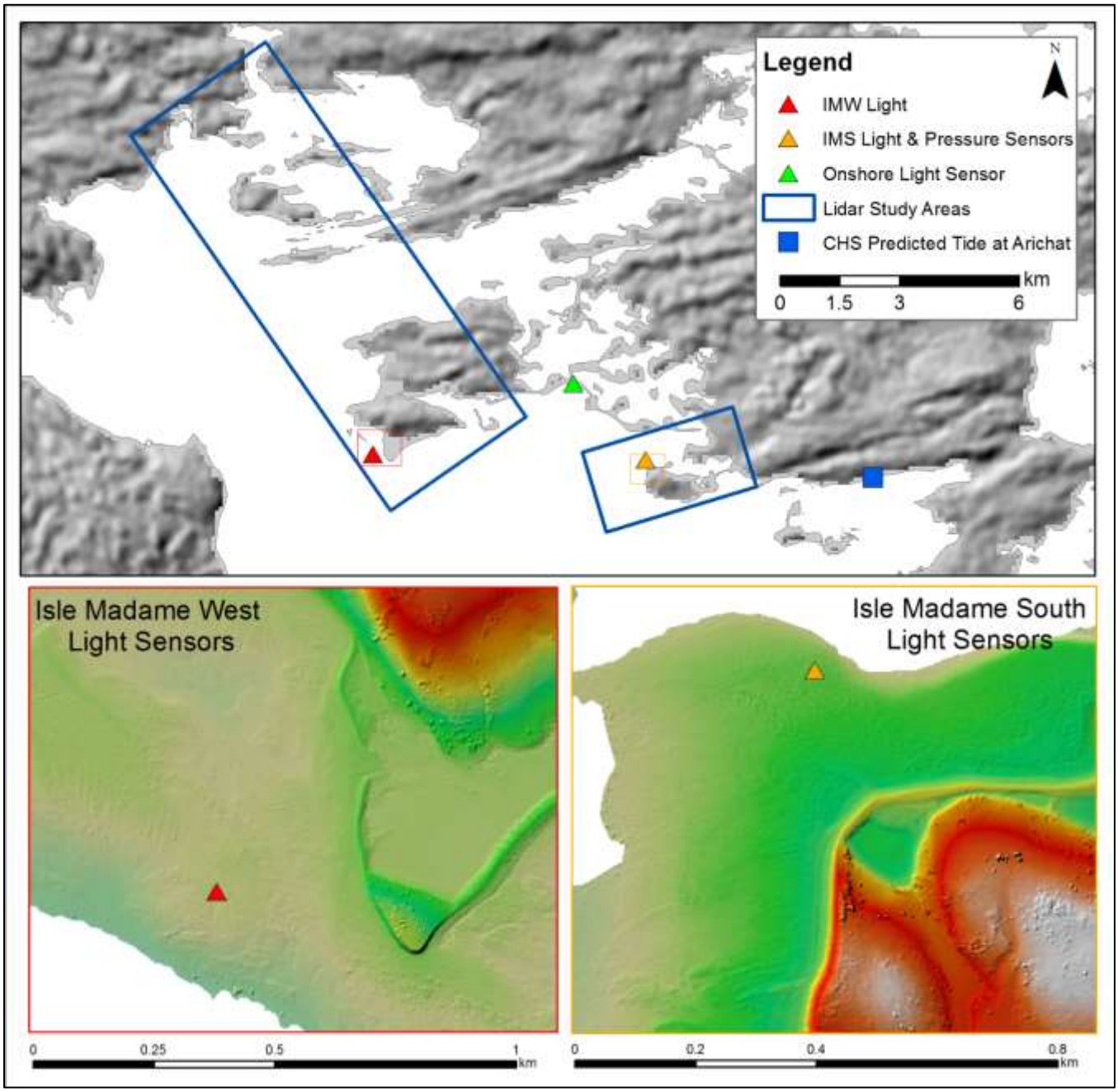

Figure 2.9: Location of underwater and onshore light sensors at Isle Madame. Red and orange boxes in the top panel refer to the zoomed in extents below. The bottom panels use colour shaded relief models of the DEMs, where red is higher elevation and green is lower elevation.

2.3.2 Vegetation and Bottom Cover Ground Truth

Figure 2.9 - Figure 2.11 show the locations of the underwater photographs collected at Isle Madame on Sept. 23 and Nov. 11. The photos were used to assign each photo location a value for percent eelgrass cover, based on the SeaGrassNet guidelines (http://www.seagrassnet.org/). A qualitative visual inspection of the photos was completed to assign a water quality metric to each photograph, where 0 was indicative of water with very low clarity, 0.5 indicated medium clarity, or somewhat clear, and a rating of 1 indicated the water at that location at the time of the photograph was very clear. The

figures show mainly clear water throughout the IMW and IMS study areas, and eelgrass found only in Figure 2.11 in the sheltered inner area away from the main channels.

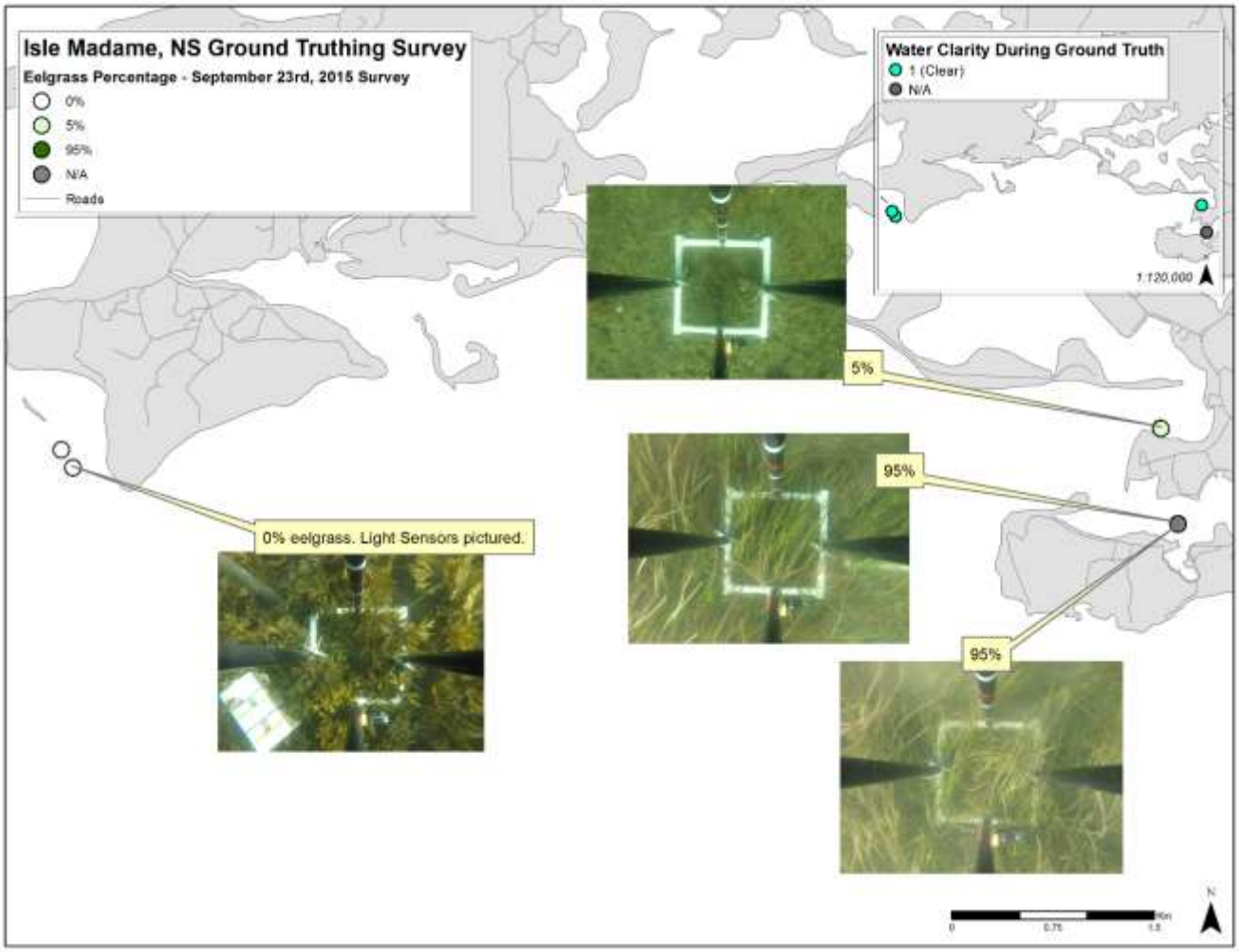

Figure 2.10: Ground truth data collected at Isle Madame on September 23, 2015 using the 1 m^2 quadrat showing different vegetation and bottom types. Eelgrass percent cover is represented colours of the symbols and was determined using the bottom photographs. The inset shows water clarity based on a visual inspection of the photographs.

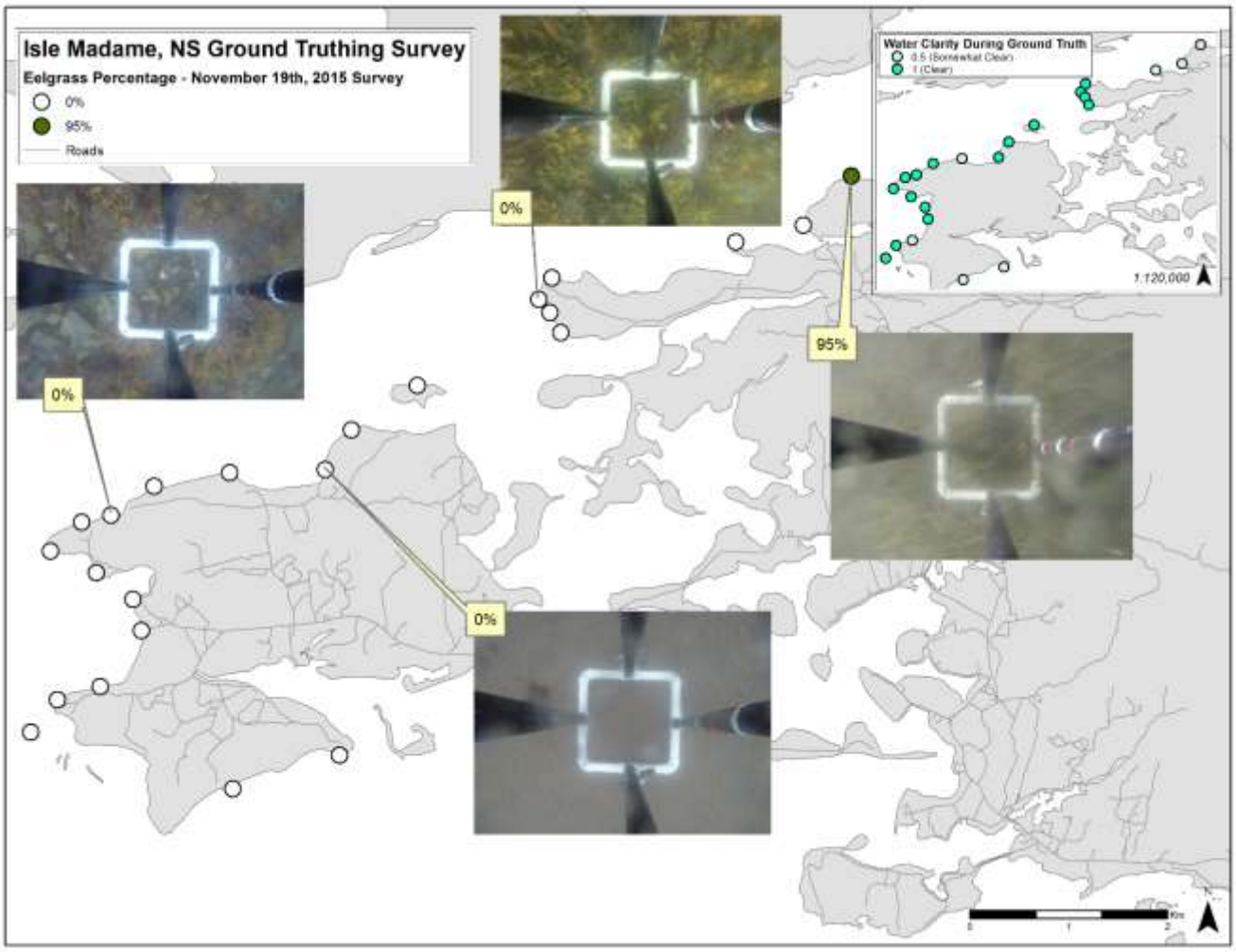

Figure 2.11: Ground truth data collected at Isle Madame on November 19, 2015 using the 0.5 m^2 quadrat showing different vegetation and bottom types. Eelgrass percent cover is represented colours of the symbols and was determined using the bottom photographs. The inset shows water clarity based on a visual inspection of the photographs.

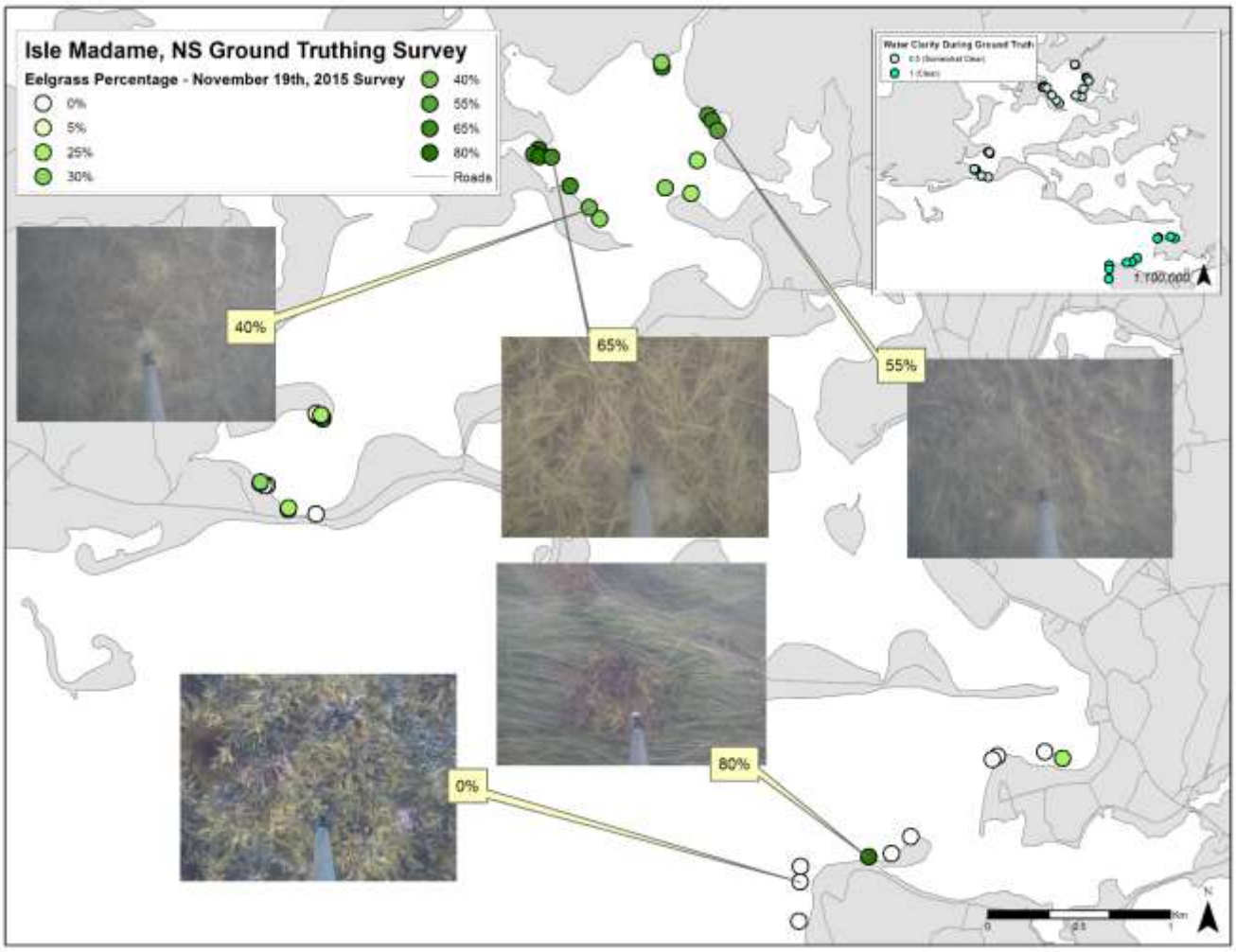

Figure 2.12: Ground truth data collected at Isle Madame on November 19, 2015 using the GoPro mounted on the pole showing different vegetation and bottom types. Eelgrass percent cover is represented colours of the symbols and was determined using the bottom photographs. The inset shows water clarity based on a visual inspection of the photographs.

2.4 Meteorological, Light and Tidal Conditions

2.4.1 Meteorology

Meteorological conditions during and prior to topo-bathy lidar data collection are an important factor in successful data collection. As the lidar sensor is limited by water clarity, windy weather has the potential to stir up any fine sediment in the water and prevent good laser penetration. Rainy weather is not suitable for lidar collection, and the glare of the sun must also be factored in for the collection of aerial photography. Before each lidar survey we monitored weather forecasts using a variety of forecasting websites (www.intellicast.com, www.windfinder.com, http://weather.gc.ca/marine/, http://weather.gc.ca/) as well as current and past conditions using the closest

Environment Canada (EC) weather station to the study sites. For Isle Madame the nearest EC weather station was Port Hawkesbury, and the EC Saint John station was used for the other study areas (Figure 1.1).

The wind was blowing at approximately 13 km/h from the northwest for the IMS survey following a day of >20 km/hr wind blowing predominantly from the northwest (Figure 2.12a). The survey at IMW was conducted with wind blowing at approximately 10 km/hr from the southeast, following several days of similar weather and a morning of especially low wind speed (Figure 2.12b).

Figure 2.13 shows the difficulty of finding a suitable time for airborne lidar surveying in late October and early November. Wind regularly exceeded 20 km/hr and in late October an event occurred with wind speeds > 40 km/hr. Wind speed was relatively low during the Campobello Island and Grand Manan survey, blowing at approximately 12 km/hr from the NW; however, wind was strong on the days preceding the survey (northwest 20 - 30 km/hr) and stirred sediment up into the water column may not have had time to settle by Oct. 27. The Saint John weather station recorded several 30 km/hr wind events between Nov. 7 – 10. Unfortunately, these events coincided with the lidar surveys at Saint John Approach, and the two surveys at Musquash. The wind was blowing from the northwest during the SJA and MQ1 surveys, but the wind had rotated to a southwestern wind for the second Musquash survey (Figure 2.13). The role that these wind events played on water clarity and lidar penetration is discussed in Section 3.2 with the lidar results.

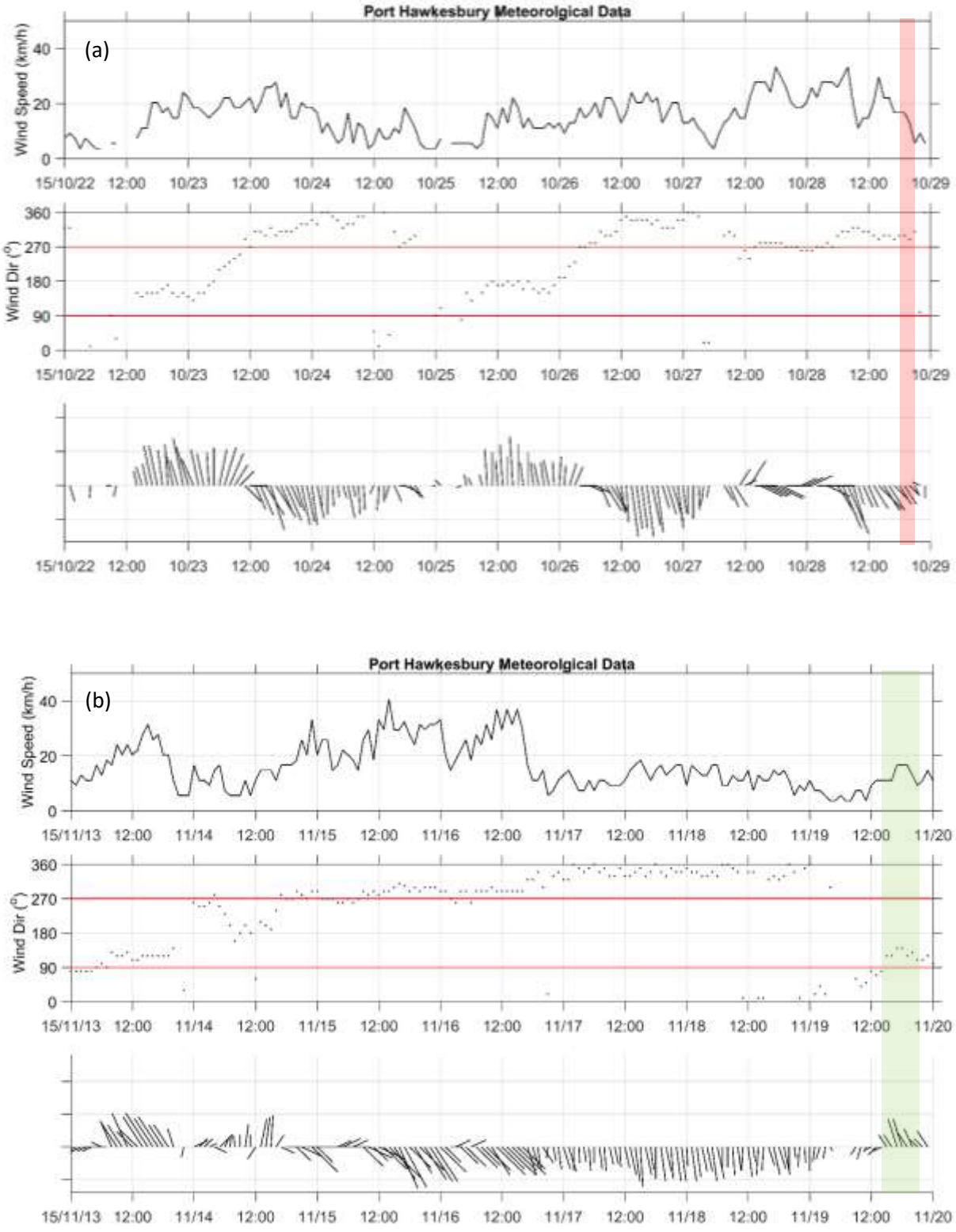

Figure 2.13: Wind speed (top panel) and direction (middle panel) collected at the EC weather station at Port Hawkesbury. The lower panel shows a vector plot of the wind, where the arrows point in the direction the wind is blowing. The lidar surveys are indicated by the red (IMS) and green (IMW) boxes. Panel (a) shows October 22 and 29, 2015 at 1 hour intervals; panel (b) shows November 13 and 20, 2015.

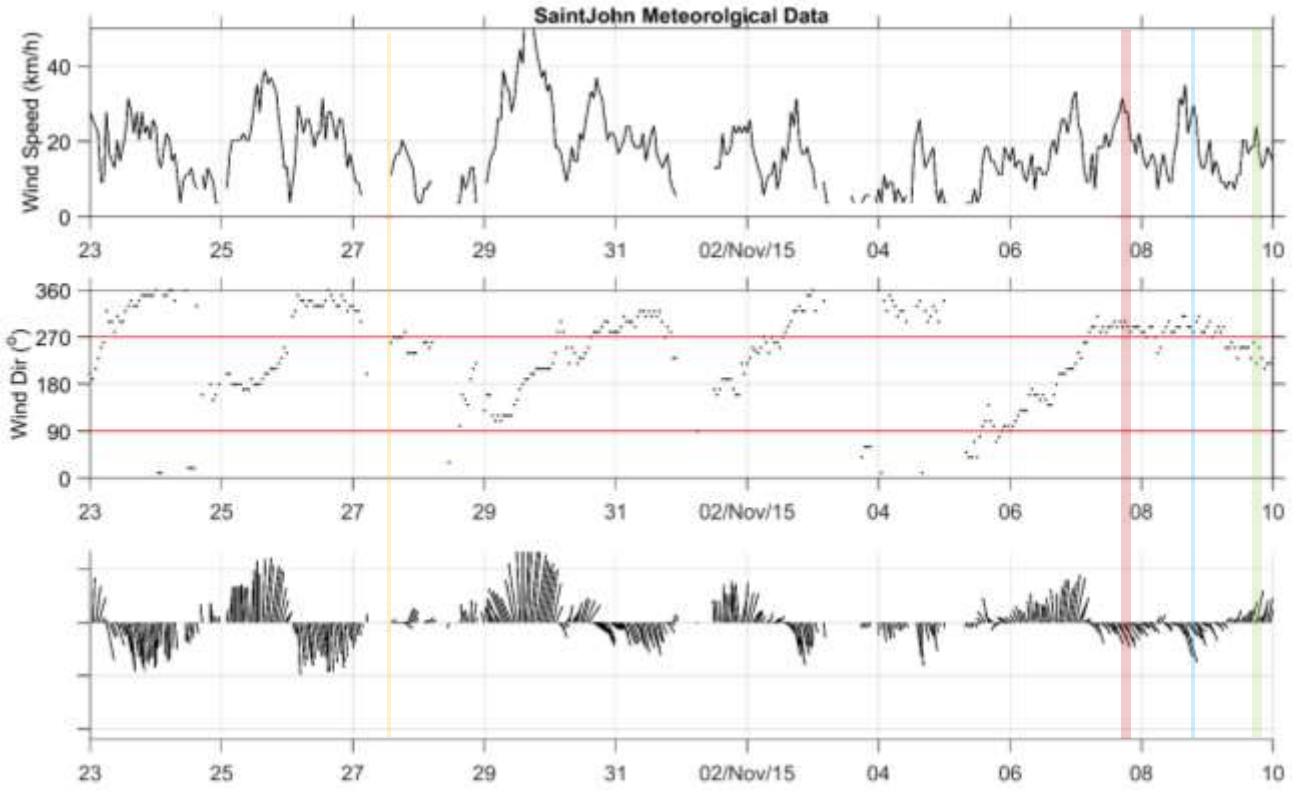

Figure 2.14: Wind speed (top panel) and direction (middle panel) collected at the EC weather station at Saint John, NB between October 23 and November 10, 2015 at 1 hour intervals. The lower panel shows a vector plot of the wind, where the arrows point in the direction the wind is blowing, and the boxes indicates the lidar surveys (yellow = CAMP, GM, red = SJA, blue = MQ Survey 1, green = MQ Survey 2).

2.4.2 Tide

Optimal data collection is a balance not only of water clarity and meteorological conditions, but also of daylight and tidal stage. The surveys were completed as near to low tide as weather and daylight permitted in order to reduce the amount of water that the laser was required to penetrate through in order to reach the seabed (Figure 2.14, Figure 2.15). Low tide surveys were possible everywhere except Campobello Island (Figure 2.14a) and Isle Madame West (Figure 2.15c).

The pressure sensor was recovered from IMS on Nov. 19 and the water level was shifted by -3.53 m to be representative of the elevation of the water surface in CGVD28. Canadian Hydrographic Survey (CHS) predicted tides at Arichat, NS were shifted by -0.7 m to represent CGVD28 (Figure 2.7). Note that the CHS data was 0.3 m less than the shift suggested by CHS to convert from Chart Datum to CGVD28 because the mean water level using the -1.0 m conversion was unusually low (-0.14 m). The value of 0.7 m was chosen empirically and gave a mean water level of 0.16 m, which agreed well with the mean water level of the observed data (0.23 m). Once both data sets were in CGVD28 they agreed well during the deployment, and during the IMS survey (Figure 2.15b); however, the sensor failed on Nov. 10 at 1:15 UTC, and did not collect water level data during the IMW survey (Figure 2.15c).

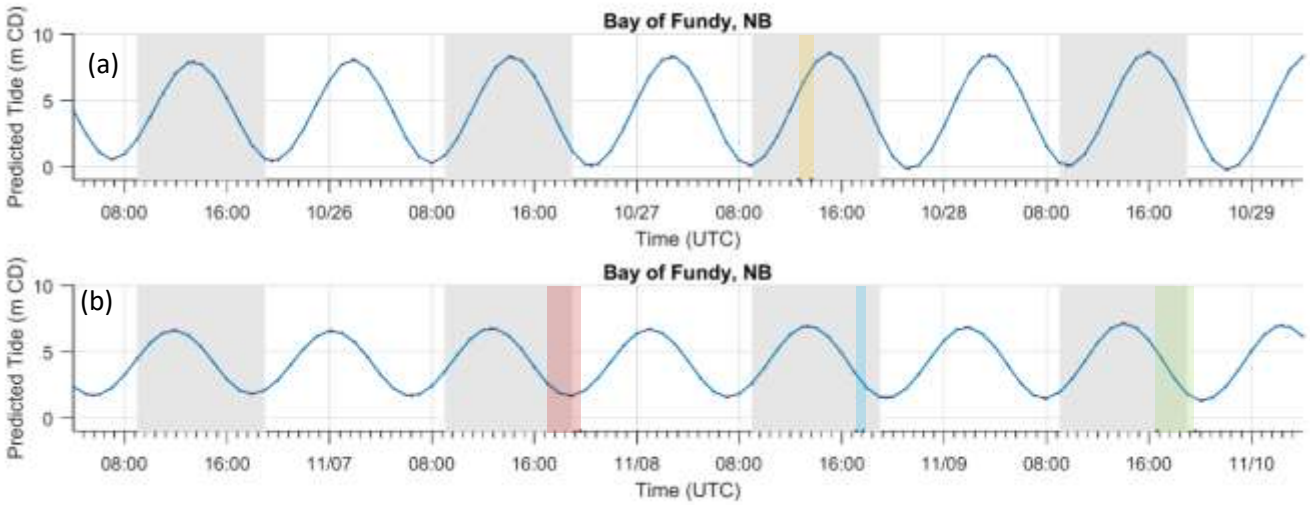

Figure 2.15: Tides for surveys at Saint John (a) October 25-29; (b) November 6 -10. Grey bars indicate daylight hours and coloured boxes indicate survey durations (orange = CAMP, GM, red = SJA, blue = MQ Survey 1, green = MQ Survey 2).

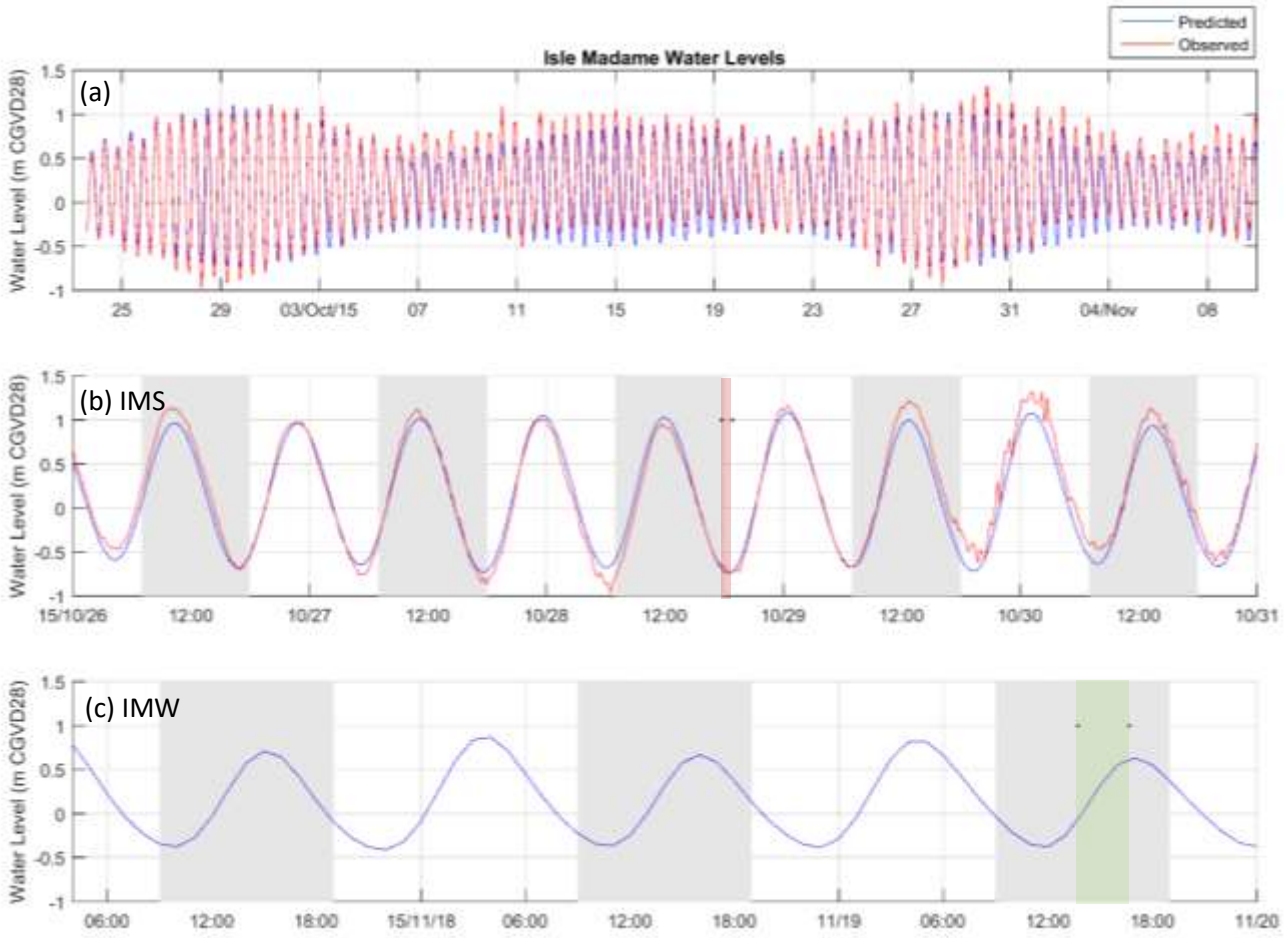

Figure 2.16: Comparison of tides predicted for Arichat, NS, by CHS and observed water level at the cinder block deployed in IMS for (a) Sept. 23- Nov. 10; (b) Oct. 26- Oct 31 with the IMS lidar survey indicated by the red box; (c) Nov. 17 – Nov. 20, with the IMW survey indicated by the green box. Grey bars indicate approximate daylight hours.

2.4.3 Light

The light sensor measures ambient light in units of Lux (lumens m^{-2}). The sensors were calibrated prior to deployment by mounting all sensors in direct sunlight for 250 minutes and grouping them based on similar readings after the calibration trial. The percent of underwater light was calculated to remove the effects of variations in cloud cover using the following equation:

$$\%\ UW\ light = 100 \times \frac{UW\ light}{OS\ light}$$

where UW = underwater and OS=onshore. Figure 2.16 shows the variations in light due to water clarity and tide at IMW and IMS; note the difference in y-axis at each study site. The light data were filtered using a median filter with a 1-hour sampling window, and the two sensors at each study location were averaged.

Figure 2.16 shows % UW light for IMW and IMS. At IMW, the elevation of the light sensors was -1.98 m CGVD28, which relates to ~1 m absolute depth at low tide and ~3 m absolute depth at high tide, and typically less than 10% of sunlight available at the surface reached the sensors. Near the later part of the deployment, this value was closer to 5%, but biofouling was not present on the sensor upon recovery, so likely the effects of different tidal cycles and wind events were responsible for the decrease in light levels. Maximum % UW light during the day of the lidar survey was ~6% (Figure 2.16b).

At the IMS sensors were deployed in deeper water at -3.53 m CGVD28, which relates to ~2.5 m absolute depth at low tide and ~4.5 m absolute depth at high tide. Figure 2.16a and c show that the IMS sensor recorded high light levels initially, but decreased to 0 shortly after deployment, and did not record any light during the lidar survey.

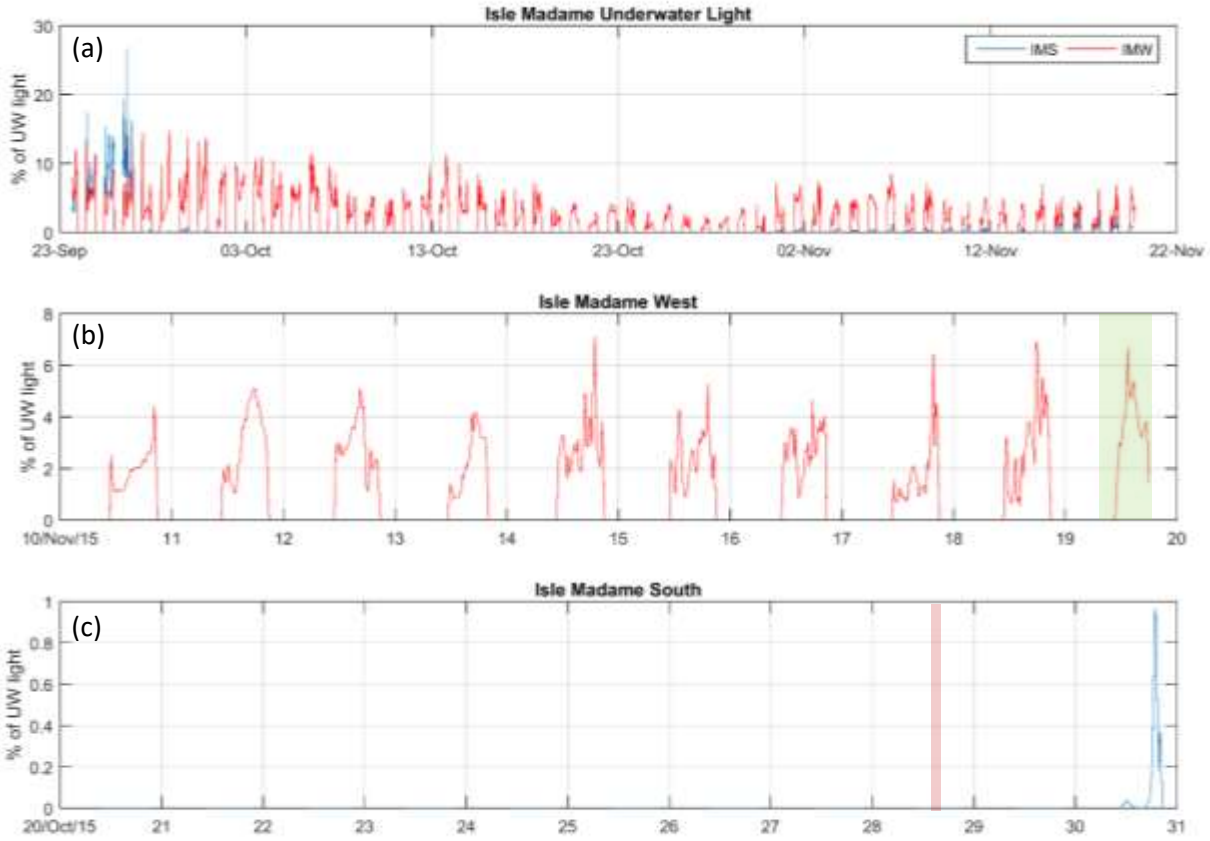

Figure 2.17: Light sensor data at (a) IMW and IMS; (b) IMW (survey duration indicated by green box); (c) IMS survey duration indicated by red box. The % of underwater light is underwater light divided by onshore light. The IMS sensor recorded very little light during the deployment time.

2.5 Elevation Data Processing

2.5.1 Lidar processing

2.5.1.1 Point Cloud Processing

Once the GPS trajectory was processed for the aircraft utilizing the GPS base station and aircraft GPS observations and combined with the inertial measurement unit, the navigation data was linked to the laser returns and georeferenced. Lidar Survey Studio (LSS) software accompanies the Chiroptera II sensor and is used to process the lidar waveforms into discrete points. The data can then be inspected to ensure there was sufficient overlap (30%) and no gaps exist in the lidar coverage.

One critical step in the processing of bathymetric lidar is the ability to map the water surface. This is critical for two components of georeferencing the final target or targets that the reflected laser pulse recorded: the refraction of the

light when it passes from the medium of air to water and the change in the speed of light from air to water. The LSS software computes the water surface from the lidar returns of both the topo (TD) and hydro (HD) lasers. In addition to classifying points as land, water surface or bathymetry, the system also computes a water surface that ensures the entire area of water surface is covered regardless of the original lidar point density. As mentioned, part of the processing involves converting the raw waveform lidar return time series into discrete classified points using LSS signal processing; points include ground, water surface, seabed, etc. Waveform processing may include algorithms specifically for classifying the seabed. The points were examined in LSS both in plan view and in cross-section view. The waveforms can be queried for each point so that the location of the waveform peak can be identified and the type of point defined, for example water surface and bathymetry.

Terrascan was utilized to further classify and filter the lidar point cloud. Because of the differences in the lidar footprint between the TD and HD sensors (TD footprint has a 0.15 m and HD footprint a 2.1 m diameter on the ground) it was decided that the HD lidar point returns were used to represent the water surface and bathymetry points and the TD lidar points would be used to represent targets above ground. The total point cloud that utilized both sensors was processed in Terrascan where the ground was classified and erroneous points both above and below the ground were defined. See Table 2.3 or the Data Dictionary that has been delivered as a separate document for the classification codes for the delivered LAS files.

Table 2.3. Lidar point classification Codes and descriptions. Note that 'overlap' is determined for points which are within a desired footprint of points from a separate flight line; the latter of which having less absolute range to the laser sensor.

Class number	Description
0	Water model
1	Bathymetry (Bathy)
2	Bathy Vegetation
3	N/A
4	Topo laser (TD) Ground
5	TD non-ground (vegetation & buildings)
6	Hydro laser (HD) Ground
7	HD non-ground
8	Water
9	Noise
10	Overlap Water Model
11	Overlap Bathy
12	Overlap Bathy Veg
13	N/A
14	Overlap TD Ground
15	Overlap TD Veg

16	Overlap HD Ground
17	Overlap HD Veg
18	Overlap Water
19	Overlap Noise

2.5.1.2 Gridded Surface Model

There are three main data products derived from the lidar point cloud. The first two are based on the elevation and include the Digital Surface Model (DSM) which incorporates valid lidar returns from vegetation, buildings, ground and bathymetry returns, and the Digital Elevation Model (DEM) which incorporates ground returns above and below the water line. The third data product is the intensity of the lidar returns, or the reflectance of the HD lidar. The lidar reflectance, or the amplitude of the returning signal from the HD laser, is influenced by several factors including water depth, the local angle of incidence with the target, the natural reflectivity of the target material, and the voltage or gain of the transmitted lidar pulse.

The original reflectance data are difficult to interpret because of variances as a result of water depth and loss of signal due to the attenuation of the laser pulse through the water column at different scan angles, as well as lack of bottom reflectivity.

2.5.1.3 Depth Normalization of the Green Laser

The amplitude of the returning signal from the bathy laser provides a means of visualizing the seabed cover, and is influenced by several factors including water depth and clarity, the local angle of incidence with the target, the natural reflectivity of the target material, and the voltage or gain of the transmitted lidar pulse. The raw amplitude data are difficult to interpret because of variances as a result of signal loss due to the attenuation of the laser pulse through the water column at different scan angles. Gridding the amplitude value from the bathy laser results in an image with a wide range of values that are not compensated for depth and have significant differences for the same target depending on the local angle of incidence from flight line to flight line. As a result, these data are not usable as is for quantitative analysis and are difficult to interpret for qualitative analysis. We have designed a process to normalize the amplitude data for signal loss in a recent publication (Webster et al., 2016). The process involved sampling the amplitude data from a location with homogeneous seabed cover (e.g., sand or eelgrass) over a range of depths. These data were used to establish a relationship between depth and the logarithm of the amplitude value. The inverse of this relationship was used with the depth map to adjust the amplitude data so that they could be interpreted without the bias of depth. A depth normalized amplitude/intensity image (DNI) was created for each study site using this technique that can be more consistently interpreted for the seabed cover material. Note that this analysis considers only bathymetric lidar values and ignores any topographic elevation points.

2.5.1.4 Aerial Photo Processing

The RCD30 60 MPIX imagery was processed using the aircraft trajectory and direct georeferencing. The low altitude and high resolution of the imagery required that the lidar data be processed first to produce bare-earth DEMs that were used in the orthorectification process. The aircraft trajectory, which blends the GPS position and the IMU attitude information into a best estimate of the overall position and orientation of the aircraft during the survey. This trajectory, which is linked to the laser shots and photo events by GPS based time tags, is used to define the Exterior Orientation (EO) for each of the RCD30 aerial photos that were acquired. The EO, which has traditionally been calculated by selecting ground control point (x, y, and z) locations relative to the air photo frame and calculating a bundle adjustment, was calculated using direct georeferencing and exploiting the high precision of the navigation system. The EO file defines the camera position (x, y, z) for every exposure as well as the various rotation angles about the x, y and z axis known as omega, phi and kappa. The EO file along with a DEM can be used with the aerial photo to produce a digital orthophoto. After the lidar data were processed and classified into ground points, the lidar-derived DEM (above and below the water line) was used in the orthorectification process in Erdas Imagine software and satisfactory results were produced.

2.5.2 Ellipsoidal to Orthometric Height Conversion

The original elevation of any lidar products are referenced to the same elevation model as the GPS they were collected with. This model is a theoretical Earth surface known as the ellipsoid, and elevations referenced to this surface are in ellipsoidal height. To convert them to orthometric height (OHt), which is height relative to the Canadian Geodetic Vertical Datum of 1928 (CGVD28), an offset must be applied. The conversions are calculated based on the geoid-ellipsoid separation model, HT2, from Natural Resources Canada.

2.6 Lidar Validation

Ground elevation measurements obtained using the RTK GPS system were used to validate the topographic lidar returns on areas of hard, flat surfaces. At IMW, IMS, SJA and MQ the GPS antenna was mounted on a vehicle and data were collected along roads within the study areas.

Boat-based ground truth data were used to validate the bathymetric lidar returns at Isle Madame only. Although various methods were used to measure depth during fieldwork, only points measured using the large pole fitted with the RTK GPS antenna to directly measure the seabed were used for the accuracy assessment; points that measured depth using sonar or a weighted rope were not considered.

For both hard surface and boat-based GPS points, the differences in the GPS elevation and the lidar elevation (ΔZ) were calculated by extracting the lidar elevation from the DEM at the waypoint and subtracting it from the GPS elevation (GPS - DEM). GPS points were subject to a quality control assessment such that the standard deviations of the Easting, Northing, and elevation were required to be < 0.05 m.

2.7 Hydrodynamic Modelling

A high-resolution 2-D hydrodynamic (HD) model was developed using the DHI Mike-21™ software module to simulate current flow and water level variations within the Isle Madame study area. The Mike software includes the capability to simulate the transport and face of dissolved and suspended substances discharged or accidentally spilled in the region. The model domain was designed to be much larger than the lidar study areas in order to properly model the circulation in the region from the mouth of Chedabucto Bay into the complex shoreline near Isle Madame and up the Strait of Canso as far as the Canso Causeway (Figure 2.17). Model inputs included bathymetry and boundaries, these are described in the following sections.

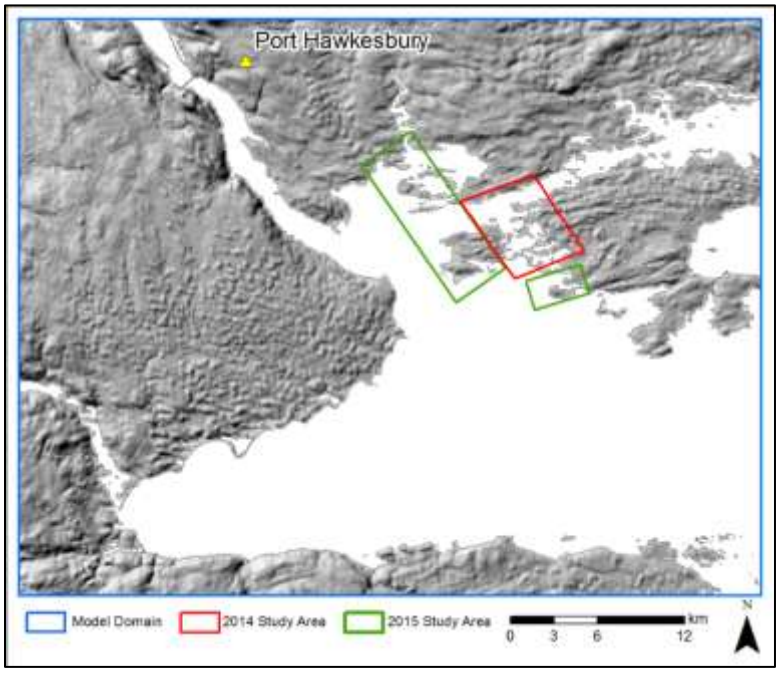

Figure 2.18: Mike 21 hydrodynamic model domain.

2.7.1 Model Grid

A variety of sources and resolutions of topography and bathymetry were required in order to complete the model depth grid (Table 2.4, Figure 2.18). The finest resolution dataset was the lidar data surveyed by AGRG in 2014 and 2015, which was sampled up to 3 m resolution for computational efficiency. Other bathymetry data included a digital compilation of bathymetry data from various sources (e.g. multibeam, single beam, seismic, etc.) aggregated by CHS (Varma et al., 2008) at between 5 and 20 m resolution; paper chart 4335 (scale 1:75,000) was purchased and digitized manually and chart 4307 (scale 1:37,500) was purchased as an Electronic Navigational Chart (ENC). A 20 m resolution database from the Nova Scotia Dept. of Natural Resources was used for topography not included in the lidar dataset.

Provider	Source	Resolution	Domain	Observations
AGRG	Lidar	3 m	Topo/Bathy	7.3×10^9
NSDNR	Rasterized 1:10 000 Contour Data	20 m	Topo	2.5×10^9

CHS	Multibeam	5 m	Bathy	990,000
CHS	Multibeam	20 m	Bathy	76,000
CHS	Chart Soundings	Variable	Bathy	6,100

Table 2.4: HD model bathymetric data sources, resolution, domain and number of observations. NSDNR: Nova Scotia Department of Natural Resources.

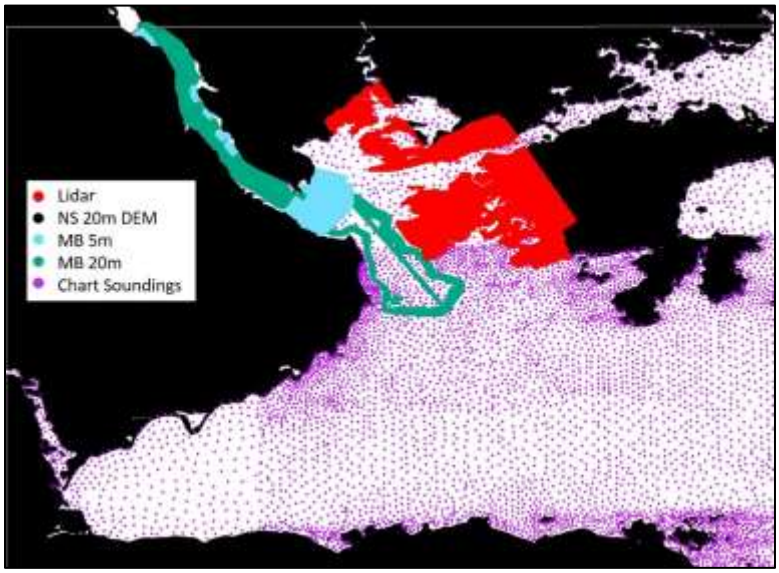

Figure 2.19: Sources of model topographic and bathymetric data.

The bathymetric and topographic datasets were merged separately using a spline interpolation algorithm to fill gaps in the different resolution datasets to create two continuous surface elevation rasters; these two rasters were then seamlessly merged with topographic elevation data (Figure 2.19). The spline interpolation technique ensured a smooth elevation surface despite the coarse and irregular point spacing of the different datasets. A nested grid model approach was used to reduce the calculations required by the model. The elevation grid was re-gridded at four different resolutions using a 3:1 resolution step Table 2.5: Nested model domains as shown in Figure 2.19.

Domain	Resolution (m^2)
A	243
B	84
C	27
D	9

Table 2.5: Nested model domains as shown in Figure 2.19.

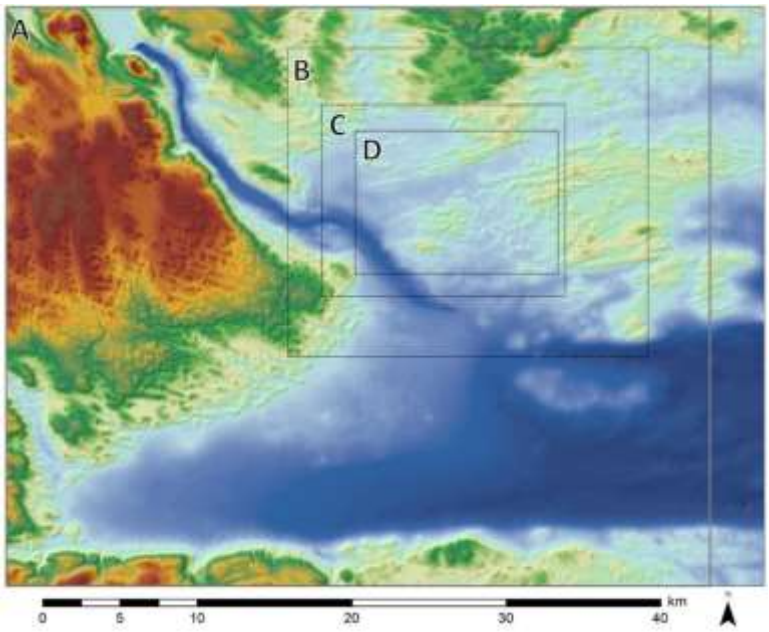

Figure 2.20: Model grid and nested model domains.

2.7.2 Boundaries

The model simulated water level variations over the interpolated bathymetry surface in response to a forcing tidal boundary condition at three different locations. Boundary A was located at the Canso causeway, and boundaries B and C were located at the eastern extent of Chedabucto Bay (Figure 2.20). Boundary A was not forced with any water level variations, and boundary conditions B and C were predicted tidal elevations at 15-minute resolution extracted from the ocean tidal predictions from the global tidal model supplied by DHI.

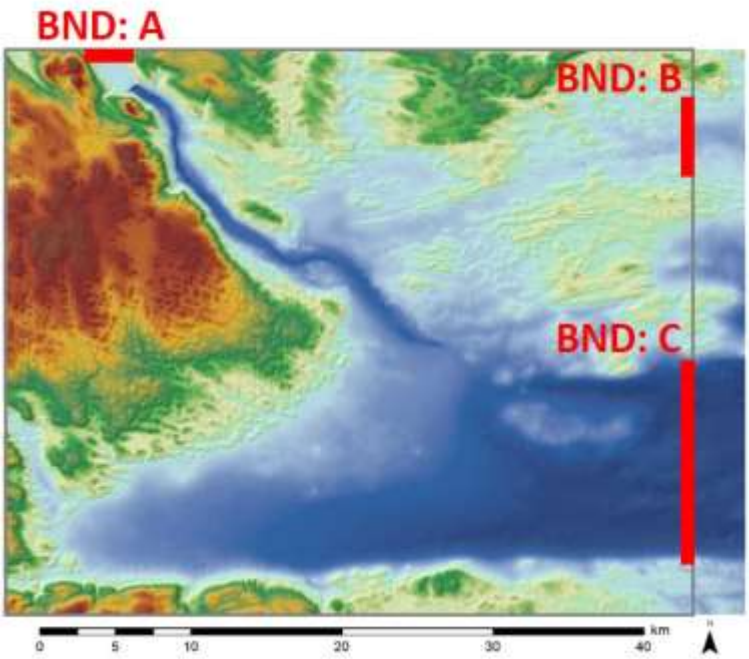

Figure 2.21: Model boundary locations.

3 Results

3.1 Lidar Validation

3.1.1 Topographic Validation

At Isle Madame there were 4658 data points collected along the roads and wharves and mean ΔZ was -0.037 m ± 0.035 m (Figure 3.1); at SJA there were 2739 data points collected along the roads and mean ΔZ was -0.087 m ± 0.038 m (Figure 3.2); at MQ there were 2113 data points collected along the roads, mean ΔZ was -0.049 m ± 0.029 m (Figure 3.3). These values are all within the expected range of accuracy for the lidar system.

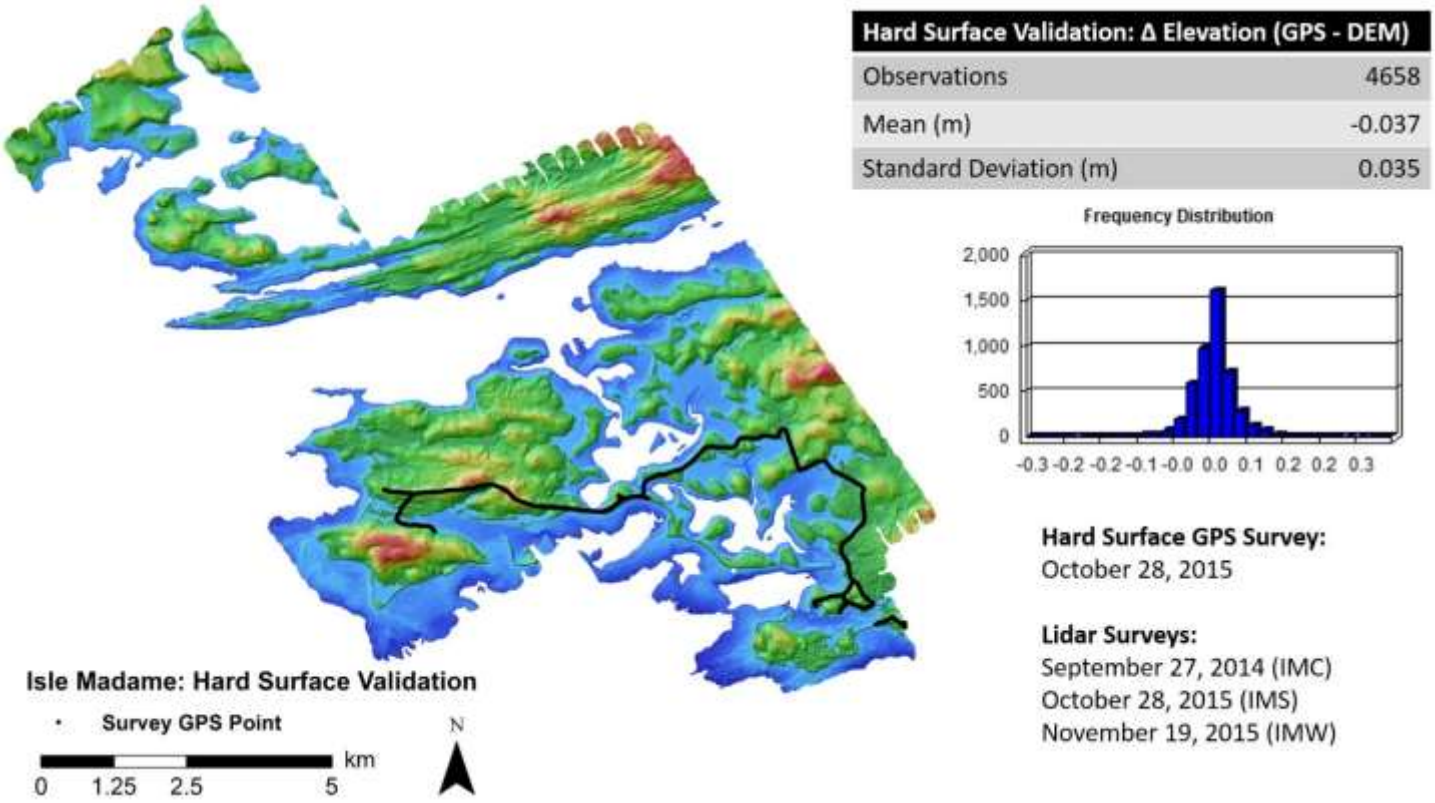

Figure 3.1 Hard surface validation at Isle Madame. Mean ΔZ was 0.04 m.

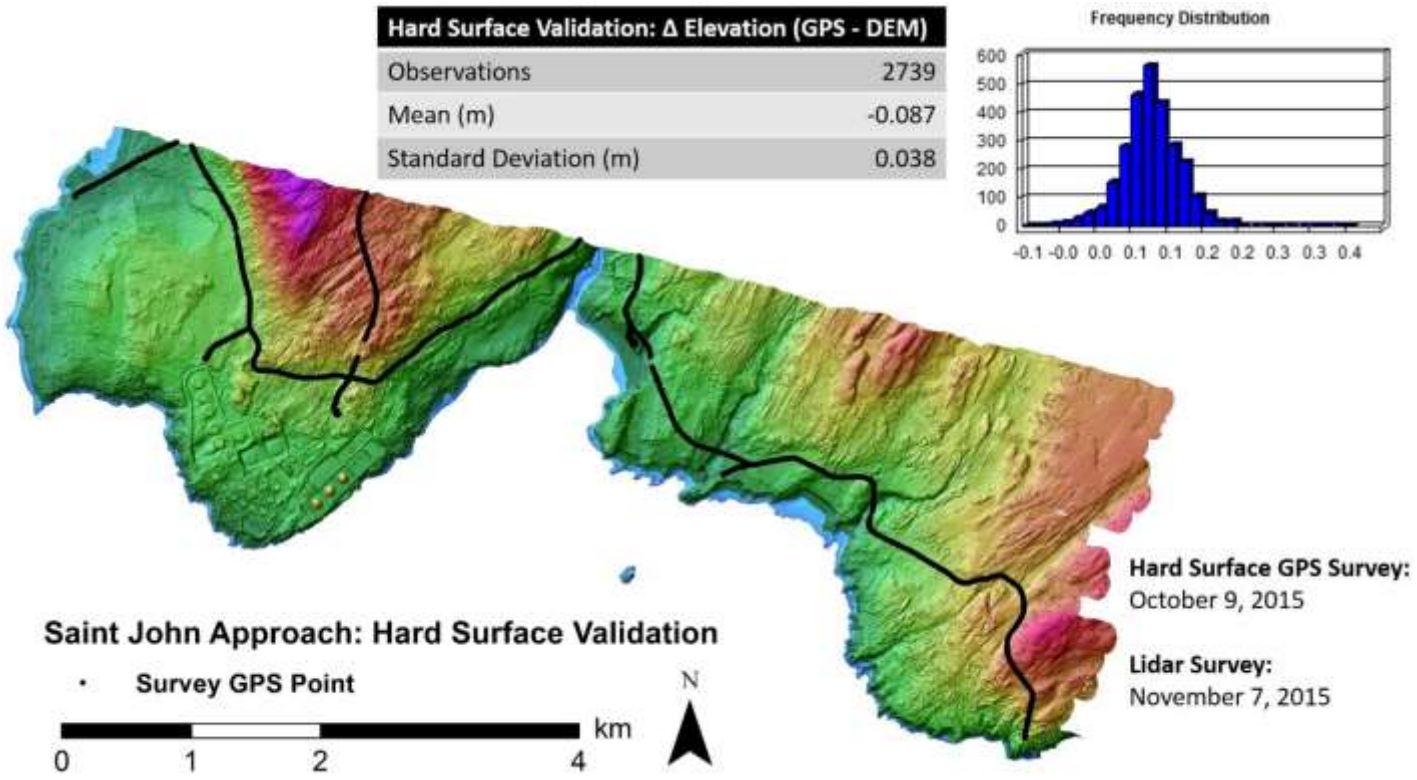

Figure 3.2: Hard surface validation at Saint John Approach. Mean ΔZ was -0.087 m.

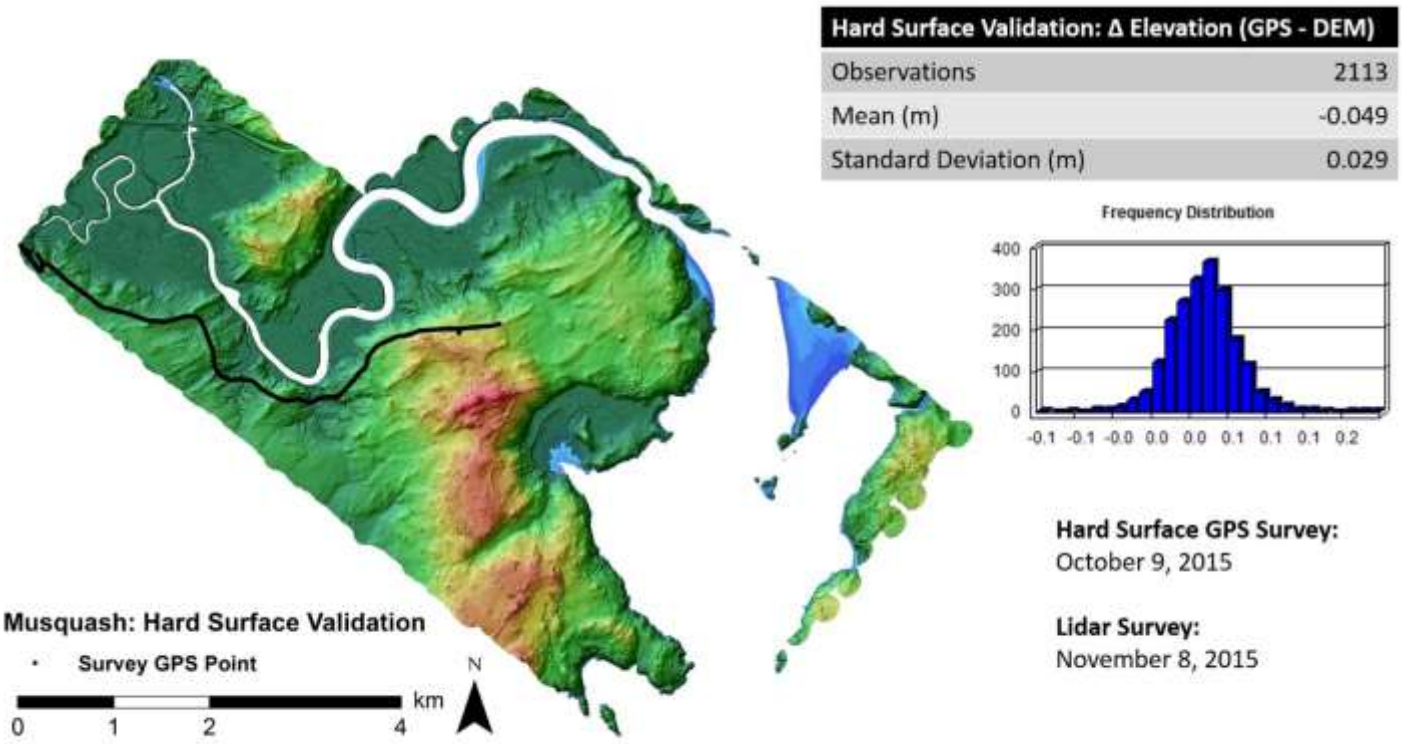

Figure 3.3: Hard surface validation at Musquash. Mean ΔZ was -0.05 m.

3.1.2 Bathymetric Validation

It was only possible to obtain bathymetric ground truth measurements for Isle Madame. For this analysis only data points obtained using the big pole with the GPS antenna threaded on it are considered; sources of error with measurements obtained using handheld code-based GPS or rope depth measurements are too great to include in the error analysis. At Isle Madame, there were 37 depth measurements; when compared to the lidar elevations the mean ΔZ was -0.19 m ± 0.102 m (Figure 3.4).

In areas where the seabed was vegetated, the lidar elevation was on average 0.21 m higher than the GPS elevations, suggesting that the laser was not penetrating through the vegetation down to the seabed. In areas where the bottom was not vegetated, the lidar elevation was on average 0.10 m higher than the seabed.

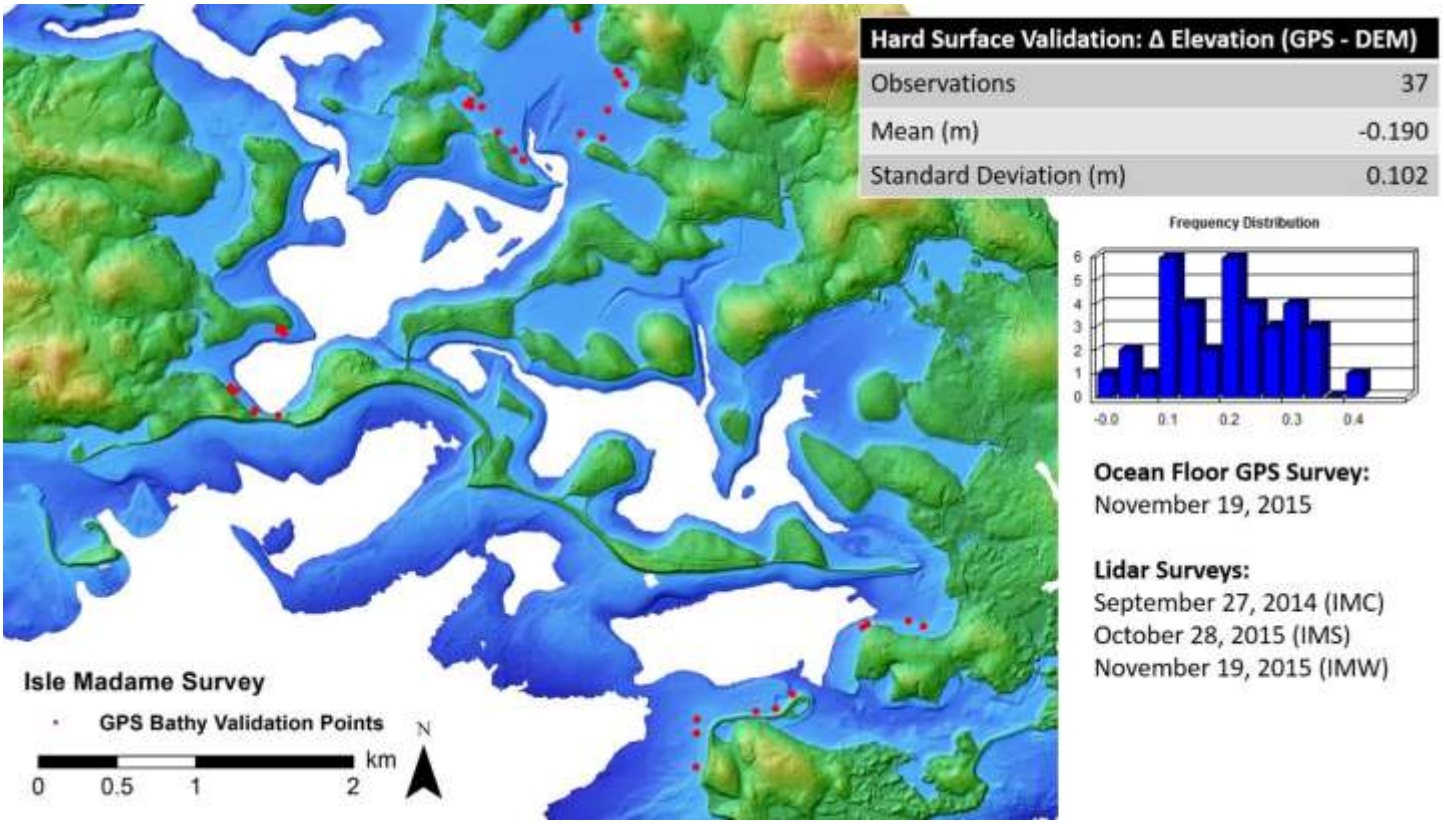

Figure 3.4: Bathymetric validation at Isle Madame

3.2 Surface Models

3.2.1 Digital Elevation Models

The lidar penetration in the study areas ranged from a maximum of -12 m at IMS, -11 m at IMW and SJA, -10 m at the SW Bay of Fundy strip, ~-8 m at GM, ~-6 m at CAMP, and ~ -3 m at MQ where the sediment-rich water prevented further penetration (all elevations in CGVD28). Figure 3.5 through Figure 3.10 present the DEMs for each study area.

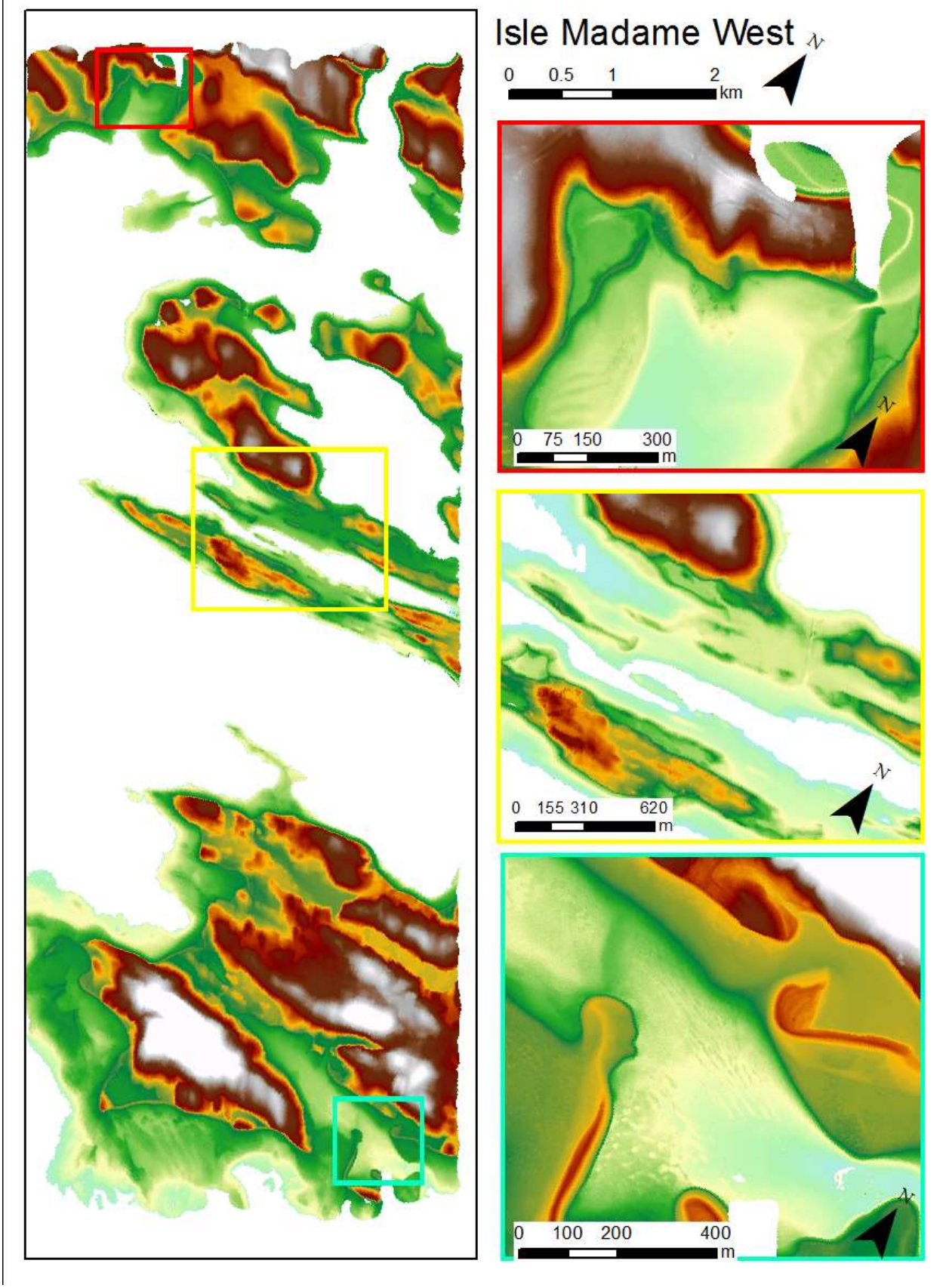

Figure 3.5: DEM for Isle Madame West showing the whole study area, and insets beside which are matched to the larger figure by border colour. Maximum lidar penetration was -11 m CGVD28.

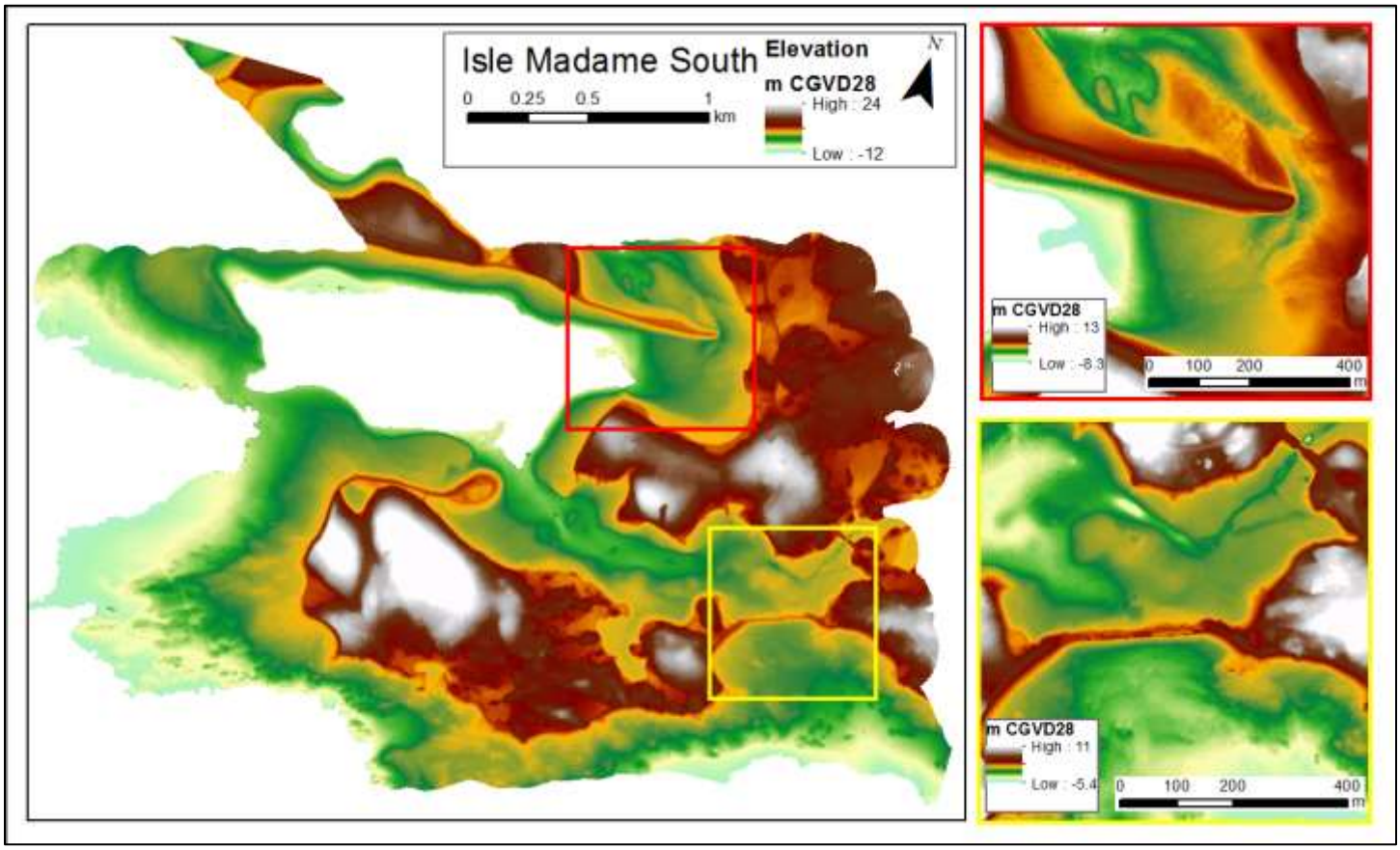

Figure 3.6: DEM for Isle Madame South showing the whole study area, and insets beside which are matched to the larger figure by border colour. Maximum lidar penetration was -12 m CGVD28.

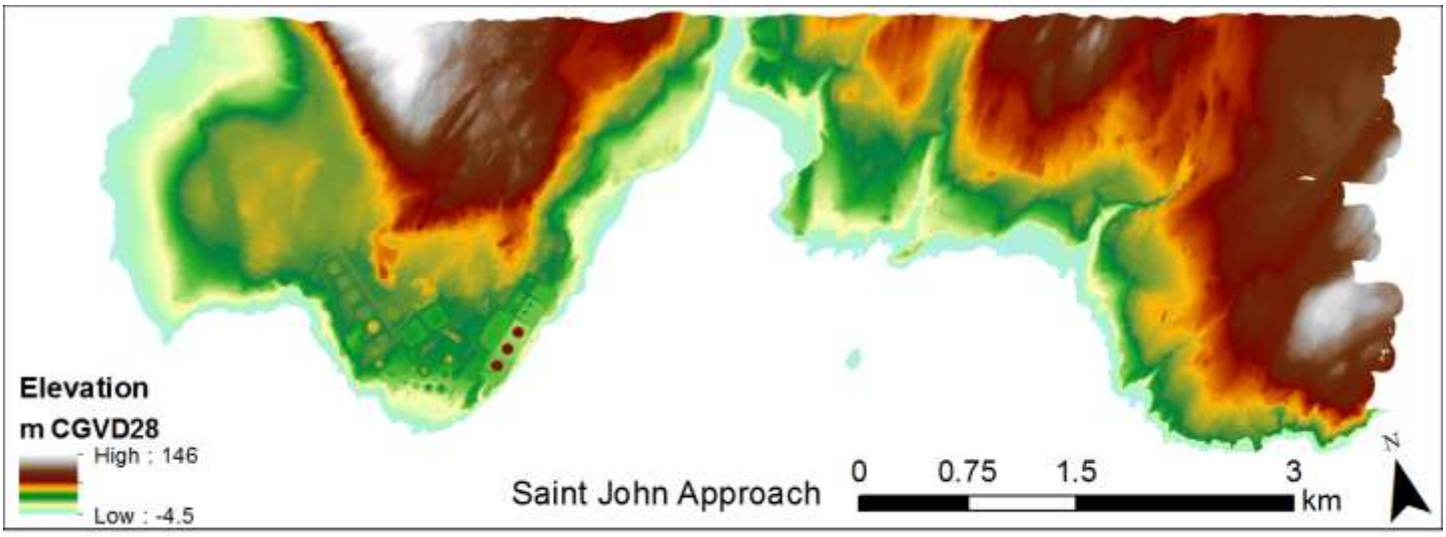

Figure 3.7: DEM for Saint John Approach showing the whole study area. Maximum lidar penetration was -4.5 m CGVD28.

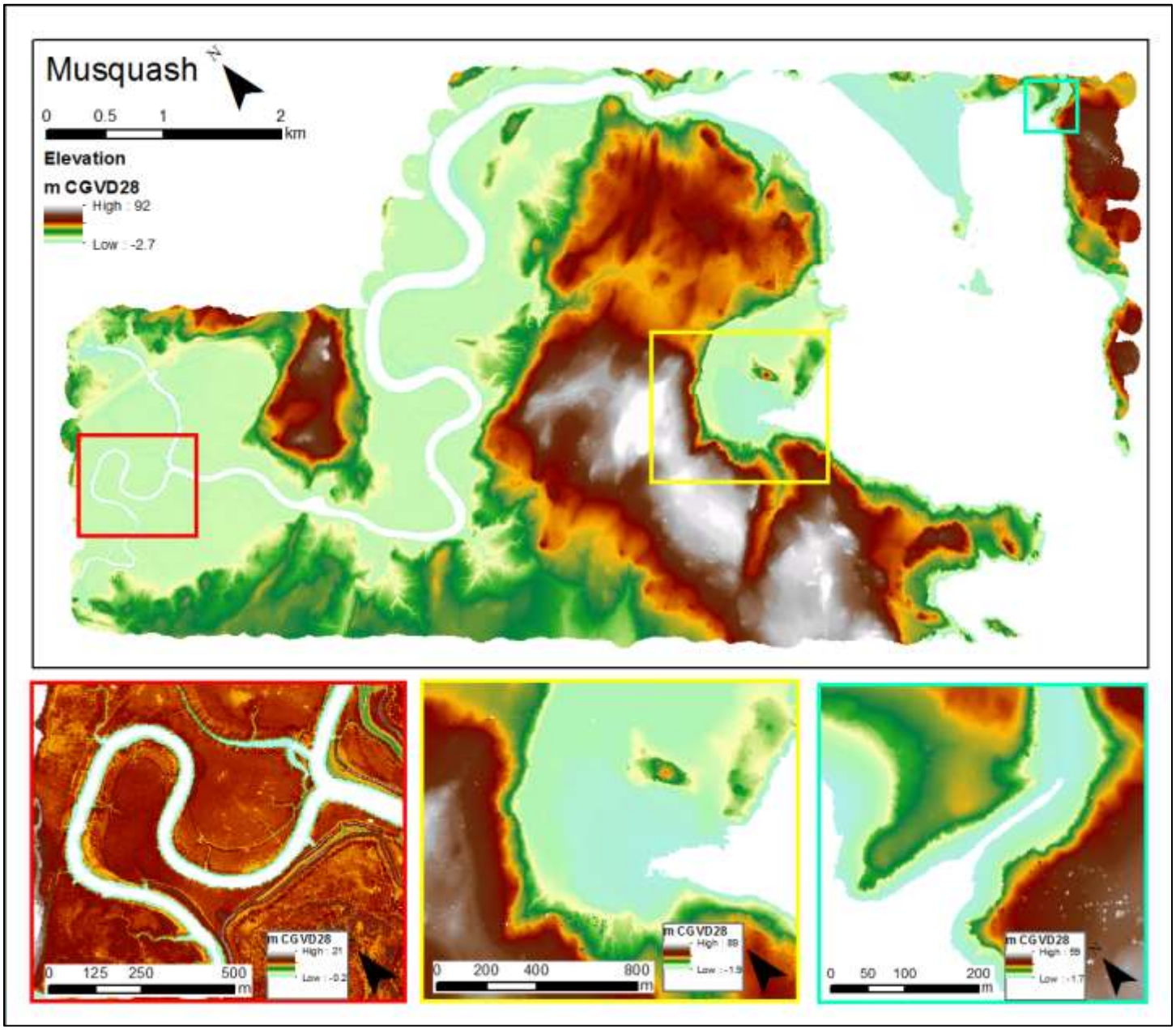

Figure 3.8: DEM for Musquash Approach showing the whole study area, and insets below which are matched to the larger figure by border colour. Maximum lidar penetration was -2.7 m CGVD28.

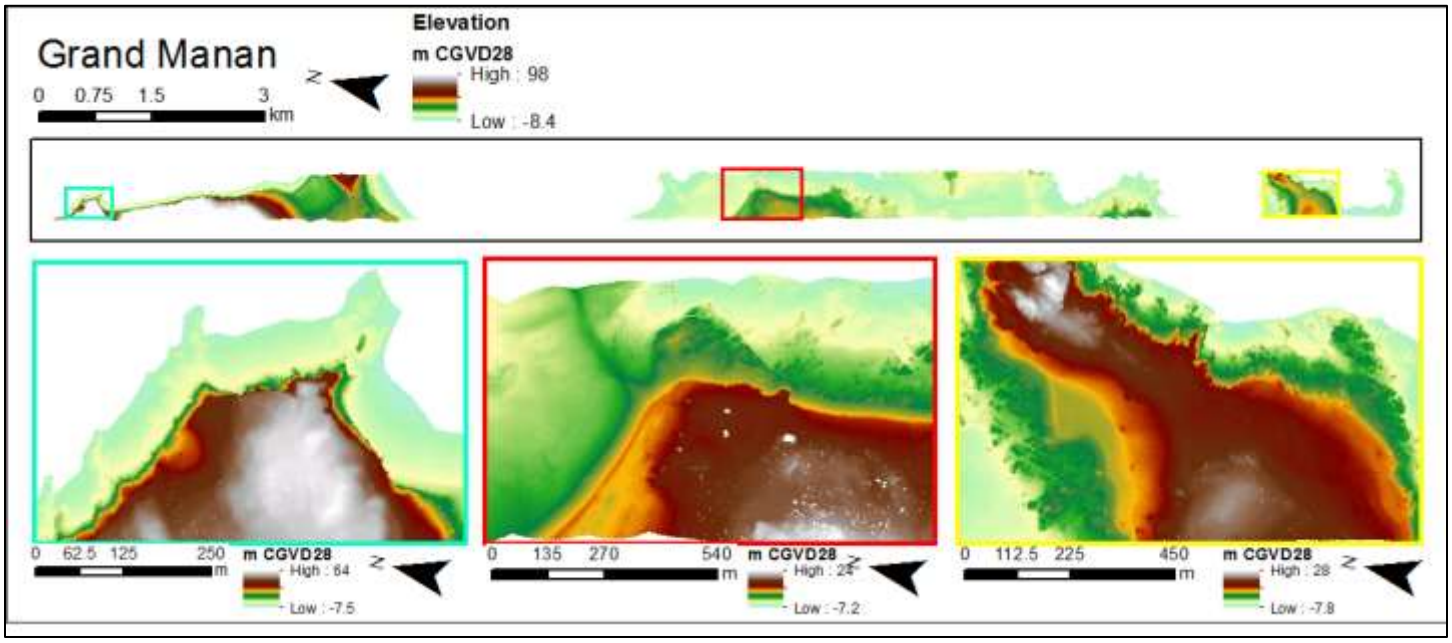

Figure 3.9: DEM for Grand Manan showing the whole study area, and insets below which are matched to the larger figure by border colour. Maximum lidar penetration was -8.4 m CGVD28.

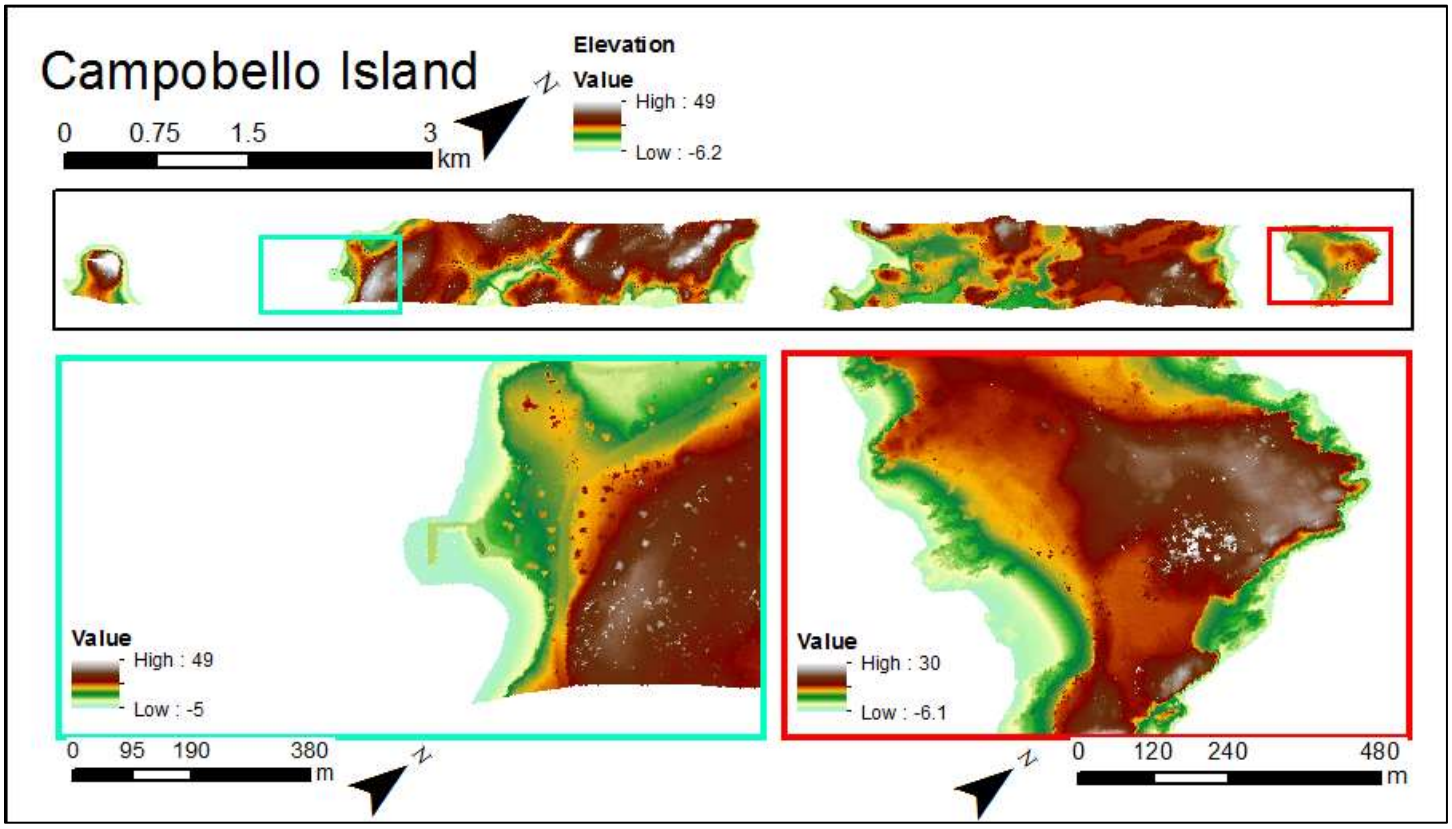

Figure 3.10: DEM for Campobello Island showing the whole study area, and insets below which are matched to the larger figure by border colour. Maximum lidar penetration was -6.2 m CGVD28.

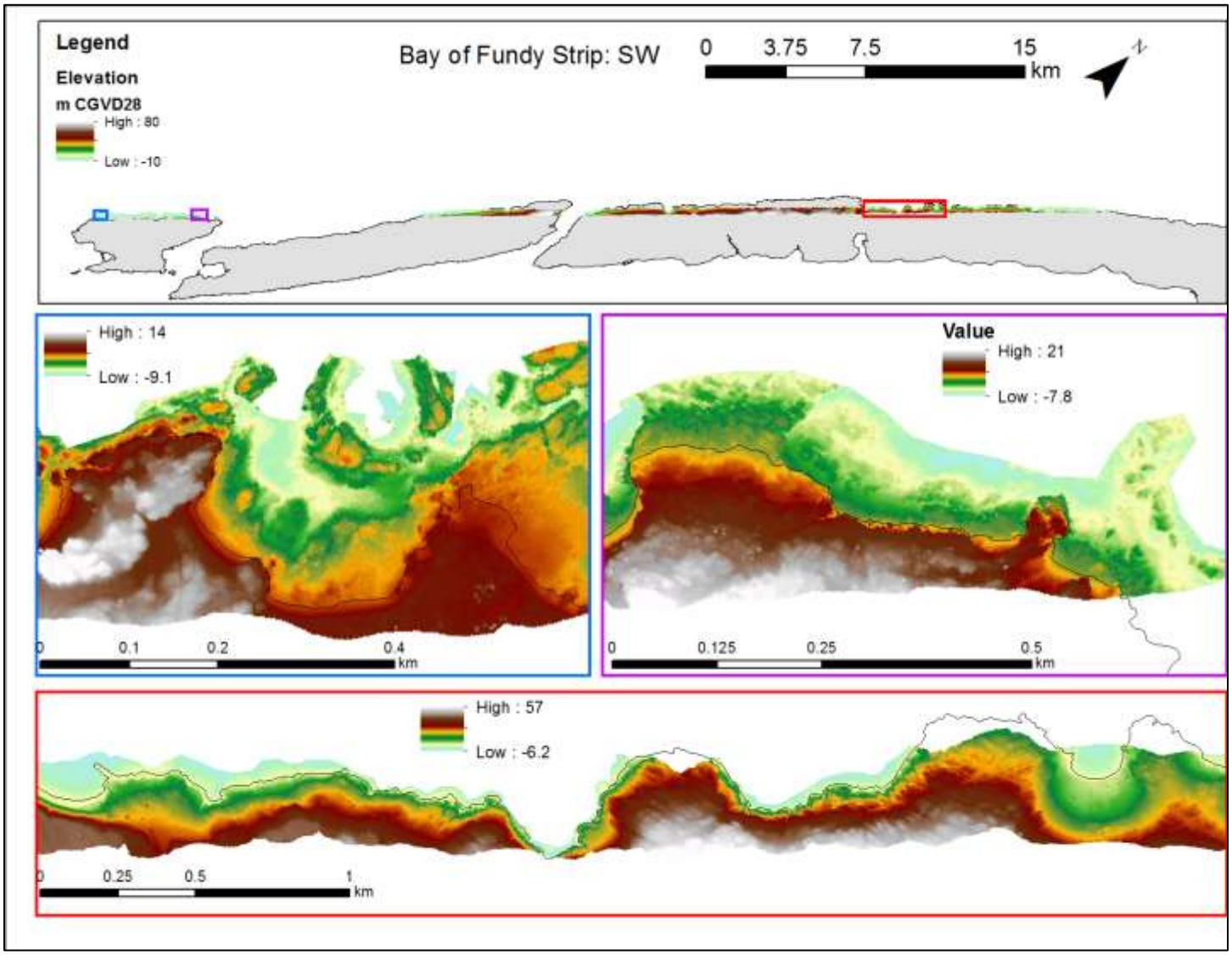

Figure 3.11: DEM for Bay of Fundy Strip SW showing the whole study area (above), and insets below which are matched to the larger figure by border colour. Maximum lidar penetration was -10 m CGVD28.

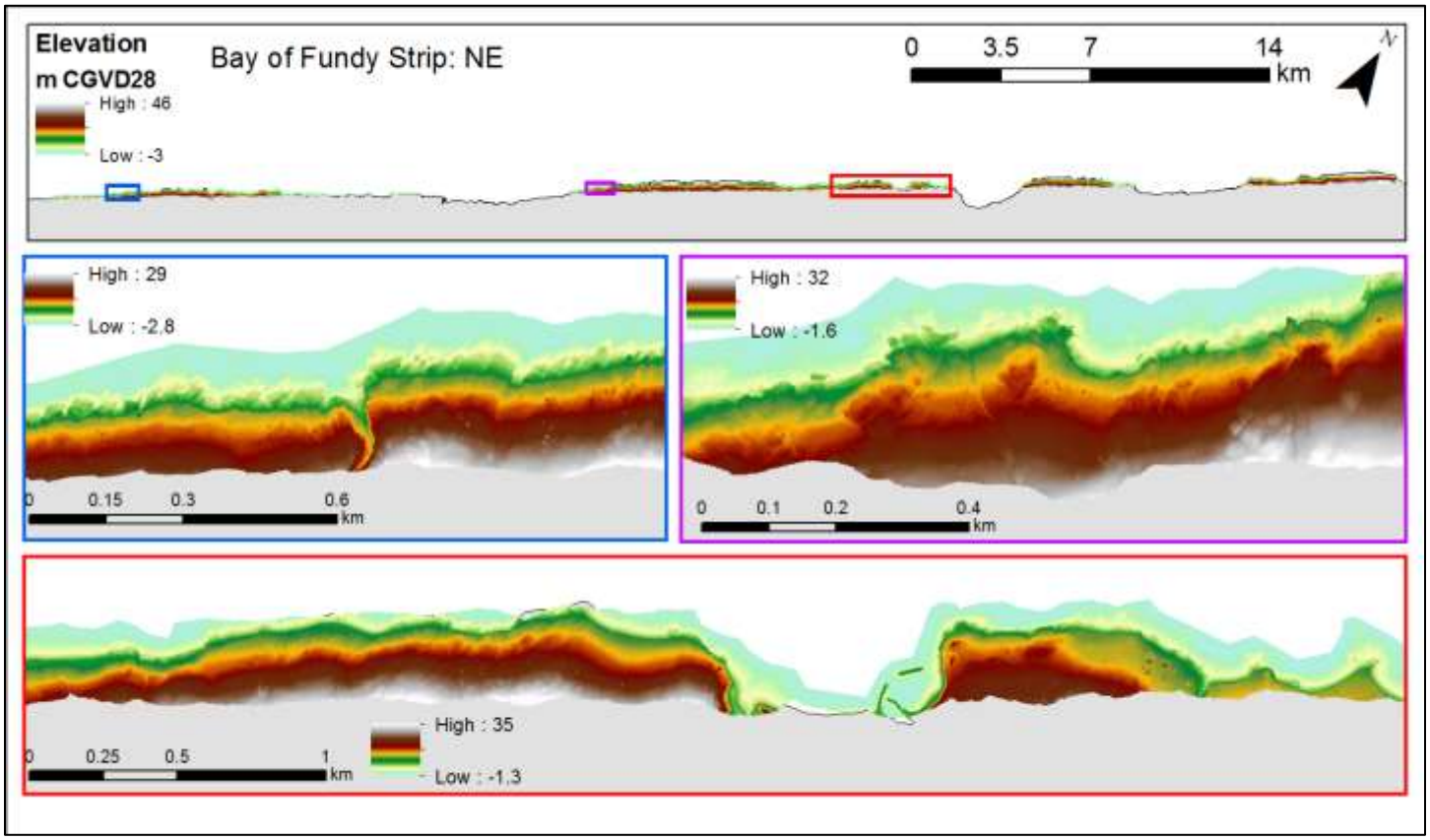

Figure 3.12: DEM for Bay of Fundy Strip NE showing the whole study area (above), and insets below which are matched to the larger figure by border colour. Maximum lidar penetration was -3 m CGVD28.

3.2.2 Colour-Shaded Relief Models

This section presents Colour Shaded Relief (CSR) models for each study area in Figure 3.11 through Figure 3.16. The CSRs emphasize the vertical relief in a map by scaling the DEM by a factor of 5 and by providing a simulated sun angle to add shadows. Each figure in this section includes several sub-panels that focus in on features at a closer scale.

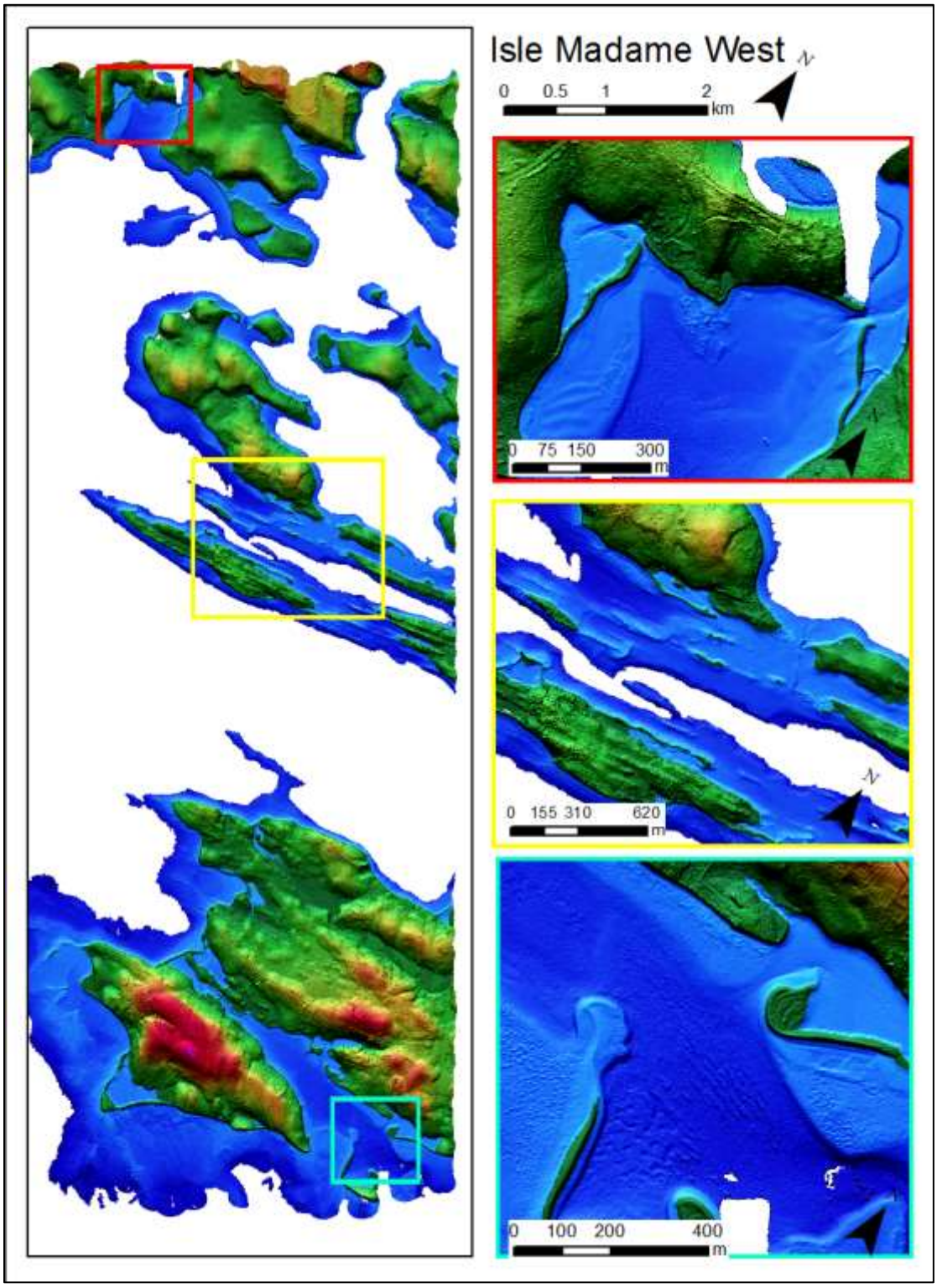

Figure 3.13: Isle Madame West Colour Shaded Relief Model showing the whole study area, and insets beside which are matched to the larger figure by border colour.

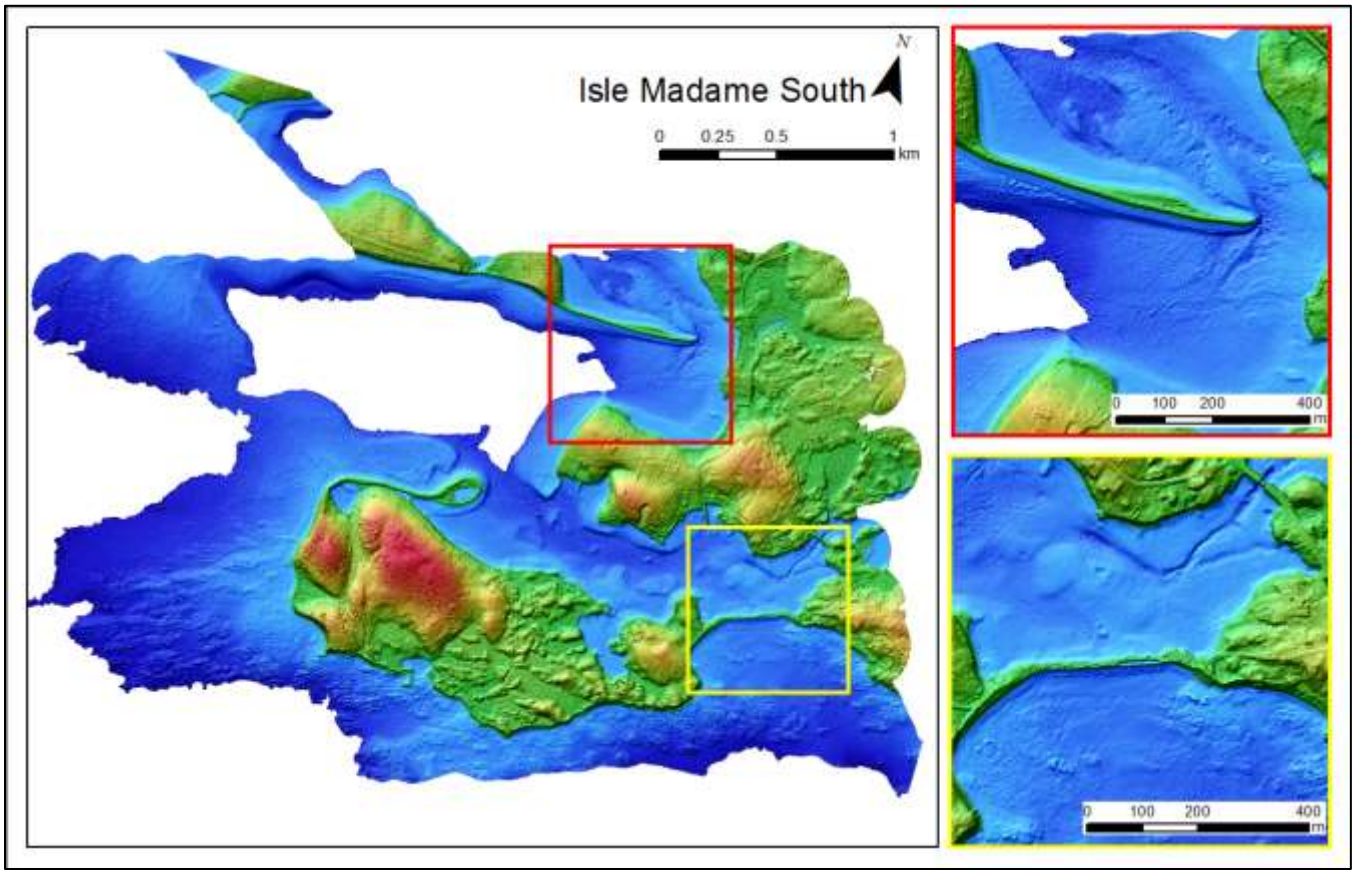

Figure 3.14: Isle Madame South Colour Shaded Relief Model showing the whole study area, and insets beside which are matched to the larger figure by border colour.

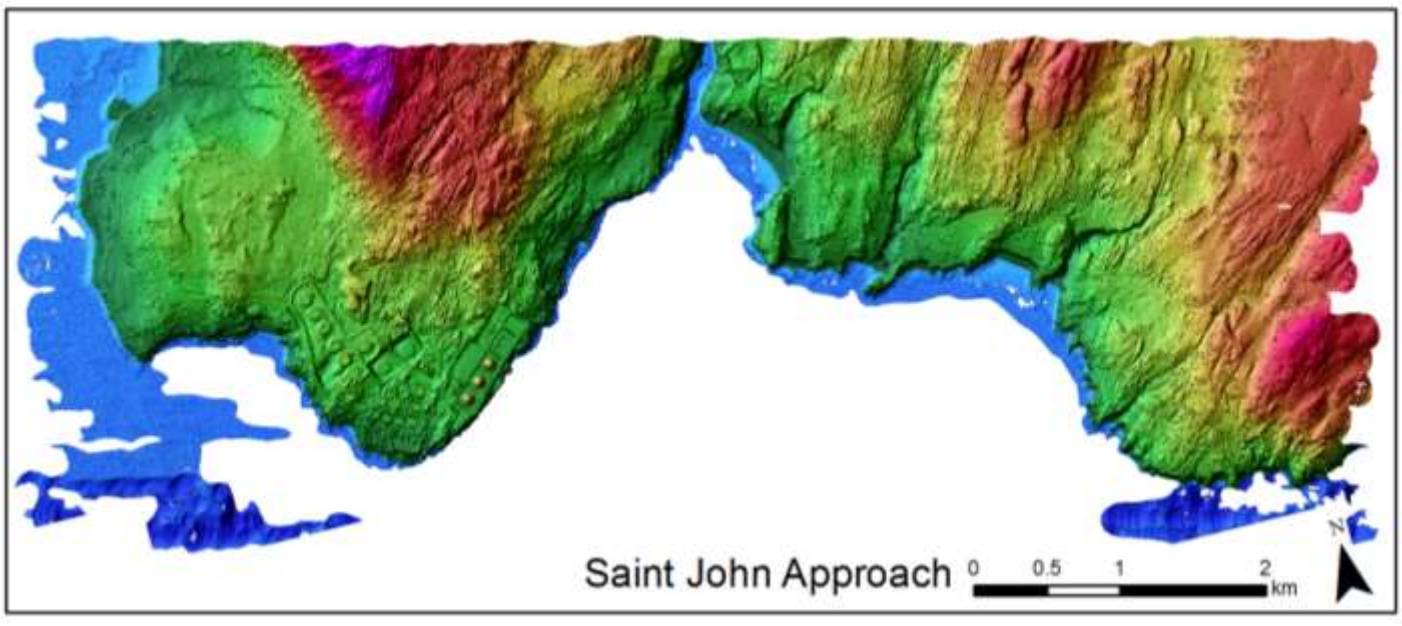

Figure 3.15: Saint John Approach Colour Shaded Relief Model showing the whole study area, and insets beside which are matched to the larger figure by border colour.

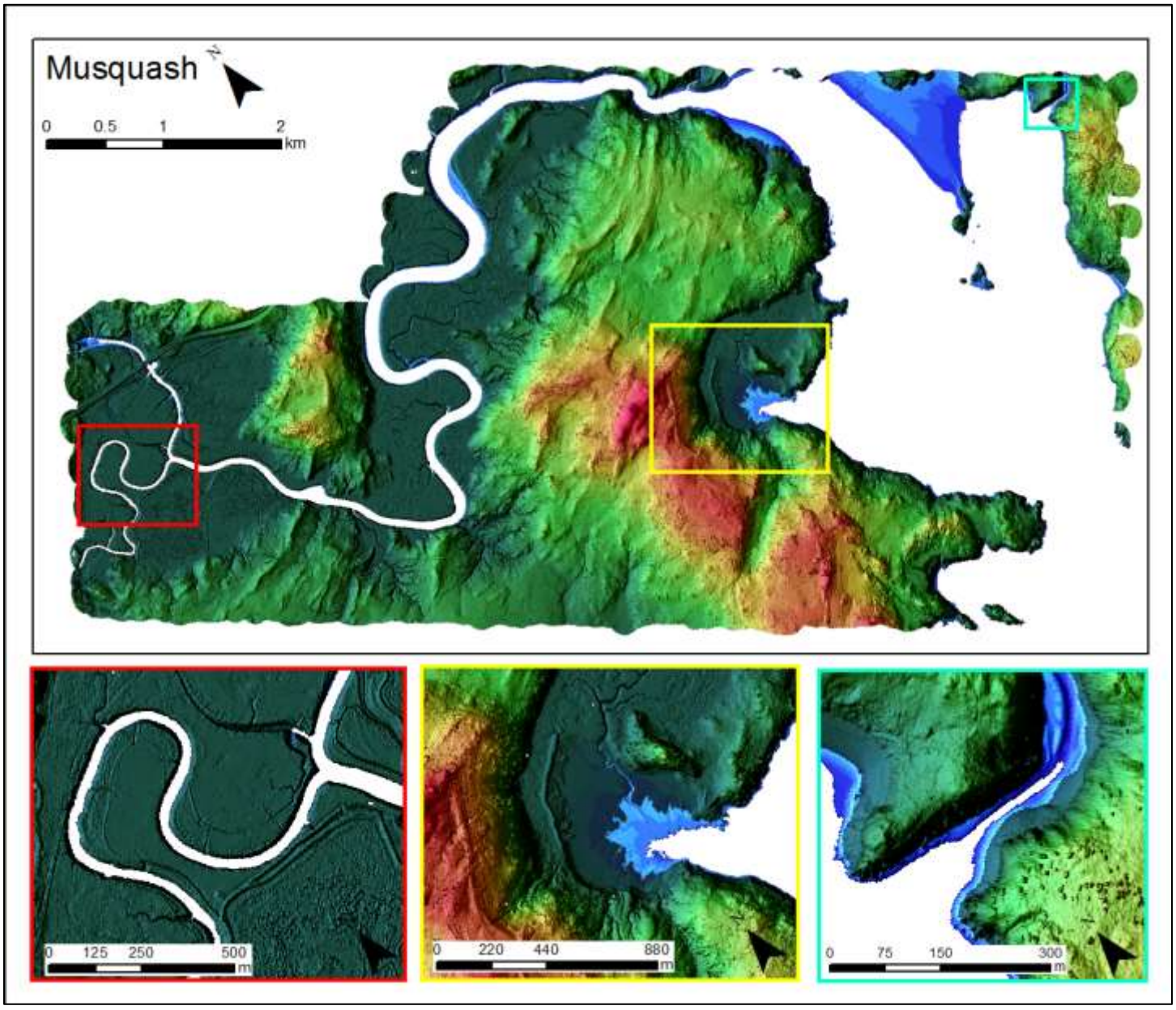

Figure 3.16: Musquash Colour Shaded Relief Model showing the whole study area, and insets below which are matched to the larger figure by border colour.

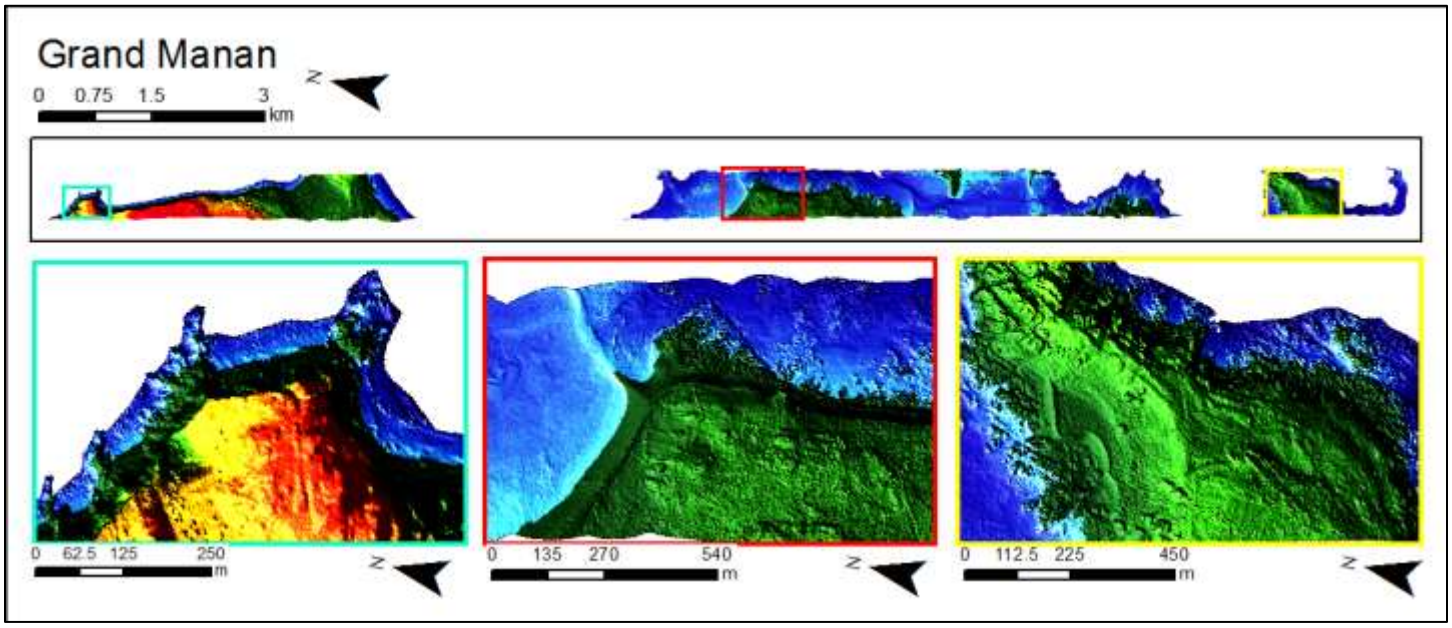

Figure 3.17: Grand Manan Colour Shaded Relief Model showing the whole study area, and insets below which are matched to the larger figure by border colour.

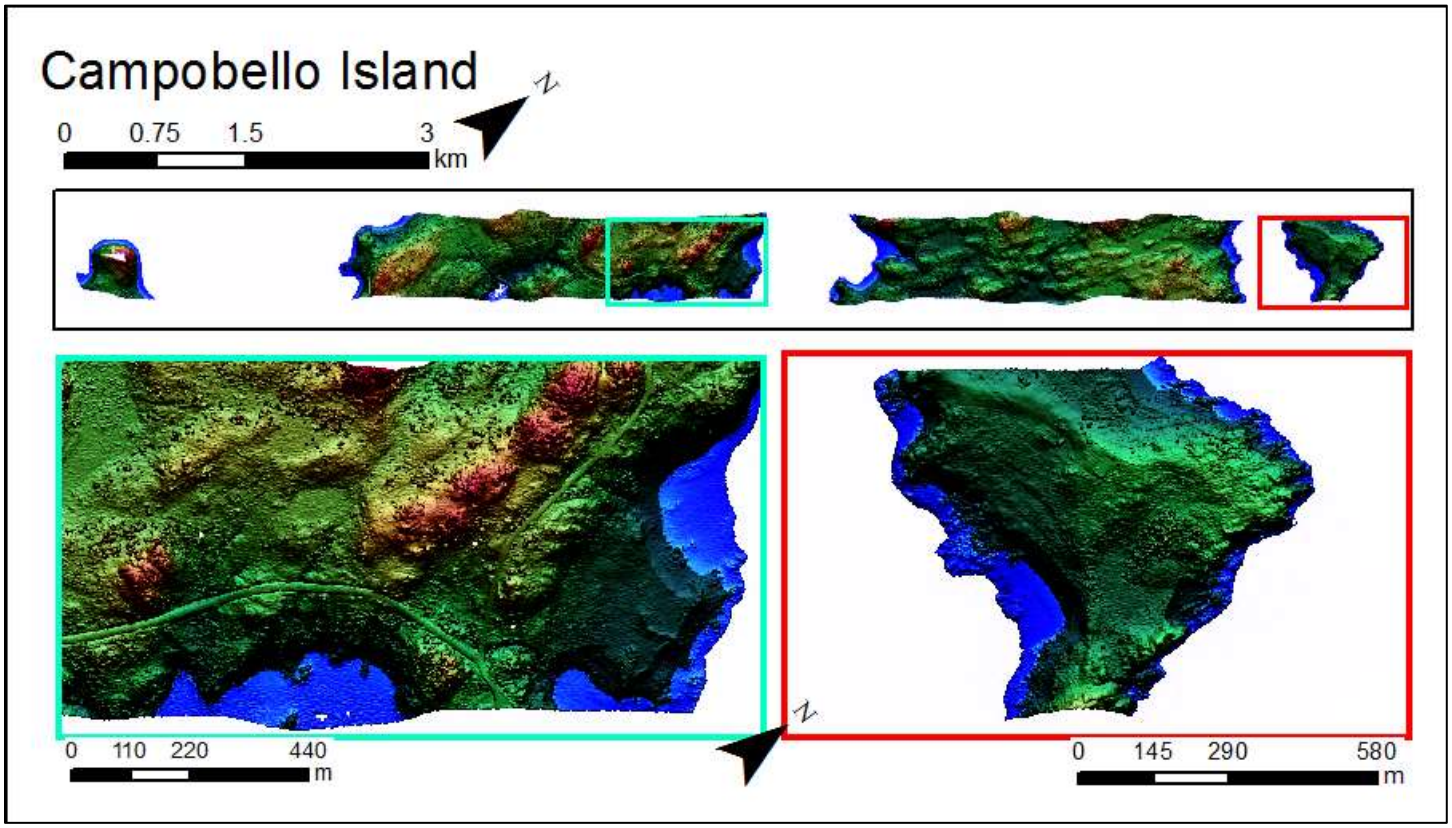

Figure 3.18: Campobello Island Colour Shaded Relief Model showing the whole study area, and insets below which are matched to the larger figure by border colour.

3.2.3 Depth Normalized Intensity

The Depth Normalized Intensity models (DNIs) can be a powerful tool to reveal submerged features and bottom type information that the air photos and DEM may not show. The intensity data also show a great deal of contrast between brightly coloured seabed and the dark colour of eelgrass.

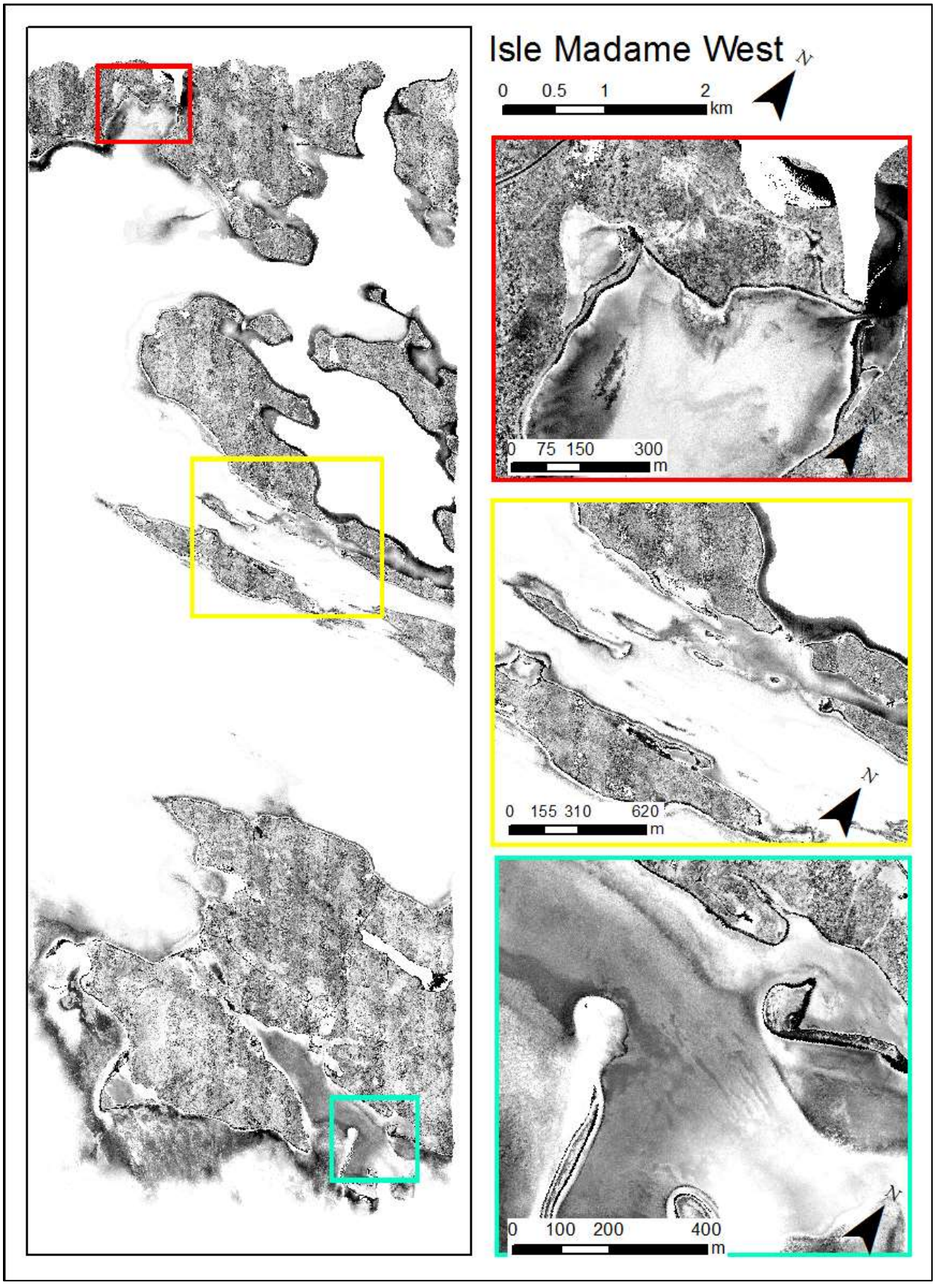

Figure 3.19: Depth Normalized Intensity for Isle Madame West.

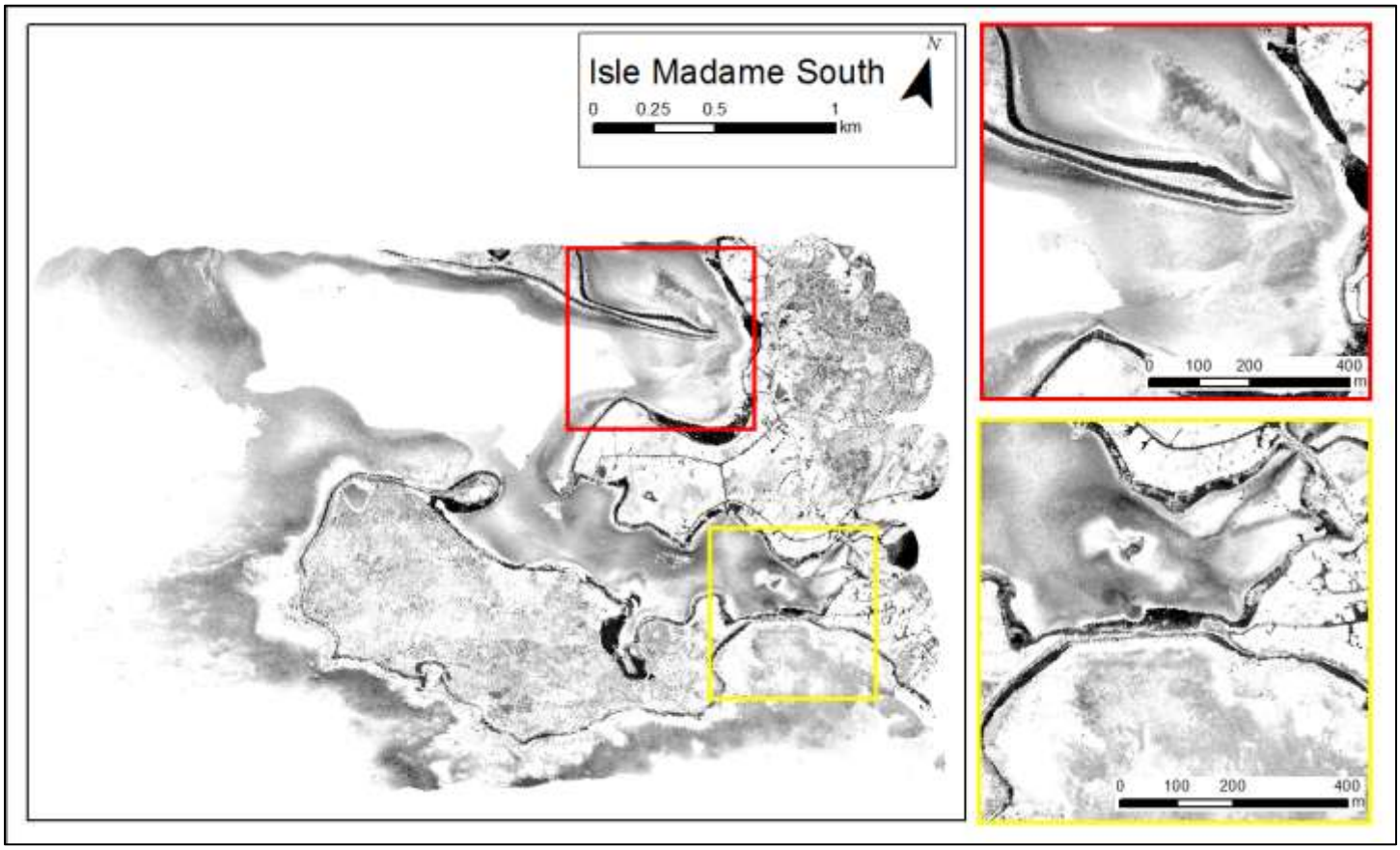

Figure 3.20: Depth Normalized Intensity for Isle Madame South.

3.3 Air Photos

The air photo products are presented in Figure 3.19 through Figure 3.24. As discussed, the mosaic generation can be a challenging process, especially during the fall when sun angle is low. However, the high quality and 5 cm resolution of the photos is clear in the sub-panel images.

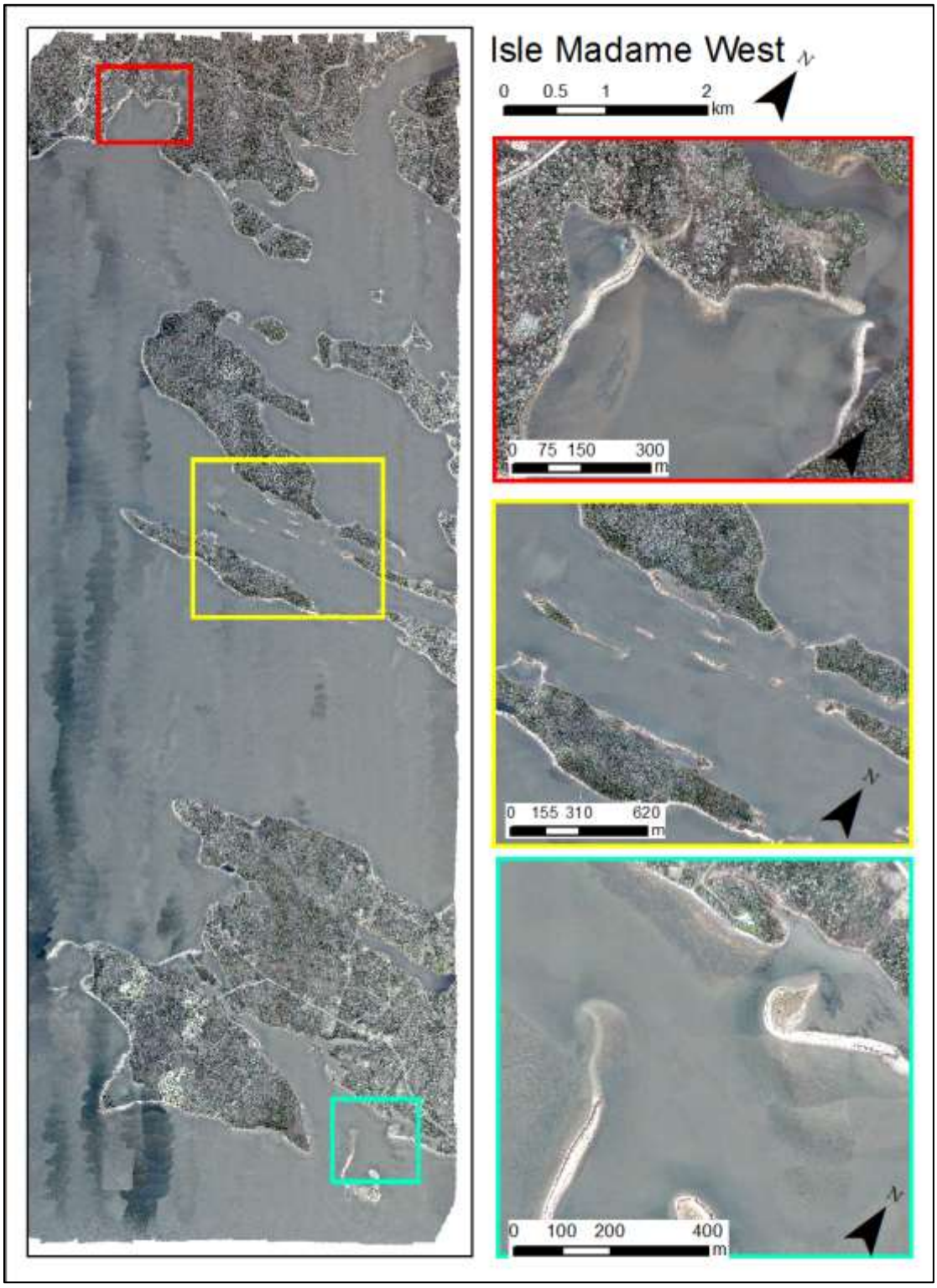

Figure 3.21: Isle Madame West Orthophoto Mosaic showing the whole study area, and insets beside which are matched to the larger figure by border colour. The zoomed in imagery highlights the features of the shoreline and the submerged vegetation and bottom type.

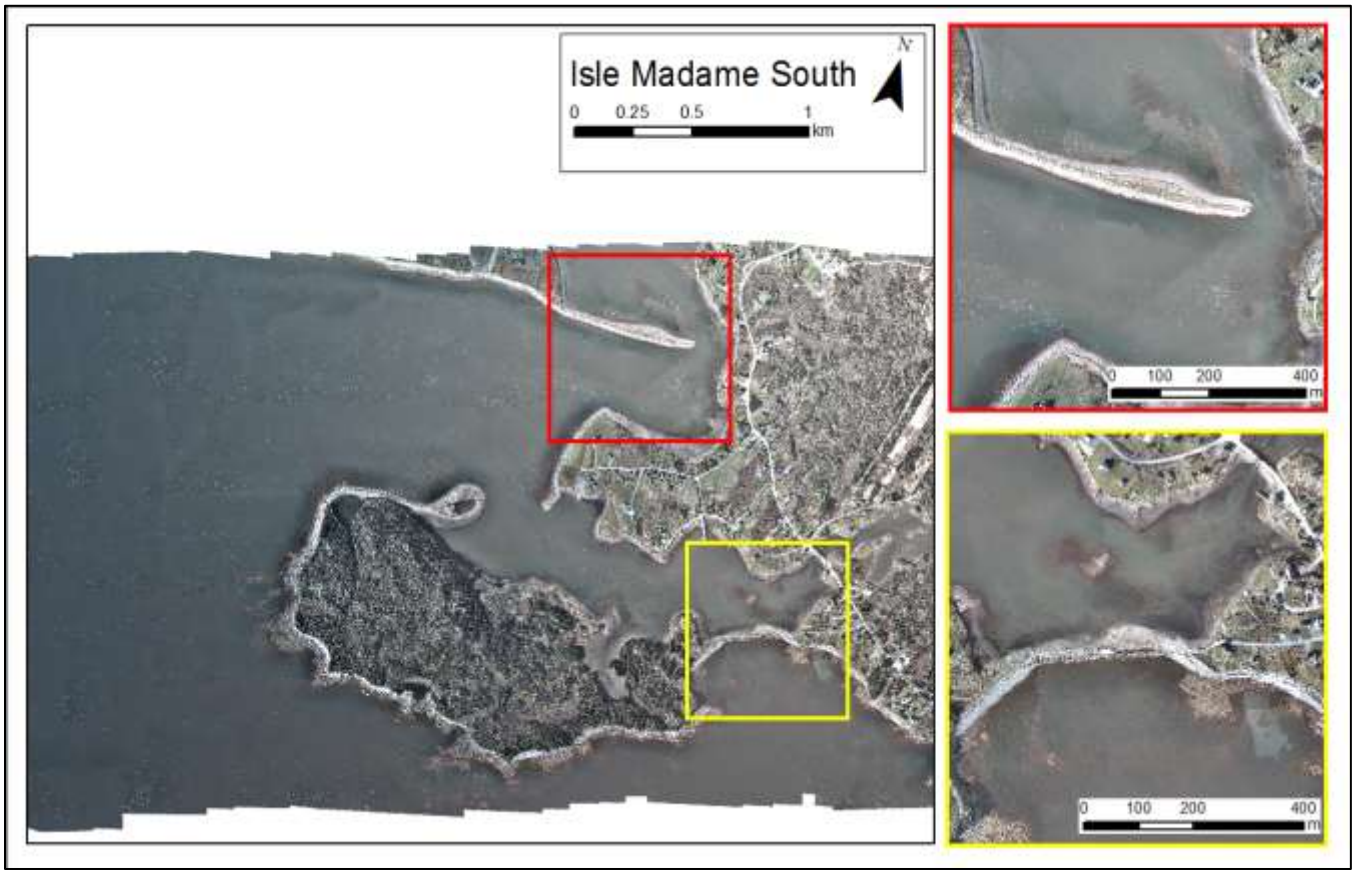

Figure 3.22: Isle Madame South Orthophoto Mosaic showing the whole study area, and insets beside which are matched to the larger figure by border colour. The zoomed in imagery highlights the features of the shoreline and the submerged vegetation and bottom type.

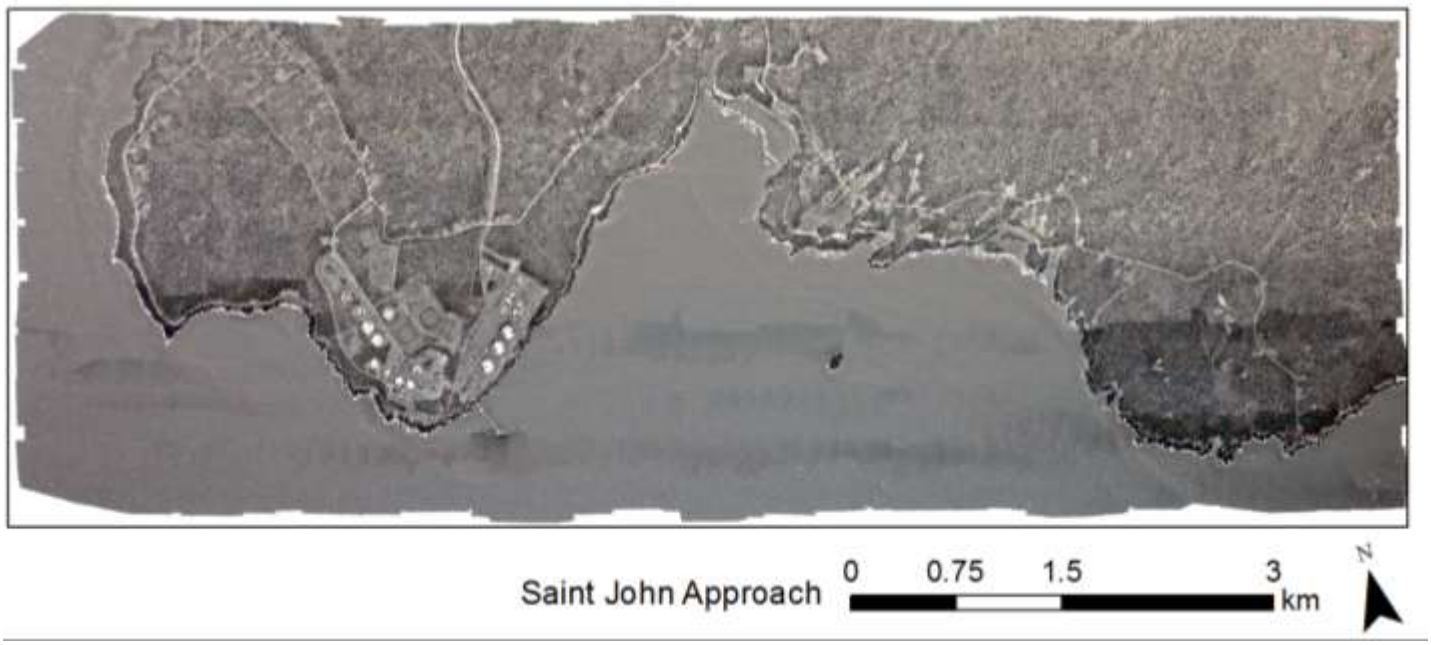

Figure 3.23: Saint John Approach Orthophoto Mosaic showing the whole study area, and insets below which are matched to the larger figure by border colour. The zoomed in imagery highlights the features of the shoreline and the submerged vegetation and bottom type.

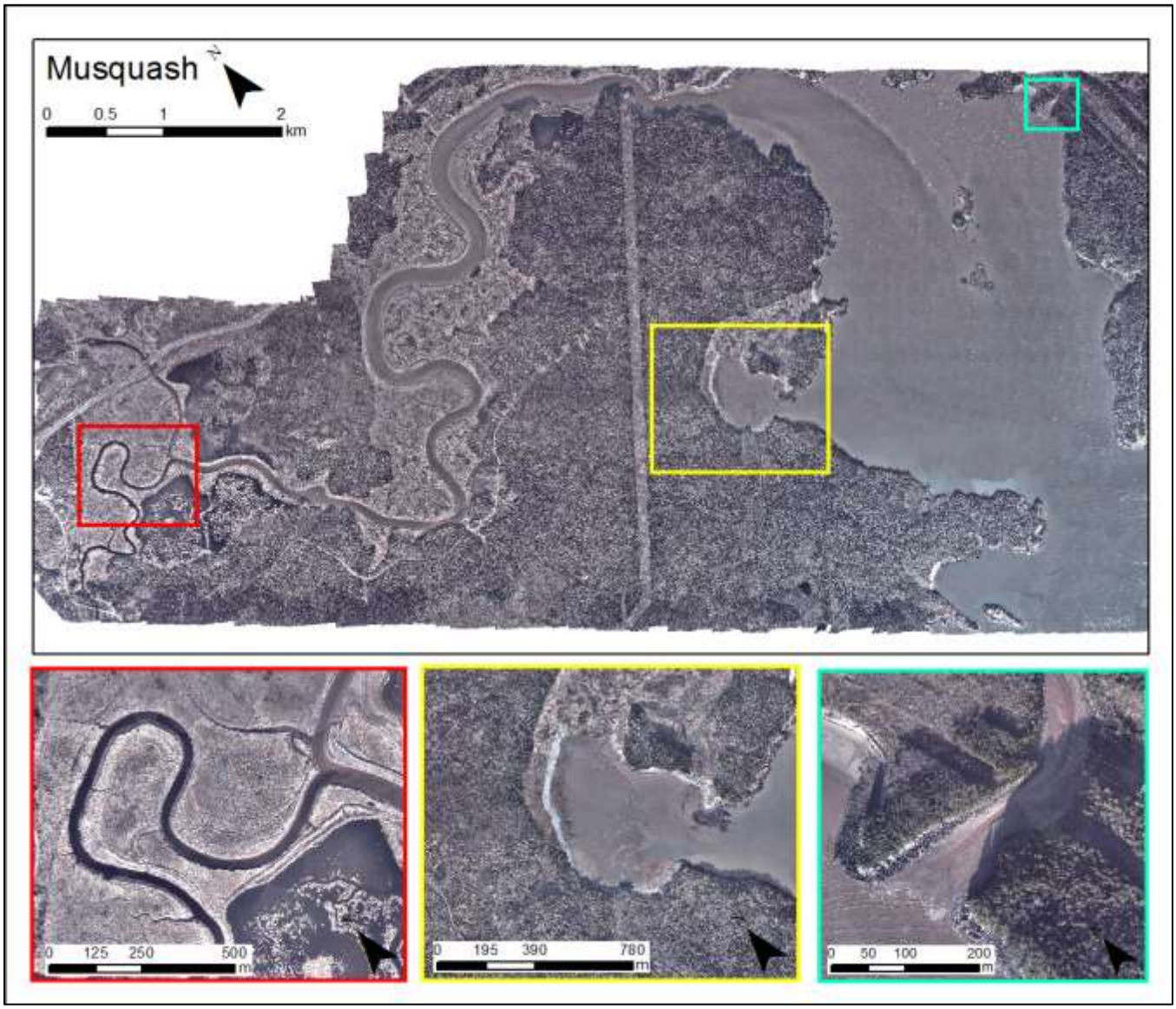

Figure 3.24: Musquash Orthophoto Mosaic showing the whole study area, and insets below which are matched to the larger figure by border colour. The zoomed in imagery highlights the features of the shoreline and the submerged vegetation and bottom type.

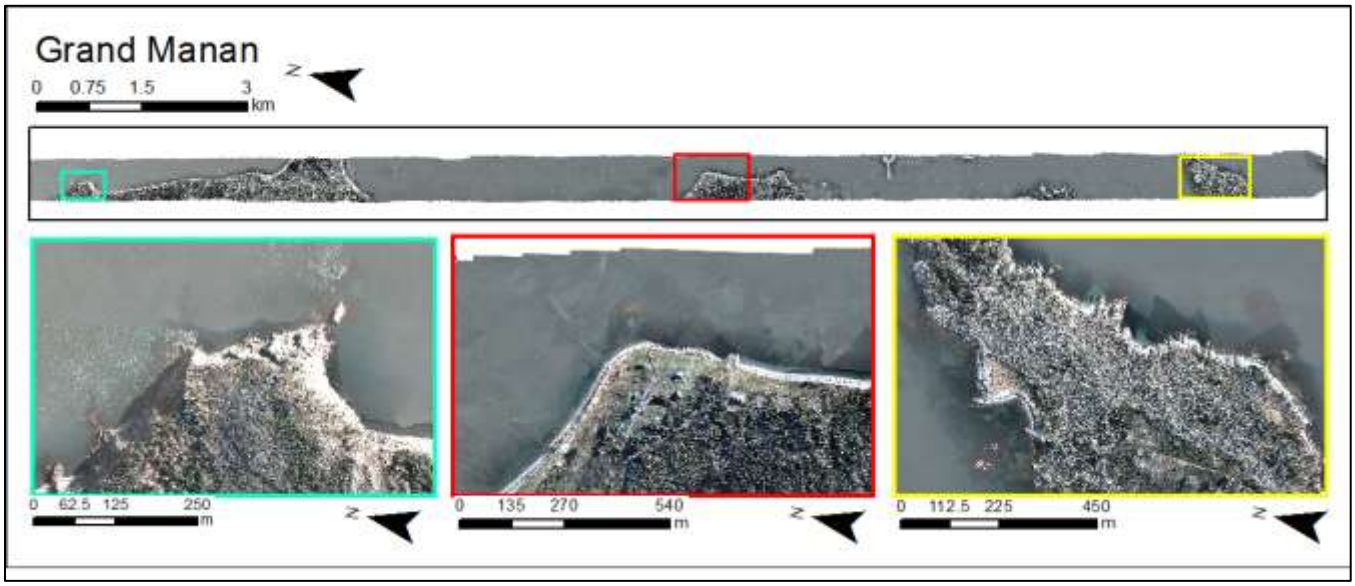

Figure 3.25: Grand Manan Orthophoto Mosaic showing the whole study area, and insets below which are matched to the larger figure by border colour. The zoomed in imagery highlights the features of the shoreline and the submerged vegetation and bottom type.

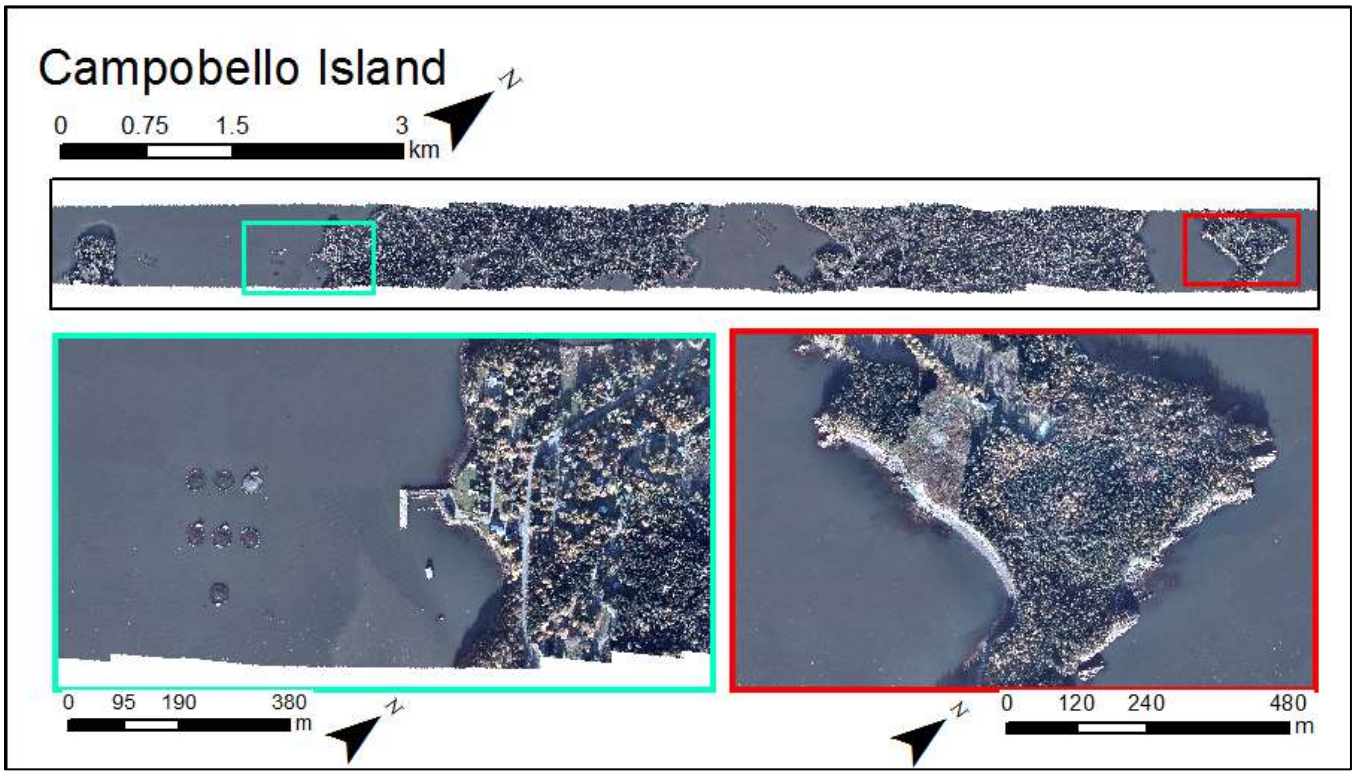

Figure 3.26: Campobello Island Orthophoto Mosaic showing the whole study area, and insets below which are matched to the larger figure by border colour. The zoomed in imagery highlights the features of the shoreline and the submerged vegetation and bottom type.

3.4 Model Results

3.4.1 Model Validation

The water surface elevation data recorded by the pressure sensor deployed at IMS, as described in Section 2.4.2, were converted to depth values and used to validate modelled water depths extracted from the model at the pressure sensor location (Figure 3.25). The modelled and observed depths comparison is represented well by a linear relationship with a Pearson's Coefficient of 0.975, with p value < 0.01 and random residual distribution (Figure 3.26). Further model validation is planned for Year 2 of this project.

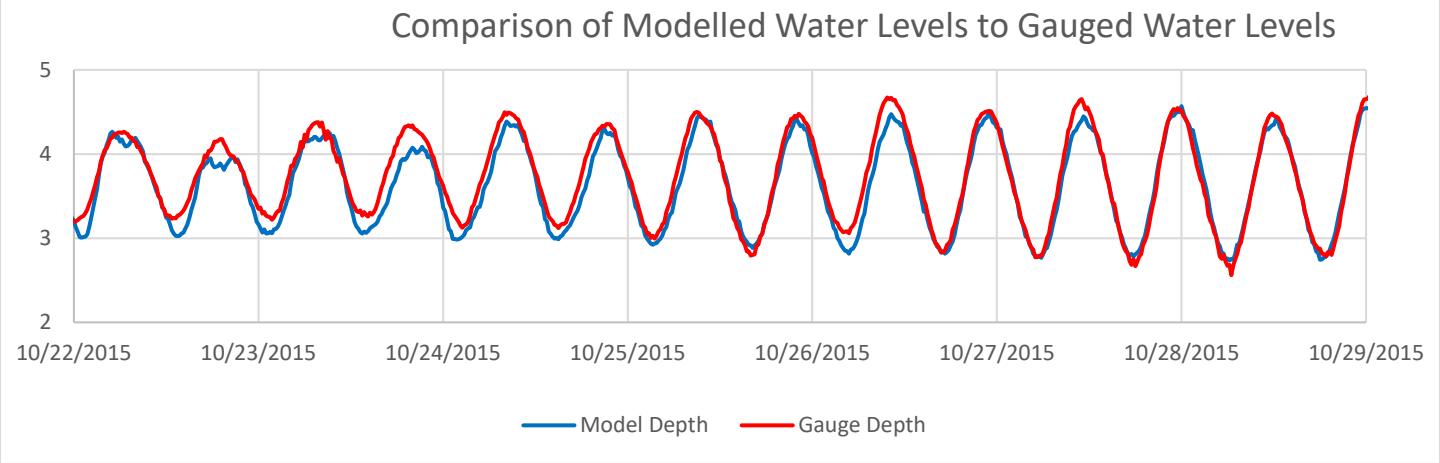

Figure 3.27: Modelled and observed water depth at the location of the IMS pressure sensor deployed between Sept. 23 and Nov. 10, 2015.

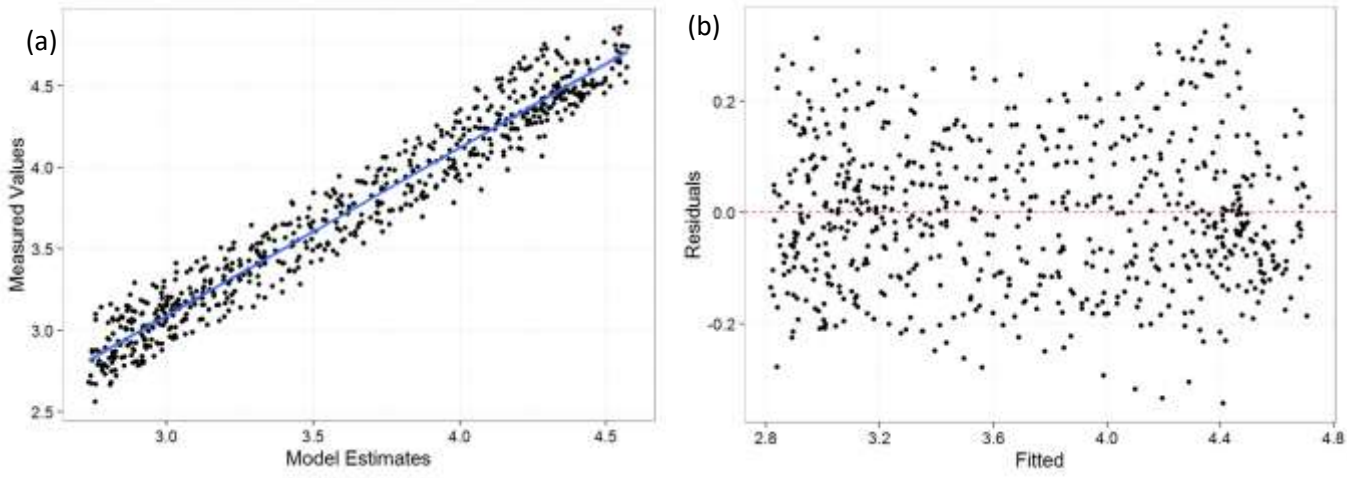

Figure 3.28: (a) Modelled depth estimates compared to measured depth during the pressure sensor deployment; the relationship has a Pearson's Coefficient of 0.975 and a p value < 0.01; (b) the residuals of the linear model show a random distribution, emphasizing the good fit of the model to the data.

3.4.2 Modelled Flows

The HD model was successful at routing flow from Chedabucto Bay through the narrow channels and complex bathymetry near Isle Madame (Figure 3.27, Figure 3.28).

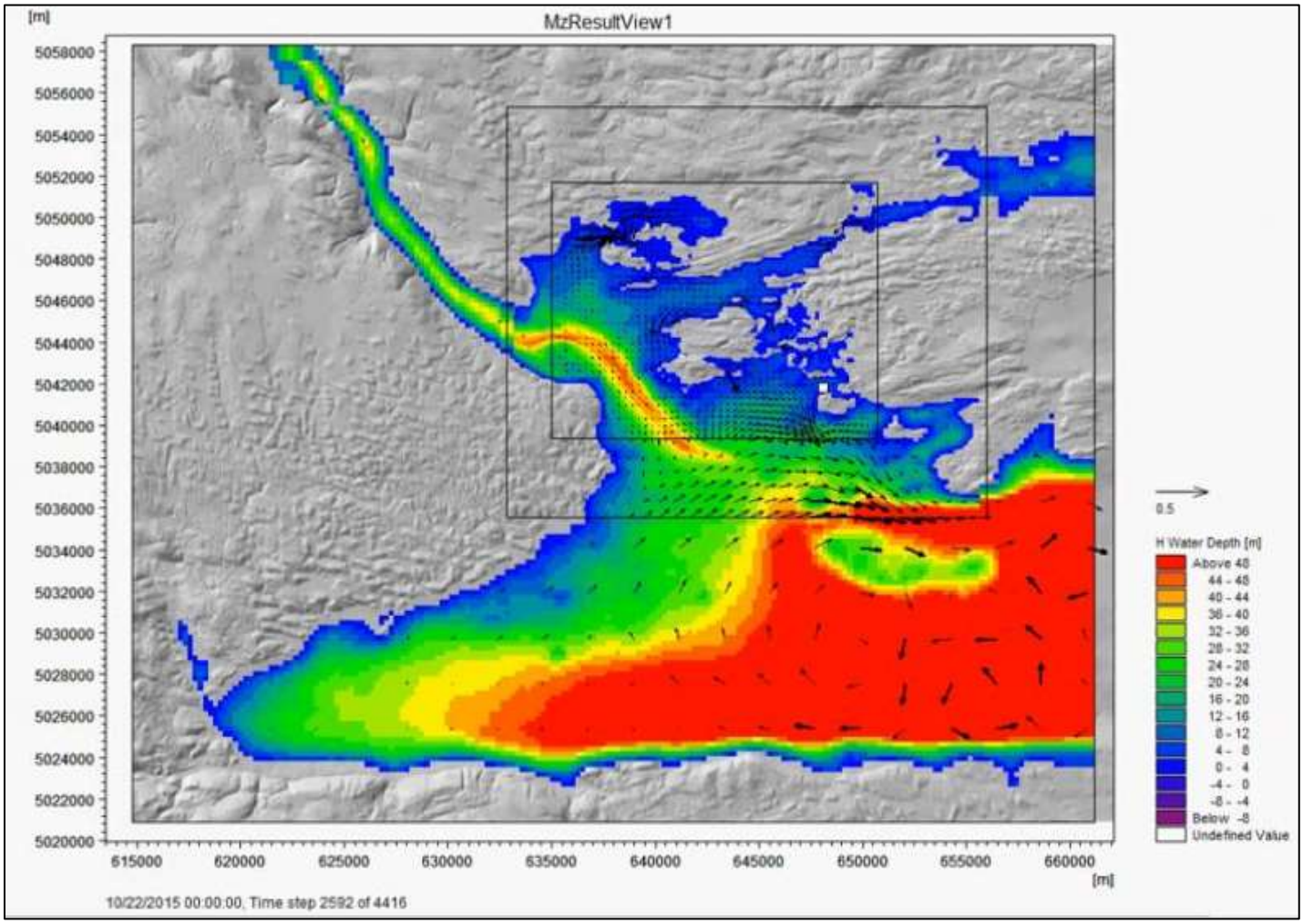

Figure 3.29: Model results for the whole domain. Vectors point in the direction of current flow and vector sizes represent flow magnitude. Coloured contours represent water depth, where deeper water is red and the shallowest water is blue.

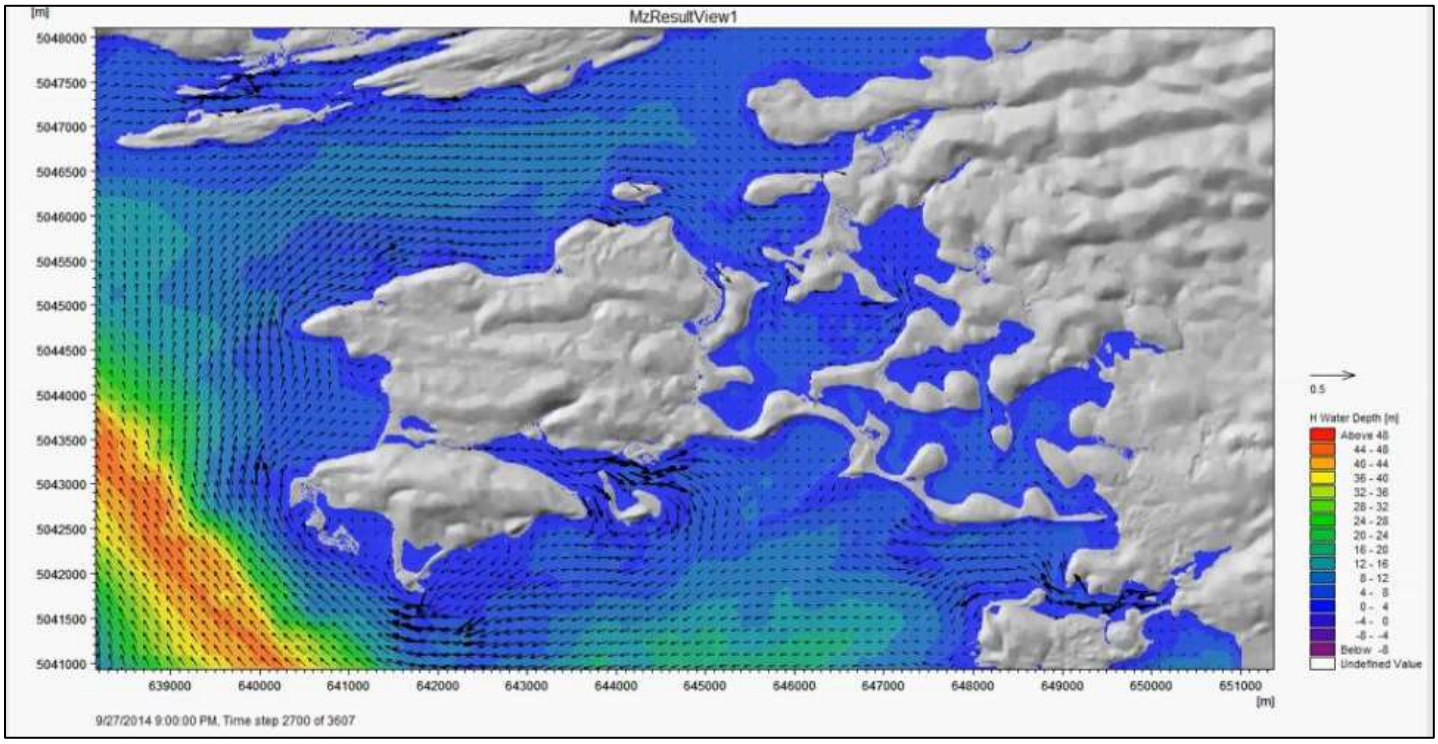

Figure 3.30: Model results for the smallest domain (D, 9 m cell resolution). Vectors point in the direction of current flow and vector sizes represent flow magnitude. Coloured contours represent water depth, where deeper water is red and the shallowest water is blue.

3.4.3 Particle Tracking

Once the model was validated and running smoothly, the particle tracking module could be activated and used to simulate the distribution of particles, such as oil. To model a past spill required knowledge of the source location of the spill, and the dispersion properties of oil. To simulate a possible spill we used characteristics of a known spill, the SS Arrow in 1970. We simulated an oil spill at three locations using a contaminant load of 1000 kg and a dispersion rate of 13 m^2/s. The movement of the oil was simulated for a section of intracoastal waterway in the 9 m resolution model (Figure 3.29). The results show how the oil spreads over the course of 32 hours, reaching a maximum spatial distribution between 17 and 20 and 20 hours after the initial particle release. By 32 hours the concentration of oil has lessened, but oil particles remain onshore, potentially causing damage to vulnerable ecosystems and habitats. The modelled distribution agrees with documentation of the actual spill in 1970 (Owens, 1971). The particle tracking model can also be used to predict future oil spills by releasing oil particles at any location in order to assess risk to vulnerable ecosystems.

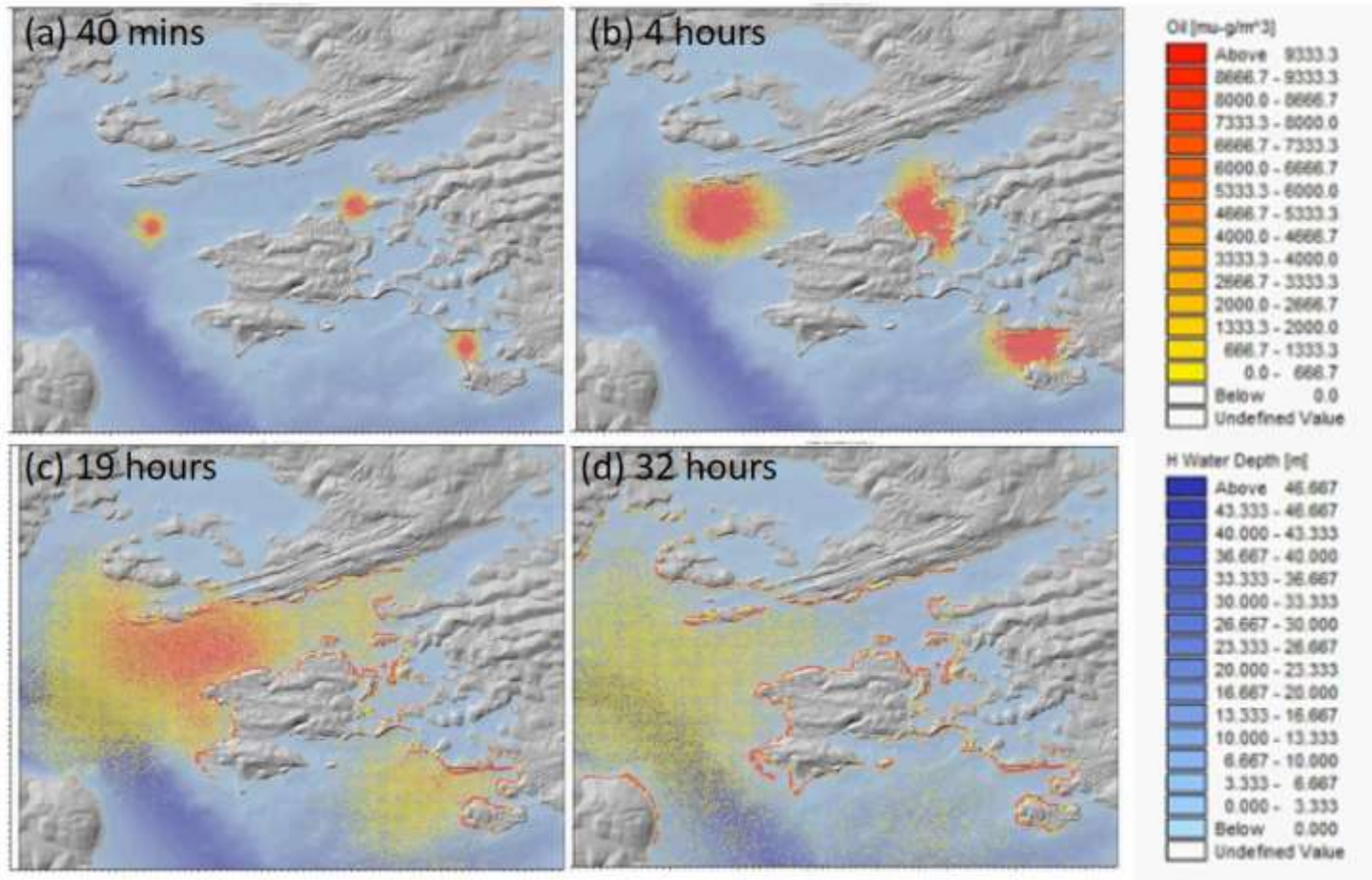

Figure 3.31: Results of simulating the dispersion of oil using the particle tracking component of the model. The panels (a) through (d) show how the oil, in micro-grams/m^3, spreads throughout the intracoastal waterway over the course of 32 hours, reaching maximum coverage between 17 and 20 hours after the initial particle release.

4 Conclusions

Topographic-bathymetric lidar surveys were flown at six study areas in Nova Scotia and New Brunswick as part of the Government of Canada's World-Class Tanker Safety Program, in collaboration with Fisheries and Oceans Canada in the fall of 2015. Depth penetration of the laser was excellent, reaching 12 m depth in the two Atlantic Ocean study areas at Isle Madame, NS, and between 10 and 3 m depth in the four Bay of Fundy sites. Digital elevation models, colour shaded relief models, and aerial photograph mosaics were generated for each study area. Validation of the topographic lidar was achieved at four study areas using differential GPS data obtained for hard, flat surfaces; mean difference in elevation between the GPS data and lidar data across all sites was -0.06 m. Bathymetric lidar was validated at the Isle Madame study area using direct seabed elevation measurements obtained using differential GPS; the mean difference in elevation between the GPS data and the lidar data was -0.19 m.

A hydrodynamic model was developed for the Isle Madame study area using the lidar bathymetry data at Isle Madame South and West combined with the 2014 dataset from Isle Madame Central. The model was validated using a pressure sensor deployed in Isle Madame for 48 days. The modelled and observed depths comparison was represented by a

linear relationship with a Pearson's Coefficient of 0.975, with p value < 0.01 and random residual distribution. The model was used to simulate flow through the complex morphology and bathymetry of the Isle Madame coastline, and to simulate the timing and dispersion of a simulated oil spill. The next stage of this project will involve the deployment of an ADCP current meter to validate the modelled currents, and to use the model to investigate shoreline vulnerability to potential future oil spills with consideration of climate change.

5 Acknowledgements

We would like to thank Fisheries and Oceans Canada for funding support. We would also like to thank David Kristiansen, Matt Roscoe, Calvin Gough, Ariel Vallis, and Sean Dzafovic of NSCC's AGRG for their assistance with collection of ground truth data for the World-Class Tanker Safety Project. Thanks to staff from Airborne Hydrography and Leica Geosystems, Leading Edge Geomatics staff for operations support and AGRG staff for administrative support.

6 References

Ekelund, A. (2015, 13 15). Airborne Hydrography AB.

ESRI. (2011, 06 29). *ArcGIS.com*. Retrieved from ArcGIS Resource Center: http://help.arcgis.com/en/arcgisdesktop/10.0/help/index.html#//009z0000007m000000.htm

Geunther, G. C., Cunningham, A. G., LaRocque, P. E., & Reid, D. J. (2000). Meeting The Accuracy Challenge In Airborne Lidar Bathymetry. *EARSeL-SIG Lidar Workshop Proceedings.* Dresden: Joint Airborne Lidar Bathymetry Technical Centre of Expertise.

Griffin, J., & Eilers, D. (2010). Lake Morphology: Application of Spatial Analysis to Better Manage and Understand Lake Morphologic Data. *21st Annual Conference of the Florida Lake Management Society* (pp. 108-110). Crystal River, Florida: Florida Lake Management Society.

Halifax Regional Municipality. (2014, June 2). *Water, Wastewater, and Stormwater Facilities & Infrastructure*. Retrieved from Halifax Water: http://www.halifax.ca/hrwc/Facilities.php

Wang, C., & Philpot, W. (2007). Using airborne bathymetric lidar to detect bottom type variation in shallow waters. *Remote Sensing of Environment*, 123-135.

Webster, T., & et. al. (2015). *Evaluating a topo-bathymetric lidar sensor to map Submerged Aquatic Vegetation in Lake Banook.* Middleton, NS: Applied Geomatics Research Group NSCC.

Webster, T., McGuigan, K., Crowell, N., Collins, K., & MacDonald, C. (2014). *ACOA 2014 Bathymetric Lidar Pilot Project Report: Cape John, John Bay, and Little Harbour, Nova Scotia.* Middleton, NS: Applied Geomatics Research Group, NSCC.

Webster, T., McGuigan, K., Crowell, N., Collins, K., & MacDonald, C. (2014). *Tabusintac 2014 Topo-Bathymetric Lidar & Eelgrass Mapping Report.* Middleton, NS: Applied Geomatics Research Group NSCC.